Dissertation
submitted to the
Combined Faculties for the Natural Sciences and for Mathematics
of the Ruperto-Carola University of Heidelberg, Germany
for the degree of
Doctor of Natural Sciences

put forward by
Janosch A. Deeg
born in Hengstfeld, Schwäbisch Hall, Germany

Oral examination: January 17th, 2014

Modulation of T cell Activation with Nanopatterned and Micro-Nanopatterned Antigen Arrays

Referees:
Prof. Dr. Joachim P. Spatz
Prof. Dr. Rainer Fink

"I was like a boy playing on the sea-shore, and diverting myself now and then finding a smoother pebble or a prettier shell than ordinary, whilst the great ocean of truth lay all undiscovered before me"

Isaac Newton

Abstract

The human immune system is a multi-talented composition of a variety of interacting elements trying to protect the host from any kind of disease. Much research has been done to elucidate a key event of this complex defense strategy, which is the activation of T cells resulting from the formation of a temporary synapse between a T cell and an antigen presenting cell. During this intercellular contact the T cell obtains pathogen-related information in order to initiate specific steps for averting the disease.

In the presented work, we introduce a novel, bio-functional substrate system simulating the antigen presenting cell's surface. The engineered platform provides defined micro- and nano-scaled presentation of crucial proteins as well as control over substrate compliance. This system enables the possibility to investigate T cell activation and synapse formation under controlled conditions. It could be demonstrated that T cells show activation-related behavior when interacting with such substrates; they adhere, polarize and start to release signaling molecules. These events prove that the substrates can substitute for the antigen presenting cell and are able to modulate the activation process of T cells. It was shown that T cells are sensitive to a surface density of 90 – 140 stimulating molecules per μm^2, but only if presented over the entire cell-surface contact area. An adhesive background consisting of proteins which support the adhesion process significantly decrease this threshold value. These insights contribute to a deeper understanding of the complex process of T cell activation and support the development of novel therapies employing the body's own defense system to control diseases.

Zusammenfassung

Das menschliche Immunsystem ist ein Multitalent, bestehend aus einer Vielzahl von interagierenden Komponenten, ständig darauf bedacht den Menschen vor Krankheiten zu schützen. Essentieller Bestandteil dieses komplexen Abwehrsystems und daher Gegenstand ausgedehnter Forschungsaktivitäten ist die Aktivierung einer T-Zelle durch Bildung einer temporären Synapse mit einer antigenpräsentierenden Zelle. Hierbei wird die T-Zelle über die Art des Erregers informiert und kann gezielt weitere Schritte zur Krankheitsbekämpfung einleiten.

In der vorliegenden Arbeit wird mit neuartigen bioaktiven Substraten die Oberfläche einer antigenpräsentierenden Zelle simuliert. Das Modellsystem erlaubt es, die Anordnung und Zusammensetzung ausschlaggebender Proteine im Mikro- und Nanometerbereich sowie die Substratsteifigkeit gezielt festzulegen und somit unter kontrollierten Bedingungen den Prozess der T-Zellaktivierung und Synapsenbildung zu untersuchen. Dabei wurde demonstriert, dass T-Zellen mit den Substraten interagieren und ein aktivierungsspezifisches Verhalten zeigen: Sie stellen Kontakt zur Oberfläche her, polarisieren und beginnen Signalmoleküle abzusondern. Dies zeigt, dass die künstlichen Zelloberflächen in der Lage sind die antigenpräsentierende Zelle zu imitieren und den Aktivierungsprozess gezielt zu steuern: Lediglich oberhalb einer bestimmten Dichte stimulierender Proteine von ca. 90 – 140 pro μm^2 konnten T-Zellen erfolgreich aktiviert werden, sofern die Proteine über den ganzen Zellbereich verfügbar waren. Bei zusätzlicher Bereitstellung von Proteinen, die den Adhäsionsprozess unterstützen, kann der Schwellenbereich signifikant herabgesetzt werden. Diese Erkenntnisse tragen zu einem besseren Verständnis der T-Zellaktivierung bei und unterstützen die Entwicklung von Therapien, die gezielt das körpereigene Abwehrsystem nutzen, um Krankheiten zu bekämpfen.

Contents

Abstract/Zusammenfassung i

List of figures v

List of tables ix

Abbreviations xi

I. Introduction 1

1. Immunology 3
- 1.1. The immune system . . . 6
  - 1.1.1. Antigen . . . 7
  - 1.1.2. MHC molecule . . . 8
  - 1.1.3. Antigen presenting cell . . . 10
- 1.2. T cells . . . 12
- 1.3. T cell activation . . . 16
- 1.4. The immunological synapse . . . 17
  - 1.4.1. Architecture of the immunological synapse . . . 19
  - 1.4.2. Discussing synapse formation and T cell activation models . . . 21

2. Biomimetic substrates for biological studies 27
- 2.1. Artificial cell environments . . . 28
  - 2.1.1. Artificial antigen presenting cell systems . . . 29

II. Substrate Fabrication 35

3. Micro- and nanopatterned antigen arrays as substitute for the APC 37
- 3.1. Block copolymer micelle nanolithography . . . 38
  - 3.1.1. Block copolymers . . . 38
  - 3.1.2. Micelle formation . . . 39
  - 3.1.3. Fabrication of nanopatterns by the self-assembly of micelles . . . 40
  - 3.1.4. Pattern analysis . . . 42

3.2. Hierarchically structured patterns . . . 46
3.2.1. Combination of photolithography and BCML . . . 47
3.3. Biofunctionalization of substrates . . . 52
3.3.1. Background passivation . . . 52
3.3.2. Immobilization of proteins on nanoparticles . . . 52
3.3.3. Determination of proteins per particle . . . 55
3.3.4. Rendering the background bio-adhesive . . . 56
3.3.5. Generation of protein islands on nanopatterns by an external device . 57
3.4. Experimental details and analyses . . . 59
3.4.1. Preparation of nanopatterns and micro-nanopatterns . . . 59
3.4.2. Analysis of patterns . . . 62
3.4.3. Functionalization of patterns . . . 67
3.4.4. Molecular occupation rate of particles . . . 69

III. Cell Experiments 73

4. T cell activation experiments 75
4.1. Monitoring activation events . . . 75
4.1.1. Calcium influx events . . . 76
4.1.2. Spreading area . . . 77
4.1.3. Polarization of microtubule organizing center . . . 85
4.1.4. Quantification of IL-2 concentration as an index of activation . . . 88
4.1.5. Investigating effects of inter-particle spacing *vs* density of particles . . 91
4.1.6. Introducing adhesive ICAM-1 molecules to the nanopatterns . . . 94
4.1.7. Introducing an additional adhesive background . . . 94
4.2. Experimental details and analyses . . . 98
4.2.1. Activation experiments . . . 98
4.2.2. Microscopy techniques . . . 101
4.2.3. Discussing evaluation methods . . . 102

IV. Discussion 103

5. Discussion 105
5.1. Nanopatterned protein arrays as a substitute for the APC surface . . . 105
5.1.1. Block copolymer micelle lithography - a simple technique to create periodic nanopatterns . . . 106
5.1.2. Number of biomolecules per individual particle . . . 106
5.1.3. Generation of nanopatterned synaptic stuctures . . . 108
5.2. T cell response to nanopatterned antigen arrays . . . 108
5.2.1. The role of adhesion during T cell activation . . . 110
5.2.2. TCR cluster and IS formation – key events during T cell activation? . 111
5.3. Nanopatterned antigen/antibody arrays and their potential contribution to clinics . . . 114

V. Conclusion & Outlook 117

6. Conclusion 119

7. Outlook 121

7.1. Future directions applying nanopatterned interfaces as APC surrogates 121
7.1.1. Towards advanced nanopatterns by upgrading binding strategies . . . 121
7.1.2. Combining nanopatterns with compliant supports 122
7.2. Determination of cellular adhesion forces 124
7.2.1. The AFM - a tool to measure adhesion forces of single cells 124
7.3. Perspectives of APC analogs in immunological research and therapies 126

Bibliography 127

Appendix 159

A. Publications 159

List of Figures

1.1. Scheme of MHC molecules . . . 9
1.2. Types of lymphocytes . . . 14
1.3. Summary of the immune response . . . 15
1.4. Procedure of antigen processing, presenting, recognition and synapse formation 18
1.5. Model for immunological synapse formation . . . 19
1.6. The architecture of the immunological synapse . . . 20
1.7. Dynamics of immunological synapse formation . . . 24

2.1. Substituting the APC . . . 30
2.2. Synapse formation on supported lipid bilayers . . . 32
2.3. Stimulation of T cells by synapse array patterns . . . 33

3.1. Process of micelle formation . . . 40
3.2. Dipping device . . . 41
3.3. Nanopatterning process . . . 42
3.4. Determination of inter-particle distances . . . 44
3.5. Nanopatterns with different inter-particle spacing . . . 45
3.6. Determination of particle size *via* an AFM . . . 47
3.7. Combination of Photolithography with BCML . . . 49
3.8. Micro-nanopatterns . . . 51
3.9. Coating the hydrophilic background with PEG . . . 53
3.10. Specific binding of proteins to nanoparticles . . . 54
3.11. Determination of occupation rate by fluorescence microscopy . . . 56
3.12. Azide-alkyne cycloaddition/Rendering the background adhesive . . . 57
3.13. Scheme of nanopatterned pMHC with adhesive ICAM-1 background . . . 58
3.14. Protein deposition by an external device . . . 59
3.15. Atomic force micrographs of structured SU-8 resist I . . . 61
3.16. Illustration of density calculations . . . 65
3.17. Topographical atomic force micrographs and corresponding height profiles . . . 67
3.18. Particle occupation rate . . . 72

4.1. Fluorescence microscopy imaging of a calcium (Ca^{2+}) influx event of a T cell 77
4.2. IRM images of T cells on pMHC-presenting nanostructures . . . 80
4.3. SE micrographs of T cells on pMHC-presenting nanostructures . . . 82
4.4. T cell adhesion on nanopatterns . . . 85
4.5. z-stack fluorescent images of a T cell exhibiting a polarized MTOC . . . 86

4.6. Fluorescent images of T cells exhibiting a polarized MTOC 89
4.7. Index of activation over particle spacing 90
4.8. Index of activation over particle density 91
4.9. Index of activation over particle spacing: micro-nanopattern *vs.* nanopattern 93
4.10. Mean contact area of T cells on surfaces presenting ICAM-1 and/or pMHC . 95
4.11. IRM images of T cells on micro-nanopatterns 96
4.12. SE micrographs of T cells on micro-nanopatterns 97

5.1. Index of activation normalized by the percentage of adhesive cells 114

7.1. Transfer of Au nanopatterns to PEG hydrogels 123
7.2. Adhesion force dynamics of T cell/APC conjugates 125

List of Tables

1.1. Innate versus adaptive immune response 8

3.1. Types of diblock copolymers 60
3.2. Calibration of the dipping device 61
3.3. Parameter values for photolithography 62

4.1. Induction/inhibition of spreading on different surfaces 79
4.2. Induction/inhibition of MTOC polarization 87
4.3. Features of micro-nanopatterns 92

Abbreviations

2D	two-dimensional	27
3D	three-dimensional	46
AFM	atomic force microscope	46
APC	antigen presenting cell	8
Au	elemental gold	37
BCML	block copolymer micelle lithography	38
BCR	B cell receptor	12
Ca^{2+}	calcium	vii
CD3	cluster of differentiation 3	19
CD4	cluster of differentiation 4	12
CD8	cluster of differentiation 8	12
CD28	cluster of differentiation 28	19
CMC	critical micelle concentration	39
CO_2	carbon dioxide	81
c-SMAC	central supramolecular activation cluster	18
CTL-4	cytotoxic T lymphocyte antigen 4	23
CuAAC	copper(I)-catalyzed azide-alkyne cycloaddition	56
DUV	deep ultraviolet	48
DNA	deoxyribonucleic acid	12
d-SMAC	distal supramolecular activation cluster	20
ECM	extracellular matrix	27
EM	electron multiplying	70
EUV	extreme ultraviolet	48
FRET	Förster resonance energy transfer	30
GFP	green fluorescent protein	106
H_2	hydrogen	41
HA	hyaluronic acid	122

$HAuCl_4$ hydrogen tetrachlroaurate(III)trihydrate . . . 40
ICAM-1 intercellular adhesion molecule 1 . . . 18
IS immunological synapse . . . 17
IL-2 Interleukin-2 . . . 16
IFN-γ interferon-gamma . . . 16
IRM interference reflection microscopy . . . 78
LFA-1 lymphocyte function-associated antigen 1 . . . 18
MCC moth cytochrome C . . . 76
MHC major histocompatibility complex . . . 8
MTOC microtubule organizing center . . . 17
NK natural killer . . . 10
NTA nitrilotriacetic acid . . . 52
OR occupation rate . . . 55
PA polyacrylamide . . . 122
PALM photo-activated localization microscopy . . . 30
PDMS poly(dimethylsiloxane) . . . 122
PEG polyethylene glycol . . . 52
PKCθ protein kinase C theta . . . 19
pMHC peptide-loaded MHC . . . 13
PS poly(styrene) . . . 39
P2VP poly(2-vinylpyridine) . . . 39
p-SMAC peripheral supramolecular activation cluster . . . 18
RGD arginine-glycine-aspartate . . . 57
RICM reflection interference contrast microscopy . . . 78
SCFS single cell force spectroscopy . . . 124
SE scanning electron . . . 44
SEM scanning electron microscopy . . . 43
SLB supported lipid bilayer . . . 30
SMAC supramolecular activation cluster . . . 19
SPM scanning probe microscopy . . . 43
SPT scanning patterning tool . . . 69
STED stimulated emission depletion . . . 55
STORM stochastic optical reconstruction microscopy . . . 55
TCR T cell receptor . . . 10
TIRFM total internal reflection fluorescence microscopy . . . 30
UV ultraviolet . . . 49
VCAM-1 vascular cell adhesion molecule 1 . . . 57
VP vinyl-pyridine . . . 40

Part I.

Introduction

Chapter

1

Immunology

In 2011 the headline of the NY Times read "An Immune System Trained to Kill Cancer". What had come to pass? By a genetic modification doctors had transformed the patient's immune cells into selective cancer-killers resulting in the elimination of all malignant cells in the patient's body. Obviously, this successful attempt was astonishing news because for many decades physicians have been thinking of training the human's own defense system to fight disease. One of the most remarkable success stories of modern medicine, vaccination, is based on such a manipulation of the immune system. For 200 years, vaccines that make use of the immune system's memory effect have widespread and have helped to dramatically reduce infection-related diseases. The fascinating memory of the immune system, which prevents the host from coming down with the same disease for a second time, has already been known since ancient times. During the fifth century BC the greek historian Thucydides reported that only those who had already suffered from the plague[1] were able to have contact to and to nurse the recently infected persons. This means that for quite a long time there has been recognition of the phenomenon that a previous infection and recovery from certain diseases guaranties protection from falling ill again. Remarkably, there are indications that even before the plague of Athens, people from ancient China had already known that a targeted infection with a pox can serve as protection of further contagion. So, the first attempts of immunization were possibly done more than 2000 years ago. However, it was not until the end of 18$^{\text{th}}$ century that western physicians realized the high potential of immunity.

In 1798, Edward Jenner, an English physician reported that a little boy, to whom he had injected the harmless material from cowpox pustule was immune against the dangerous smallpox. This successful attempt to prevent humans from risky diseases resulted in a widespread acceptance of the vaccination and eventually, in one of the biggest successes of immunization campaigns in the 20$^{\text{th}}$ century, the eradication of

[1] The plague was a pandemic, which is known in literature as the *plague of Athens*. It took lives of approximately one quarter of the citizens of ancient Athens, however, until today it is not exactly clear which disease they were facing.

pox.

Nowadays, the term “immunology” not only denominates such effects which are used for immunization but covers a broad range of biomedical science dealing with the immune system of all organisms. It is applicable in several disciplines of medicine from the *classical immunology* including fields of epidemiology to the *clinical immunology*, which studies diseases caused by disorders of the immune system. In addition to that, *diagnostic immunology* uses the specificity of the bond between antigen and antibody in order to detect substances with a variety of analytic techniques. The *reproductive immunology* investigates interactions between the reproductive system and the immune system in order to understand fertility problems or pregnancy complications while the *immunotherapy* attempts to use components of the immune system to treat diseases.

The field of immunology has gained wide attention over the past decades, as it became obvious that a deeper comprehension of the human immune system is crucial in order to develop better treatments for any kind of disease. Not only to prevent people from illness through immunization but also to cure disease by teaching the immune system and letting it defend the host with its own methods. The advantage of such an approach is that side effects, which are caused by external medication that targets not only the pathogen but also healthy tissue, can be reduced or even entirely avoided. Moreover, the human’s own defense system is much more specific than any external substance or method that is applied in order to combat a disease. It is and keeps on being highly efficient since it remains in the body while drugs are cleared out.

Immunotherapy against cancer is one strategy, which has received considerable attention over the past decades, as illustrated by the successful attempt mentioned in the beginning paragraph. Until now, the most widespread method to cure malignant neoplasm is surgery in combination with chemotherapy based on cytotoxic drugs or radiation therapy. One major drawback is that patients are faced with heavy side effects of these therapies. Both chemotherapeutic agents and radiation not only destroy cancer cells but also severely harm the host’s healthy tissue. Furthermore, in case that cancer cells have already left the original tumor site and developed metastases the success of the mentioned therapies converges against zero. In contrast to such approaches, immunotherapy is theorized to reduce adverse effects by training and/or programming the patient’s own immune system in a way that it recognizes and destroys tumor cells scattered throughout the body, without damaging healthy cells. This idea is both simple and ingenious: Why not take advantage of the already existent defense system to combat mutated cells? Since this system is very specific, side effects can most probably be minimized and at the same time the efficiency is much higher than that of externally applied methods. The difficulty would “only” be instructing this system how to

precisely recognize the target.

Since there are many different types of cancer and multiple factors play a role an all-purpose medical treatment against cancer is very unlikely to exist. Until today there are basically three different approaches:

- a simple cancer vaccine can prevent the host from developing cancer.
- immune cells can be modified *in vitro* to target mutated cells
- therapeutic antibodies can recruit immune cells to eliminate malignant cells.

All these methods use the specificity and efficiency of the host's immune system to fight malignant cells. In future therapies a combination of such methods could help to dramatically minimize development as well as spreading of cancer.

A major break-through was the aforementioned immunotherapy recently reported by a research group around Professor Carl June at the University of Pennsylvania [1, 2]. Several patients were cured from leukemia using an *ex vivo* modification approach of immune cells: Doctors extracted T cells[2] of the patient's blood and using gene transfer technologies they modified T cells in such a manner that they expressed certain binding domains on their surface. Now, equipped with these new receptors T cells were able to specifically target and eliminate leukemia cells as soon as they were re-introduced into the patient's blood. Within the first days of the treatment patients showed very intense symptoms which were similar to symptoms of an influenza, for example strong fever and very low blood pressure. However, after a few days the fever was gone and astonishingly, so were the leukemia cells. It even turned out that the modified T cells were able to establish memory, which means that as soon as new leukemia cells appeared, they became eliminated. Such an approach of directing the immune response was theoretically developed some decades ago, however, it took some time before such a pioneering success was reported. Previously, methods had failed for various reasons: cells within the body did not replicate, they lost their specificity, they were not functional, they simply died or in the worst case they attacked not only malignant but also healthy cells. All these obstacles were apparently sufficiently overcome in the approach used by Professor June, even though it is not clear why and which circumstances made the approach being successful.

Considering the astounding news coming along even with this lack of clarity, it becomes obvious that much effort will be put into the further development of such novel methods. First of all a deep comprehension of the immune system, followed by a controlled guidance of the immune response is necessary to successfully establish im-

[2] T cells are a type of immune cells; for details see section 1.2.

munotherapy approaches. Therefore, exploring the human immune system will probably take up a major part of medical research in the 21st century. One fundamental part of this task is to develop a thorough understanding of the behavior of immune cells. Both chemical, as well as physical conditions influence cellular actions and in order to understand how cells function it is crucial to investigate their response within a controllable environment.

The intention of this presented research is exactly that: it applies artificial cell environments in order to explore the behavior and response of immune cells depending on different external conditions within a precisely controllable environment. It is widely known that a cell's surrounding plays a key role for their behavior and even determines cell fate. In the present study, we applied artificial cell environments which allow for a precise control over the nanoscale presentation of biomolecules. What are the needs in terms of the chemical and physical parameters to make immune cells function in the intended way and to drive them into a specific direction? Providing control over the micro- and nanoenvironment of a cell contributes on the one hand to elucidating fundamental questions regarding the way the immune response operates. On the other hand it explores opportunities of culturing and controlling the behavior of immune cells *in vitro*. New insights and expertise in both fields are essential requirements for the development of novel medical treatments that make use of the exceptional abilities of our immune system and could eventually initiate a new age of medical care.

1.1. The immune system

Physical health of the human body is not a matter of course but the result of a complex interplay of different strategies, which constantly try to protect the human body from any kind of diseases. This entire set of components and functional units interacting together in a very intelligent systematic manner is called the immune system. The collective and very well coordinated response of all cells and molecules constituting the immune system is denominated as immune response.

The immune system can be characterized by several attributes namely: specificity, diversity, flexibility, adaptability, complexity and memory; it is able to detect a wide variety of agents, from viruses to parasites and bacteria or infected and mutated host cells. It distinguishes them from the organism's own and healthy cells in order not to attack functioning tissue. Moreover, it is capable of establishing memory in order to react much quicker upon second contact with pathogens. Most of the components are cellular in nature and not associated with any specific organ but rather embedded or

circulating in various tissues located throughout the body. This omnipresence enables the system to act wherever it is required and that the response is not restricted to certain areas. Basically, action against pertubations can happen *via* two different subtypes of the immune system:

- the innate immune system
- the adaptive immune system

The innate immune system includes all the initial non-specific strategies which happen in a generic manner. Among these are for example physical and chemical barriers to pathogens or the recruitment of certain immune cells to sites of infection, using specialized chemical factors. Within several minutes the pathogens are detected and after some hours completely eliminated. The innate immunity is based on pathogen-specific receptors, which are already encoded in the genetic material, and can be found in all classes of plant and animal life. The genetic determination of the protein structure is responsible for the ability to react immediately, however, restricts flexibility [3].

Most of our infections are already entirely repelled by this first line of defense. In case that the innate system fails, the second line of defense, the adaptive immune system becomes active. It is unique to vertebrates[3] and in contrast to the innate system it is capable of adapting to harmful foreign elements that enter the body from time to time. Such an acquired response is said to be "adaptive" since it adapts to unknown threads and moreover, prepares for future challenges. Compared to the innate system it provides a stronger and long-lasting response including a memory function. Each pathogen which enters the body is "remembered" by a signature antigen and in case of re-infection the system is now able to react much faster and amplified than in the case of first contact. The basis of the adaptive system is the ability of immune cells, especially the so called T cells (see section 1.2), to distinguish between self antigens and foreign antigens, and therefore the adaptive response is said to be antigen dependent [3]. In Table 1.1 the main characteristics of the two different defense strategies are summarized.

1.1.1. Antigen

Antigen means *anti*body[4] *gen*erator and originally denominated any biological substance that specifically binds to the respective antibody. However, nowadays any molecule or molecular fragment which can be recognized by an antigen receptor is

[3] Vertebrates are species featuring backbones.
[4] An antibody is a large Y-shaped protein serving as marker in order to identify foreign substances.

Table 1.1.: Innate versus adaptive immune response (adapted from: http://nfs.unipv.it/nfs/minf/dispense/immunology/lectures/files/evolution_immunity.html)

	Innate	Adaptive
Self /non self discrimination	(✓) reaction against foreign	(✓) reaction against foreign
Immediate response	(✓) within minutes	(**x**) few days
Specifity	(**x**) limited, same response is mounted to a wide variety of agents	(✓) specific response to agents that initiated it
Diversity	(**x**) very limited	(✓) extensive, wide variety of antigen receptors
Memory	(**x**) subsequent exposures to agent generate same response	(✓) subsequent exposures to agent generate faster and amplified response

termed antigen. Most antigens are proteins or peptides but they might also be carbohydrates, lipids or any other material with the elementary attribute that antigen receptors are able to bind to them [3]. Antigens may originate either from the body itself or from any other external source. Accordingly, they are termed "self" antigens or "non-self" antigens, respectively. Non-self antigens can mainly be found on the surface of foreign substances which have entered the body such as bacilli or pollen, while self antigens are present on the surface of the body's own cells. Additionally, there are specialized immune cells which are able to present foreign antigens on their own surface to other immune cells in order to generate an immune response (see subsection 1.1.3). Moreover, if host cells are infected by viruses or in case of mutation they usually start to expose non-self antigens on their membranes. In general, self antigens are well tolerated by the immune system while non-self antigens are attacked, since they are identified as invaders from the outside or as any other harmful substance such as infected cells. Hence, the antigen is a very important indicator, by which the immune system is able to differentiate between "friend or foe" so to say.

1.1.2. MHC molecule

The presentation of any antigenic structure on a so-called antigen presenting cell (APC) surface happens *via* the so-called major histocompatibility complex (MHC) molecule. MHC molecules are cell surface proteins with an antibody-like Y-shaped structure.

They are members of the so-called immunoglobulin superfamily, which is a large group of cell surface and soluble proteins that are involved in the recognition, binding, or adhesion processes of cells.

Due to their antigen presenting function MHC molecules are also responsible for mediation of the interaction between two immune cells or immune cell and any other body cell and therefore, play a central role within the cell-mediated immunity [4, 5]. Until today three subgroups of the MHC gene family have been identified:

- MHC class I
- MHC class II
- MHC class III

The focus commonly goes to MHC class I and class II since these two molecules are responsible for antigen presentation [6]. They are either able to bind antigens by themselves (classic) or are at least somehow involved in the process of antigen presentation (non-classic). The MHC molecules class I and class II are characterized and distinguished by (see Figure 1.1):

- the origin of antigen which is presented by them
- the type of cell which is able to bind to them
- their chemical structure

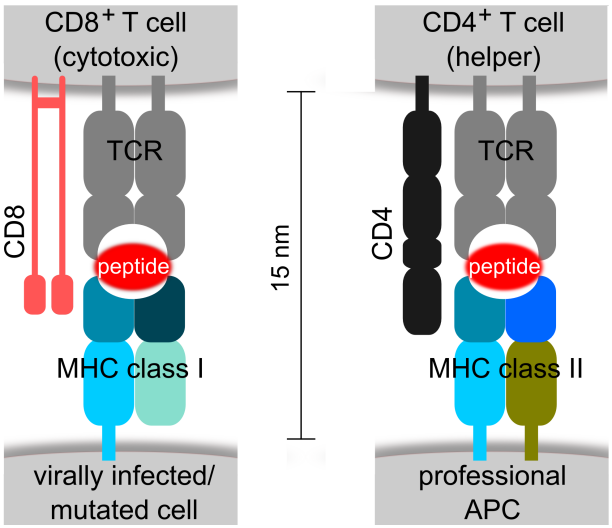

Figure 1.1: MHC class I and class II and their role as mediators during antigen presentation and recognition | Antigen presented *via* MHC I can be recognized by the TCR and the CD8 co-receptor which is expressed by primarily cytotoxic T cells while antigen presented *via* MHC II is recognized by the TCR and the CD4 co-receptor which is mainly found on helper T cells. According to their co-receptors, T cells are classified as $CD8^+$ or $CD4^+$ T cells. For further details see following sections.

With the help of classic MHC class I proteins intracellular antigens[5] are presented to $CD8^+$ T cells while by means of classic MHC class II molecules extracellular antigens[6]

[5]This can either be self antigen, non-self antigen from mutated cells or from pathogens (mainly viruses), which had entered the cell.

[6]Extracellular antigen includes all external harmful material which was purposefully ingested by the cell.

are presented to $CD4^+$ T cells (for details regarding $CD4^+$ and $CD8^+$ T cells see section 1.2).
Non-classic MHC class II are not expressed on cell membranes, but can be found in internal membranes and help to load the antigenic peptides onto classic MHC class II proteins. Through non-classic MHC class I molecules, cells are also able to interact with other immune cells, but for many of these molecules the binding partner remains unknown [5].

All nucleated cells of the human body express the MHC class I on their surface while the MHC class II are expressed only by certain types of cells. In the present thesis the classic MHC class II molecule whose binding partner is the so-called T cell receptor (TCR) (see section 1.2) of the $CD4^+$ T cells will be of interest.

To conclude, depending on the antigen in combination with the type of MHC molecule, specialized immune cells, mostly T cells, are able to differentiate between own/foreign substances or healthy/damaged tissue [3].

1.1.3. Antigen presenting cell

Most cells of the human body are able to present antigens on their surface loaded on MHC molecules and APCs can be split into two categories:

- non-professional APC
- professional APC

Non-professional APCs generally express only MHC class I molecules; however, some cell types, including fibroblasts or vascular endothelial cells, are able to express also the MHC class II protein, following stimulatory signals originating from certain cytokines. Cytokines are signaling molecules, which bind to a matching cell-surface receptor causing, among others, effects such as up- and/or down-regulation of several genes, production of other cytokines or expression of certain cell surface receptors [3].

In general, the presentation of antigen on MHC class I proteins is an indicator if cells are in a healthy state or not. Certain immune cells, predominantly cytotoxic T cells (see section 1.2), constantly check for foreign antigen on other cell's surfaces. In the case that their TCR detects some unexpected alien antigen presented *via* MHC class I, cytotoxic T cells destroy that cell immediately by inducing apoptosis, the programmed cell death [7].

Additionally, there is another strategy to recognize infected cells, which is still controversially discussed and seems to be incomplete: The so-called "missing self" or "altered self " which is part of the innate response. According to this hypothesis the natural

killer (NK)[7] cells which are able to detect harmed molecular structures within cells or tissue recognize such aberrant material not by 'presence of the unexpected' but by 'absence of the expected'. Upon discovery of host cells with low levels of MHC class I they start to attack and destroy such missing self cells. However, nowadays it is known that missing-self is one of several contributing elements in a delicate balance [8, 9].

Professional APCs are active members of the adaptive immune system. They posses the ability to endocytose[8] external antigen by professional APCs. Once inside the cell the adsorbed pathogen becomes processed into smaller fragments, normally peptides, which are then transported to the outside and loaded on MHC class II molecules [10]. Such peptides or antigens[9] feature a unique structure and hence, contain specific information about the internalized harmful object. Antigen presentation is required since antigens such as free viruses or bacilli do not stimulate T cells directly. Instead, APCs feature the specialized machinery required to efficiently activate naive/memory T cells (see section 1.2) upon contact formation due to antigen recognition. Antigen recognition occurs *via* the TCR and "informs" the T cell what kind of dangerous object or material is being present in the host [11]. This procedure usually takes place in the lymph nodes which are a kind of "meeting point" of professional APCs and T cells. Antigen detection and presentation by APCs is a very essential step to initiate a new/an established adaptive immune response [3]. Hence, conversely to antigen presentation of non-professional APCs, the purpose of presenting foreign antigen through professional APC is not to show that themselves are damaged or infected but to alarm and stimulate other immune cells in order to generate an immune response and immunological memory [3].

The most important professional APCs are:

- dendritic cells
- macrophages
- B cells

Dendritic cells pick up antigen at sites of infection as part of the innate immune response and then travel to lymphoid tissue in order to present the foreign antigen to naive T cells [12]. Macrophages are very versatile cells playing many roles. Their main

[7] NK cells are cytotoxic lymphocytes belonging primarily to the innate immune system. They are autonomous and do not need any additional information, stimulation or interaction in order to remove virally infected or abnormal cells which is why they were termed "natural" killer cells.
[8] Endocytosis denominates a cellular process by which substances are engulfed by cells.
[9] Note: Actually, only the part of a pathogen or toxic material which binds antibody or TCRs is termed antigen. However, in general linguistic usage both the original object as well as the small fragment is denominated as antigen.

function is to remove necrotic or apoptotic material but along with dendritic cells they are also involved in initiating an immune response by presenting antigen to T cells [13]. B cells are lymphocytes and according to their name they express the so-called B cell receptor (BCR). With the BCR they are able to recognize antigens in their native form, e.g. soluble antigen in the blood or lymph. Like dendritic cells they are able to process antigen and load it on MHC II molecules and thereby stimulate T cells. Besides antigen presentation, a major function of B cells is antibody production and evolution into memory B cells in order to establish immunity [14].

1.2. T cells

T cells are probably the most prominent members of the immune defense since they play a pivotal role in orchestrating the entire immune system. They are a type of lymphocytes and can be distinguished from other lymphocytes such as B cells and NK cells by expression of the TCR. With this receptor they are able to recognize foreign antigen displayed through MHC molecules on the surface of APCs . Unlike B cells or NK cells, they are not able to detect free antigen or antigen on the surface of the pathogen itself.

T cells develop out of haematopoietic stem cells[10] in the bone marrow and become committed to their lineage in the thymus. They have evolved sophisticated mechanisms for generating a diverse repertoire of TCRs relying only on a small set of genes. A genuine recombination system is employed which shuffles the deoxyribonucleic acid (DNA) of T cells and hereby creates a vast variety of unique receptors [15] enabling them to recognize millions of potential antigens. However, an individual T cell is not multi-sensitive but only specific to one individual antigen. Once fully developed, T cells enter the bloodstream and again leave it as soon as they reach a peripheral lymphoid organ. They migrate through the lymphoid tissue and re-circulate between that tissue and the bloodstream always scanning for antigens presented by APCs. As long as T cells have not come in contact with their specific antigen they are called naive T cells. Naive T cells are very important for the host since they guarantee that the immune system is able to respond to unfamiliar pathogens [3].

Before naive T cells are released to the thymus a selection process results in T cells which express either the co-receptors cluster of differentiation 8 (CD8) or cluster of differentiation 4 (CD4) on their surfaces[11]. CD8 and CD4 are crucial for binding the TCR to the MHC class I or class II molecule, respectively. Therefore, the type of

[10] Haematopoietic stem cells are those blood cells out of which all other blood cells originate.
[11] In the following “CD” always stands for “cluster of differentiation”.

receptor is a characterizing attribute of T cells and accordingly, they are divided into two major subgroups of T cells:

- $CD4^+$ T cells
- $CD8^+$ T cells

$CD8^+$ T cells are generally classified as having a pre-defined cytotoxic role since upon encounter of a specific antigen, which indicates malignancy, infection or some other damage of the APC, they start to kill this cell showing non-self antigen. There exists a high affinity between CD8 and the MHC class I molecule which keeps the cytotoxic T cell and the target cell closely bound together during antigen-specific activation and following elimination.

The main group among $CD4^+$ T cells are the so-called helper T cells. This type of T cell was used in the present study. The description "helper" indicates that they themselves do not directly eliminate any pathogens but possess a supporting function during the immune response. Helper T cells become activated as soon as their TCR detects its specific antigen loaded on a MHC class II molecule (peptide-loaded MHC (pMHC)[12]), expressed on the surface of professional APCs. Upon activation, they start to divide rapidly and secrete cytokines that regulate or assist in the active immune response. Cytokines can for example induce growth and activation of cytotoxic T cells, stimulate B cells and initiate antibody production or maximize the activity of phagocytes[13].

In general, $CD4^+$ as well as $CD8^+$ T cells that have detected their specific antigen and therefore, show cytokine releasing or cytolytic activities are no longer called naive but effector T cells [16]. The lifetime of naive T cells if not encountering their specific antigen is short and only lies within days [17, 18]. In contrast, the so-called memory T cells keep persisting a long time after an infection has been resolved (months to many years) [19]. They can be either $CD4^+$ or $CD8^+$ T cells and are considered to be "antigen-experienced" as having encountered antigen during a prior infection [20]. Upon further contact with familiar pathogens or other known harmful material they are able to respond much faster and stronger compared to the first contact [21]. In most of the times this quick reaction due to the established memory prevents the host of falling ill again, since the time period is not sufficient for the pathogen to replicate and seriously harm the body.

[12] In the following paragraphs the term pMHC will always refer to a MHC class II molecule loaded with a specific antigen (peptide).

[13] Phagocytes are cells which protect the body by ingesting harmful foreign material, bacteria, and dead or dying cells. Some types of phagocytes are professional APCs such as macrophages or dendritic cells.

One last important subgroup of T cells are the so-called regulatory T cells which maintain tolerance to self-antigen. They feature a function known as "self-check" which prevents excessive reactions by suppressing immune responses of other immune cells [22].

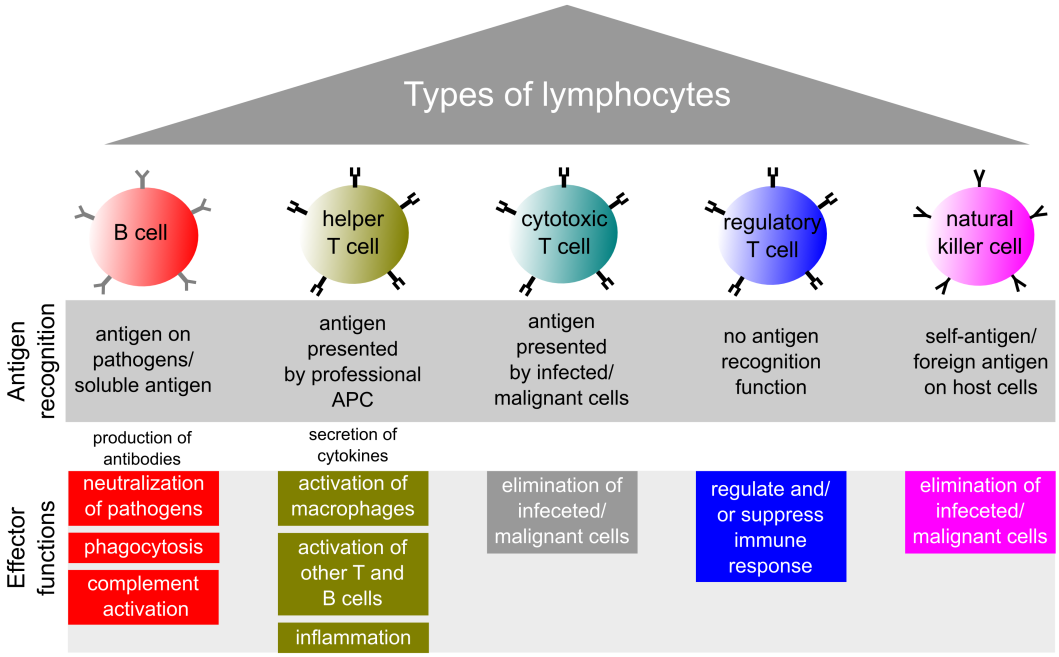

Figure 1.2.: Types of lymphocytes and their effector functions | The lymphocyte family includes five different immune cells: B cells recognize soluble antigen and pathogens and develop into antibody producing cells; Helper T cells recognize specific antigen on the surface of APCs, they get activated and start to induce further immune response processes; Cytotoxic T cells as well as NK cells recognize infected or malignant cells and eliminate them directly with the difference that NK cells only exhibit a very limited receptor diversity and are supposed to use a strategy which is known as missing self (see subsection 1.1.3); Regulatory T cells prevent an excessive immune response including actions against healthy tissue.

In Figure 1.2 all types of lymphocytes are summarized. As mentioned, B cells are mainly responsible for antibody production while most of the T cells constantly scan for material which is "labeled" with a certain antigen that has been recognized as a foreign/harmful substance. Upon encounter, some of the T cells directly try to destroy or neutralize this material or they at least attempt to induce an immune response by activating other cells of the immune system, which then will eliminate the harmful substances. Additionally, there are T cells trying to control the immune response in a way that the reaction does not exceed a certain necessary level.

Figure 1.3 summarizes the different types and strategies of the immune responses and their connections between each other. Immune response can be basically divided into the humoral immunity that is mediated by macromolecules (such as antibodies)

and the cell-mediated response, that does not include antibodies but rather different types of cells. Both types, the humoral and the cell-mediated immunity are part of the innate as well as adaptive immune system.

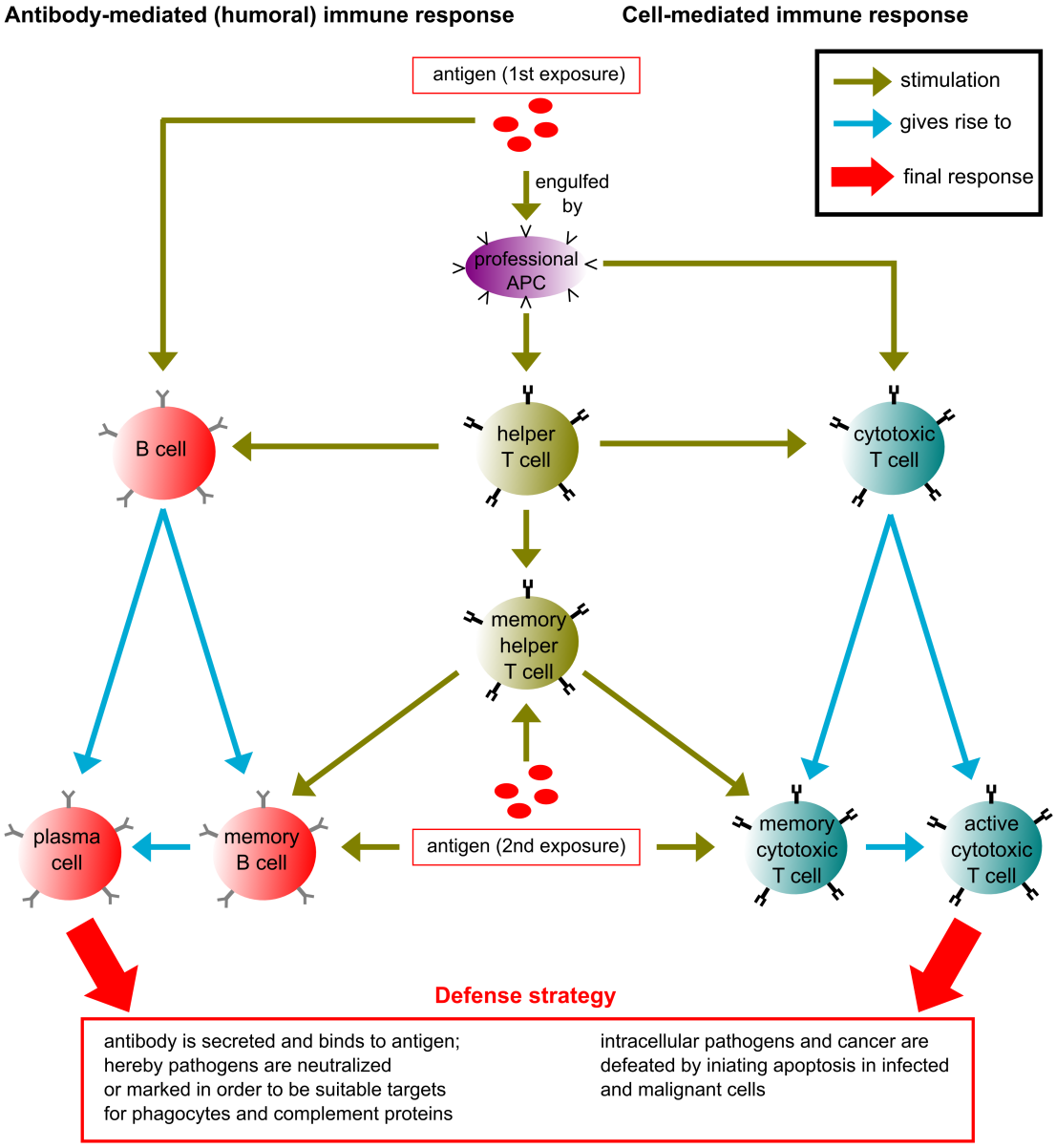

Figure 1.3.: Summary of the immune response | (Adapted from: Biology by Campell and Reece 2008 Pearson Education, Inc. [23] and lecture about the immune system at the University of Illinois, Chicago (http://www.uic.edu/classes/bios/bios100/lectures/immune.htm).

1.3. T cell activation

A key feature of antigen specific T cells is their extraordinary ability to recognize a very small amount of foreign antigens (sensitivity) incredibly quick within an enormous amount of surrounding self-pMHC (selectivity) [24]. They are able to differentiate between non-stimulating and stimulating pMHC complexes even though the difference between these can be only a single conservative amino acid change. Moreover, the recognition happens on the fly, since cells only brush past each other at high velocities. Only upon detection of a specific peptide a temporary stable cell-cell contact starts to form (see section section 1.4) which eventually results in the activation of the T cell including several further events.

T cell activation in general denominates any stimulation of T cells by their specific antigen. This can be naive T cells which have never been in contact with antigen and upon first contact turn into effector T cells, or memory T cells which encounter corresponding antigens and start to induce a fast and effective immune response against such familiar pathogens. Stimulation of naive T cells, often denominated as "priming", turns $CD8^+$ into cytotoxic T cells capable of directly killing pathogen-infected cells, while stimulated $CD4^+$ T cells develop into a diverse array of effector T cells depending on the additional types of signals which they obtain during priming [16]. In most cases they develop into helper T cells secreting signaling molecules and alerting other immune cells through:

- stimulation of B cells in order to induce antibody production
- inducing growth and proliferation of other T helper cells in order to enhance the response
- stimulation of cytotoxic T cells or macrophages, which eliminate the pathogen
- transformation into memory T cells

The stimulation of other cells can either happen through a direct cell-cell contact, i.e. formation of a synapse (e.g. between T and B cell) or *via* cytokines such as the growth factor Interleukin-2 (IL-2) or interferon-gamma (IFN-γ), which stimulates other T cells or macrophages, respectively.

The whole procedure of antigen presentation and subsequent activation of a T cell is shown in Figure 1.4 and runs as follows: the first step is the uptake of foreign material by a professional APC which becomes processed in the inside of the APC, then transported to the outside and loaded on MHC class II molecules in order to present it to T cells. The stimulation of T cells always starts with the recognition of

such an antigen presented by the APC. As soon as the TCR of the T cell detects some "suspicious" material the T cell gets a signal to arrest [25], followed by a Ca^{2+} influx [26, 27]. A cytoskeletal remodeling event polarizes the T cell's microtubule organizing center (MTOC) to a position just beneath the cell-cell interface in order to establish a stable junction at the interface [28] initiating the full activation during this time-limited intercellular contact between T cell and APC [29, 30]. This contact formation is a complex process in which many surface molecules assemble into a highly ordered, spatially structured pattern (see following section 1.4) [31]. The formation of the mature immunological synapse (IS) takes between 10 – 15 min (for primed T cells) and ≈ 30 min (for naive T cells), although the cell-cell connection can last up to several hours [32, 33]. Subsequently, the freshly activated T cell loosens its contact and again starts to migrate through the body thereby inducing a variety of immune responses including for example proliferation, differentiation or stimulation of other immune cells. The process of establishing an IS between T cell and all the involved components and signals have been subject of extensive research over the last two decades due to its central role in adaptive immunity.

1.4. The immunological synapse

In general, a synapse is a specialized structure that forms between two cells and functions as a signal transmitter, site of adhesion and recognition [34]. Immediately, the long lasting synapse between neurons comes to mind; however, cells of the immune system also form intercellular junctions, which are more transient than neuronal connections but nevertheless structured and essential for the immune response. The formation of a synapse between immune cells is a relatively new (≈ 20 years) discovery but it quickly turned out that this early step of contact formation is of immense importance for the subsequent immune response. Therefore, and because of its relevance to the presented project, this section will shortly depict the discovery of the IS and the current state of knowledge.

The term "synapse" denominating the intercellular junction of T cells and professional APCs was first used by Norcross in 1984 [35]. Ten years later Paul and Seder described an "immunological synapse", which forms between a T cell and a B cell and revived the the term synapse regarding the temporary connection of immune cells. They found several molecular interactions and speculated that some of these may function mainly to strengthen the adhesion of the APC and the T cell, but others clearly provide important co-stimulatory signals [36]. In 1998 Abraham Kupfer and his col-

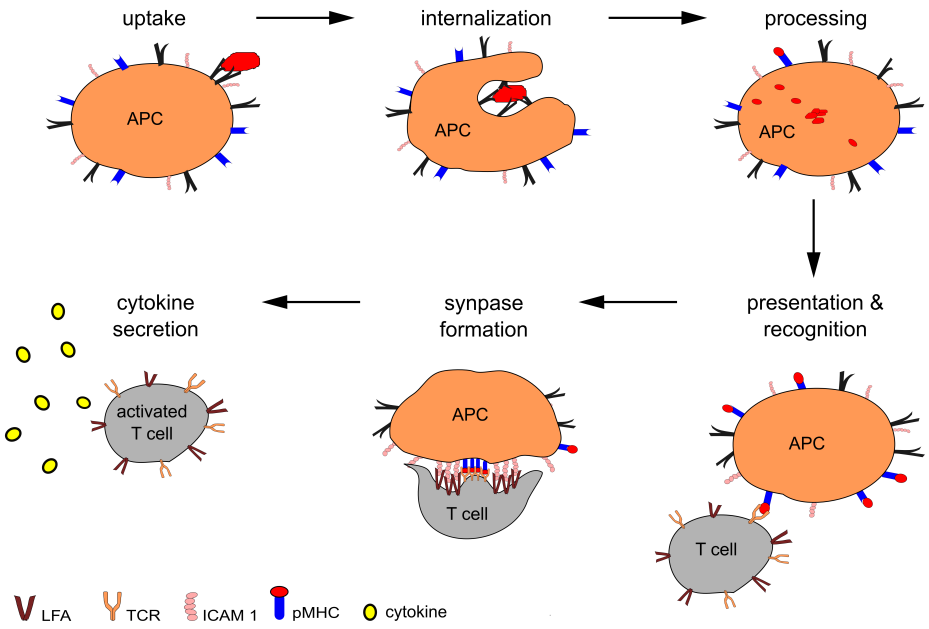

Figure 1.4.: Procedure of antigen processing, presenting, recognition and synapse formation | A professional APC internalizes foreign material and generates peptides out of such pathogen derived proteins (processing). These peptides are then loaded onto MHC molecules on the APC surface (presentation) where they can be identified by the TCR of the T cell (recognition). Upon recognition of a pMHC cells start to form a temporary intercellular junction between each other (immunological synapse formation), persisting up to several hours. Subsequently, the connection is separated and the T cell starts to migrate and secrete signaling molecules in order to induce further immune response.

leagues from the National Jewish Medical and Research Center in Denver were the first who reported the detection of activating receptor clusters within the contact zone of both cells [29]. They described two distinct spatial domains, which was a central region, termed central supramolecular activation cluster (c-SMAC) surrounded by the peripheral supramolecular activation cluster (p-SMAC). This pattern is typically referred to as a "bull's eye" structure. They proposed the c-SMAC to be the area of TCR ligation and the surrounding "doughnut" to be a stabilizing region where especially the integrin lymphocyte function-associated antigen 1 (LFA-1) binds to its specific ligand intercellular adhesion molecule 1 (ICAM-1). Eventually, the term IS describing this highly molecular structured intercellular junction between T cell and APC was coined by Michael Dustin, Professor at the University of New York. He and his co-workers confirmed and extended the findings of Monks et al. [30]. They proposed the IS to be a molecular machine which controls T cell activation and suggested a three step model for the formation process (see Figure 1.5) consisting of:

- junction formation

- pMHC transport
- stabilization

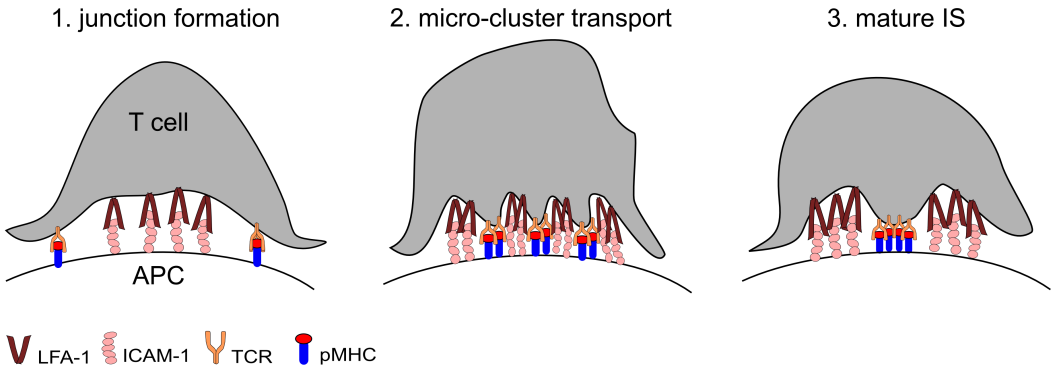

Figure 1.5.: Three step model for immunological synapse formation | Side view of T cell forming an immunological synapse with an APC. 1.) Junction formation: LFA-1 anchors the central region of the nascent immunological synapse, providing a fulcrum for cytoskeletal protrusive mechanisms that force an outermost ring of T cell membrane into close apposition with the substrate. This allows TCR sampling of pMHC complexes. Early signals from the TCR and CD4 stop migration. 2.) pMHC transport: This step happens within minutes and Grakoui et al. speculated that this is mediated by actin-based transport mechanisms. 3.) Stabilization: The clustered pMHC complexes are "locked-in" (Taken from [30]).

From then on it was clear that this highly structured arrangement of certain molecular bonds and the resulting signaling processes play a crucial role during the process of T cell activation. A diversity of functional roles have been attributed to the IS such as biophysical support [30], controlled extinction of signaling [37, 38], a conduit for directed exchange of cytokines [39, 40] or a specific site for receptor signaling [41]. However, despite intensive research, many details and factors controlling synapse formation, dissolution and its exact function are still unclear and understanding the immunological synapse remains one of the major challenges of current immunological research [42, 43].

1.4.1. Architecture of the immunological synapse

The mature IS consists of well-defined, concentric peripheral and central supramolecular activation cluster (SMAC)s [29–31, 44, 45] and is depicted by a "bull's eye structure" (see Figure 1.6). The major components of the central cluster are complexes involved in signaling processes such as pMHC – TCR bonds, cluster of differentiation 3 (CD3) and cluster of differentiation 28 (CD28) or the protein kinase C theta (PKCθ), which are all expressed by the T cell and function as co-stimulatory signaler [46, 47]. Both,

CD3 and CD28 are transmembrane proteins but while CD3 is directly connected to the pMHC – TCR bond, CD28 binds to other surface molecules expressed by the APC such as CD86. PKCθ is selectively expressed by the T cell and interacts with several other molecules inducing further signals essential for full T cell activation and cytokine production. In contrast to the c-SMAC, the periphery is considered to mainly stabilize the whole structure through adhesion molecules such as the T cell's integrin LFA-1 and its counterpart ICAM-1 or the T cell adhesion molecule CD2 binding the ligands CD48 or CD59 on the APC surface [30, 31, 45, 48]. Several years after the discovery of those two spatially distinct domains researchers proposed a third concentric ring encircling the periphery. The distal supramolecular activation cluster (d-SMAC) was detected to contain large extracellular domains such as the signaling molecule CD45 [49] or CD43 [50–52]. This distal region was thought to be responsible for maintaining sustained TCR signaling, however the formation of the d-SMAC may not be essential for full T cell activation [53].

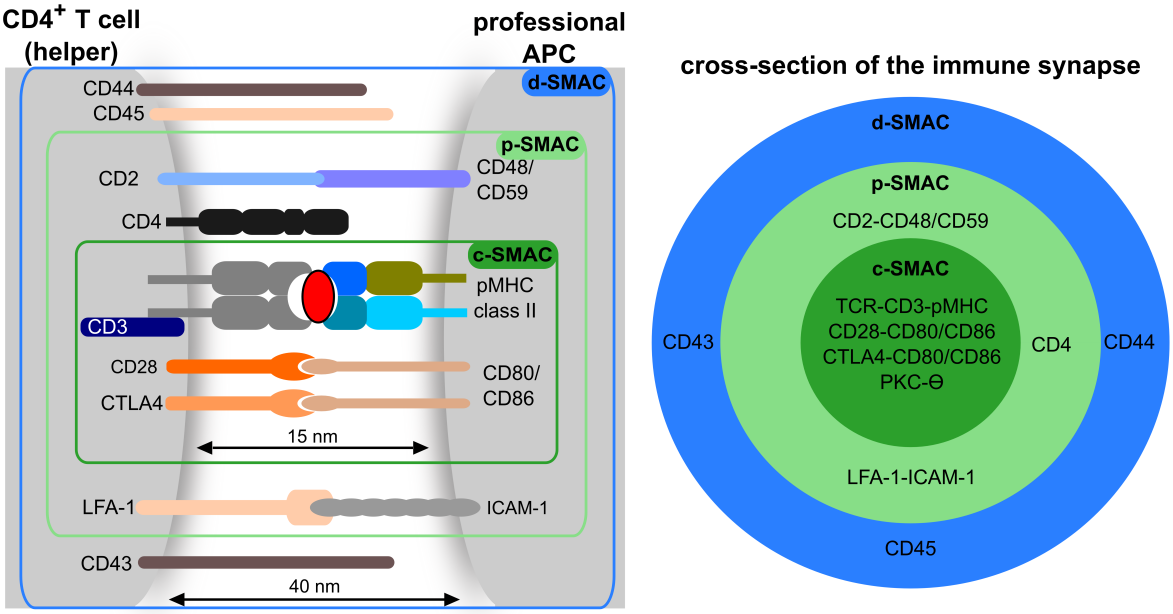

Figure 1.6.: The architecture of the immunological synapse | Left side: Side view cross section of the different involved molecules and molecular bonds within the molecular synapse; Right side: Cross section from above showing the architecture of the immune synapse with its different regions and receptors [31].

Besides such a "model" synapse a variety of other patterns and different stages of receptor clustering have been observed [54, 55]. For example, immature T cells show dynamic multifocal synapses [56, 57] and dendritic cells have been reported to lack a d-SMAC [53] but exhibit multifocal synapses in the c-SMAC [58, 59]. Furthermore, the interaction between T cell and APC is not only a stable connection but rather a

continuos change from only temporary stable to transient states. For instance, imaging of lymph nodes *in vivo* suggests that T cells seem to interact with the APCs by forming ISs and also immunological kinapses, respectively. In contrast to the IS the immunological kinapse is only a brief contact during which small accumulations or microclusters of TCRs are produced. For example, $CD4^+$ T cells and dendritic cells can form stable multifocal ISs or only transient kinapses, both producing Ca^{2+} flux and eventually resulting in a proliferative response. Hence, it seems that not only stable but also transient T cell/APC connections can induce T cell activation and consequently, the IS would appear not to be an absolute requirement for full T-cell activation [53, 60].

1.4.2. Discussing synapse formation and T cell activation models

Until today, the role and the development of the mature IS regarding the activation of T cells is still not entirely understood; neither how individual early chemical and physical cues are translated into further activation events and how they impact the formation of a mature IS, nor to which extent the mature synapse has to build up in order to completely activate a T cell.

For instance, there is evidence that the composition of the IS depends on the cell type and that T cells can get fully activated without forming an entirely developed synapse but rather multifocal structures [58]. The time course of cSMAC formation does not match early signaling events such as tyrosine phosphorylation or Ca^{2+} influx [57]. Thus, immediate recognition and/or clustering events are considered to be the major initiators for further signaling cascades. Different initial conditions result in diverse substructures; for instance, different protein densities lead to different supramolecular structures like diffuse receptor clustering, multifocal or nanoscale clusters of receptors at the interface. And in turn, the distinct structures can result in distinct responses of the T cells in terms of cytokine secretion or proliferation and differentiation [55, 56].

A variety of components and actions were proposed to have influence on the development of the IS and could explain the high sensitivity of T cells to antigen combined with the apparent immunity to stochastic noise. It is widely accepted that upon detection of a specific antigen presented on a MHC molecule, TCR crosslinking causes the multimerization of TCR – CD3 complexes and induces further activation related events [61]. Several reports have theorized that at first, the physical-chemical properties of pMHC – TCR interactions such as affinity [62, 63], dissociation rate of the complex [64], or association rate [65] determine TCR crosslinking and T cell response [66, 67]. Two major models suggest the equilibrium dissociation constant K_D [68] or the off-rate k_{off}

[69] to be the decisive parameters: K_D describes the sensitive number of pMHC – TCR complexes at equilibrium, k_{off} the duration of the interactions. However, due to the difficulty of observing pMHC – TCR interactions directly within a real IS, correlations between ligand potency and binding parameters are difficult to determine [70].

To some extent, high resolution microscopy could recently contribute to shed light on the interaction kinetics between the TCR and the pMHC on the molecular level [70]. For example, it has been reported that synaptic pMHC – TCR binding dynamics (measured between $CD4^+$ T cells and synthetic surfaces) differ significantly from binding in solution, such that affinity was much higher in synaptic conditions (association rate 100-fold higher, while dissociation rate only 4 – 12-fold higher) [71]. Imaging of the initial contact period of T cells with synthetic surfaces has revealed that detection of antigen and pMHC – TCR bond formation occurs within seconds after antigen encounter, followed by initiation of an active cell spreading within minutes [72].

The initial detection of agonist peptide and the following clustering events of pMHC – TCR complexes can be regarded as one of the most crucial parts during synapse formation. T cells carrying the CD8 receptor have been reported to become stimulated by as few as 10 – 50 pMHCs [73, 74] and perhaps even fewer [75], to initiate cytotoxicity, whereas $CD4^+$ T cells are thought to require 40 to 400 ligands [76–78]. However, Irvine et al., for example, suggested that even a single pMHC – TCR bond may trigger a transient Ca^{2+} influx and that only 10 pMHC molecules lead to characteristic synapse formation between $CD4^+$ T cells and live APCs [79] emphasizing the discrepancy of findings. More recent studies propose numbers of pMHC – TCR bonds ranging from four to 300 for the minimal microcluster unit mediating initial and also sustained TCR signaling [33, 80, 81]. Such incipient clusters develop as transient structures at the immediate contact area and are sequentially formed at new contact regions during cell spreading. The number of microclusters per cell is reported to be around 100 – 300 [82], each of them composed out of very few up to 300 TCRs. After maximal spreading they translocate in an actin-dependent process with time towards the center of the interface forming the c-SMAC [33]. The appearance of TCR microclusters correlates with the onset of intracellular Ca^{2+} flux, an indication for T cell triggering [81, 82]. This led to the conclusion that the microclusters, rather than larger features of the immune synapse, are centers for signaling activity [83]. Nowadays, such initial cluster formation is regarded as an essential step towards T cell activation and microclusters seem to be able to mediate both initial as well as sustained TCR signaling [83].

According to Yokosuka and Saito the activation of T cells would be induced by two spatially distinct signaling compartments: first, a TCR signaling by the microclusters in the periphery and second, a co-stimulation through the c-SMAC where the TCR

microclusters become enriched with co-stimulatory molecules such as CD28 [84]. At the late phase they propose an accumulation of cytotoxic T lymphocyte antigen 4 (CTL-4)[14] in the cSMAC competing with CD28 resulting in an eventual blocking of signaling [85]. CTL-4 would therefore act as an "off" switch down-regulating T cell stimulation. The same mechanism is also known to regulate the activity of cytotoxic T cells [86] being the reason for the terming of CTL-4. The whole procedure is displayed in Figure 1.7 and for further details see the review *"Receptor signaling clusters in the immune synapse"* [83].

Besides the almost self-evident, contributing factors like binding affinities between the pMHC and the TCR, a variety of further elements are believed to play key roles during the process of T cell activation. Wulfing et al. found MHC molecules loaded with endogenous peptide to overtake a co-stimulatory role [87], confirmed by Hailman and Allen who additionally, found a helper role of the CD4 molecule [88]. Such a "self help" would be an explanation for the fact that only very low numbers of foreign pMHC molecules are required for T cell stimulation but at the same time a significant higher amount of TCR–MHC bonds assembles into micro clusters. Moreover, within such TCR clusters an extensive cooperativity among multiple receptors is implicated [89] and may result from conformation-induced clustering [90], kinetic segregation [91], or lipid-mediated assembly [92].

Several models have been suggested to explain the well coordinated transformation into a structural molecular pattern of the mature IS. Historically, the first reports proposed that molecules at the T cell/APC interface segregate according to size, with small "accessory" molecules, such as CD2 and CD4, contributing to the formation of a close-contact zone, within which the TCR engages pMHC, and from which large molecules, such as LFA-1 and CD43 are excluded [93]. This hypothesis was supported by trying to stimulate T cells with elongated MHC molecules which led to abrogation of T cell antigen recognition, emphasizing the importance of molecular sizes for T cell activation [94]. The pattern segregation is assumed to occur due to effects of membrane bending energy combined with receptor–ligand binding/diffusion equilibria [95], however, active transport of receptor clusters to the c-SMAC mediated through the cytoskeleton has also been reported to occur [96]. Until today, the cytoskeleton has come to be regarded as a main player for the construction an maintenance of the synapse. It seems responsible for shaping and remodeling the cell and eventually provides a scaffold for signaling components [97]. It is involved in active diffusion of participating ligands and integrin clustering [98] as well as in force generation and mechano-sensing processes [48, 99] within the IS. As a logical consequence, the Young's

[14]CTL-4 is a protein receptor of T cells responsible for down-regulating immune response.

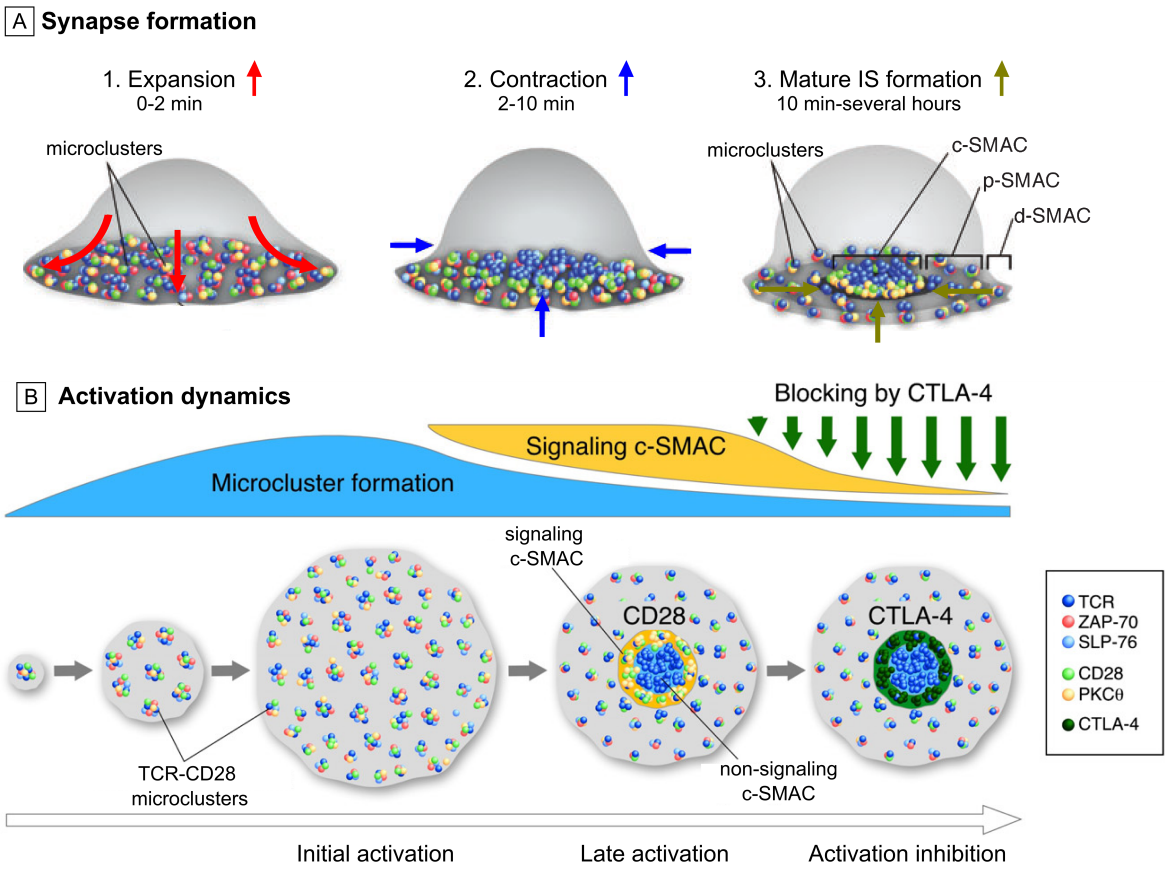

Figure 1.7.: Dynamics of immunological synapse formation on planar lipid bilayers A) 1.) Upon settling a T cell on a lipid bilayer presenting pMHC, ICAM-1 and CD80 starts to form TCR – CD28 microclusters; 2) After reaching full expansion the T cell starts to retract and microclusters accumulate in the central region fusing with other receptors; 3) Approximately 10 min later the immunological synapse with its three distinct regions has formed; D) Detection of pMHC results in formation of TCR – CD28 (containing also other T cell surface membrane proteins such as Zap-70 and SLP-76, or the protein kinase PKCθ) microclusters and induce early signaling. The microclusters move towards the center generating the c-SMAC and inducing sustained co-stimulation signals. At the late phase accumulation of CTLA-4 in the central region leads to inhibition of activation by pushing CD28-PKCθ out of the cSMAC (adapted from [84, 85]).

modulus of an activating substrate might influence T cell activation and in turn the elasticity of an APC would impact the stimulation process [100]. There is multiple evidence that integrin-ligand interactions are mechano-sensitive [101] and Hosseini et al. could show that the development of adhesion forces due to integrin-ligand interaction between a T cell and an APC correlates well with the dynamics of synapse formation [102]. Moreover, it has been demonstrated that surface-anchored pMHC triggers the TCR much more effective than soluble antigen [103], raising the question whether the TCR is force sensitive. This finding was further confirmed by Li et al., who showed that external physical forces acting on TCR – anti-CD3[15] complexes can trigger TCR signaling by inducing a conformational change [105].

Until today a detailed physical description of the signaling reactions within TCR microclusters and the IS remains largely incomplete. Much needs to be learned about the exact impact of the immediate, very rapid and sensitive antigen detection process and the influence of binding dynamics and affinities on downstream signaling and following activation related events. Furthermore, the fact that T cells may react to very few individual agonist peptides and at the same time maintain such extreme sensitivity without spontaneous triggering in the absence of foreign antigens has still not sufficiently been resolved. A key to many previous findings was the ability to manipulate TCR cluster assembly in living T cells. For this purpose synthetic APC-mimicking surfaces have become an essential support to ultimately determine, and experimentally verify, the molecular mechanisms of TCR triggering and the subsequent IS formation. Presumably, in future research they will further confirm their crucial role for establishing a complete picture of the intriguing process, T cell activation.

[15] Anti-CD3 binds to the TCR – CD3 complex and hereby induces T cell activation. Stimulating T cells by means of anti-CD3 is a common and well-established method in immunological approaches [104].

Chapter

2

Biomimetic substrates for biological studies

Culturing cells on synthetic substrates is a widespread method in cellular research since artificial cell environments provide possibilities, which would be impossible to accomplish under *in vivo* conditions. For example, only planar two-dimensional (2D) synthetic surfaces mimicking APC surface conditions, allowed for the discovery of the IS. Using such biomimetic substrates the molecular arrangement of the synaptic pattern and the dynamics of IS formation could be optically accessed. At the same time they provided control over biomolecular composition of the T cell/APC interface and hence, allowed for altering conditions the T cells were confronted with.

In general, a wide variety of artificial cell environments haven been used since many decades to study the behavior of cell. Within organisms, most cells are dynamically interlinked to their extracellular neighborhood and therefore, the parameters of the surrounding have quickly come into focus of researchers. Cells sense and respond to both physical as well as chemical characteristics [101, 106] and multiple environmental cues such as elasticity [107–109], topography [110, 111], anisotropy of the adhesiveness [112] or molecular composition [113] can influence their morphology, dynamics, proliferative behavior and often decide over cell fate. This phenomenon is based on a rich range of sensory mechanisms and is widespread in almost every cell type.

Considering this outstanding impact of the extracellular matrix (ECM) on cellular function it becomes obvious why biomimetic substrates have gained wide attention over the past decades. Nowadays, the control of environmental parameters through the artificial ECM is an integral component of biological research as it determines the success of cell culturing methods, allows for addressing a variety of unanswered questions, and moreover, allows for exploring and directing cellular behavior. Especially, for investigation of the IS synthetic substrates have proven to be a indispensable part of research, and accompany immunologists since they started to explore the contact formation of immune cells.

2.1. Artificial cell environments

Research regarding many cellular processes, such as adhesion, stimulation or cell death requires at best a fully controllable environment. Explicitly that means control over parameters that are expected to affect the studied cellular process; obvious ones such as temperature and humidity, and others like composition of the culture media or chemical and mechanical properties of the micro- or nano-environment [114]. While temperature or media composition are comparatively easy to adjust, the physical appearance of the environment within cellular dimensions remains challenging to control. Intensive research was done to develop synthetic ECMs which mimic *in vivo* conditions by precisely adjusting environmental parameters like substrate compliance, density and orientation of biomolecules [115, 116] or certain structural dimensions [117].

In recent years, the development of structures, substrates and controlled operations in the nano- and micrometer regime has accelerated more and more and has strongly contributed to the development of novel synthetic cellular environments. The micro- and nanotechnology has discovered new interesting effects and materials such as quantum dots [118], photonic crystals [119] or nanotubes [120] and one of the biggest impulsion is the speculative vision of tiny electronic devices using atoms as minimal unit, such as quantum computers [121, 122]. Even though the bio-medical, bio-physical, bio-molecular and tissue-engineering research had not been primarily connected with this field of research they also benefitted from it: novel microscopy techniques and new materials consisting of a broad diversity of components e.g. nanofibers [123], polymers [124] or supported lipid bilayers [125, 126]. This variety of new materials exhibiting many different characteristics started to serve as platforms for cellular research and cell culture. Additionally, the ability to pattern and arrange bioactive proteins in a desired manner within the micro- as well as nanometer regime opened the door for creating and designing a cell's environment in dimensions which are of relevance for a cell. It is now possible to systematically explore cellular behavior on an adequate length scale and at the same time monitor processes with the help of new imaging technologies.

The surface patterning techniques, which have appeared during the last 50 years use either bottom-down, denominating the directed deposition of molecules by an external device or bottom-up approaches, including primarily the controlled self-assembly of molecules [127]. These technologies opened the door to the sub-cellular space and a control of the cellular environment was suddenly possible. The opportunity of defining molecular patterns with nanometer accuracy in combination with control over matrix rigidity, topography or matrix actuation resulted in a wide spectrum of artificial cellular micro- and nano-environments which have been used to study effects on cell

adhesion [101, 128, 129], dynamics [130], apoptosis [131], activation [30, 54, 132, 133], proliferation[100, 134], differentiation [113, 135–138] and have made a major contribution towards understanding how cells function.

Furthermore, a cell's environment is of high importance not only in terms of basic research but also when culturing and expanding cells *ex vivo*. For several medical approaches such as generating artificial tissue [139–141], controlled differentiation of stem cells [142, 143] or immunotherapy [144–146] harvesting and growth conditions remain a major challenge. In all cases the environmental characteristics of the cell's surrounding play a crucial role and eventually determine the success of the method. For example, growing synthetic tissue needs scaffolds providing stability and certain structural dimensions, mechanical properties and proper chemistry in order to ensure molecular bio-recognition and make cells replicating and assembling the intended way [147–151]. Above all, immunotherapy requires methods to quickly expand cells, to keep them functional, to modify or to activate them *ex vivo* in order to create a strong immune response when re-introduced into the patient [152–154]. Hence, providing the cell with an appropriate environment is an essential step towards the positive outcome of both novel medical approaches as well as fundamental research, as presented in this thesis.

2.1.1. Artificial antigen presenting cell systems

A strategy to study biological phenomena like the activation of T cells is to engineer APC analog systems, which, at best, deliver all essential physiological signals required for the appropriate stimulation of the T cell. Since receptor crosstalk and clustering of receptors was shown to be important for the formation of the synapse [83], and in turn for activation of T cells, the chemical composition, including also the ligand arrangement of the APC must be well-controllable and precisely adjustable. Moreover, regarding for instance immunotherapy, a large number of therapeutically potent T cells are required. Synthetic APCs can function as a substitute to expand and activate them since such systems constitute a more general and effective ready-to-use approach compared to any live APC. Functional live APCs are difficult to obtain and culturing and expanding them *in vitro* is very costly and time-consuming. Because of these reasons, during the past decade much effort has been put into the development of synthetic APCs presenting ligands of interest to the receptors of the T cell, as schematically exemplified in Figure 2.1. Such novel artificial cell substitutes provide research platforms for exploring T cell behavior as well as culture platforms for expanding and directing immune cells *in vitro* [109].

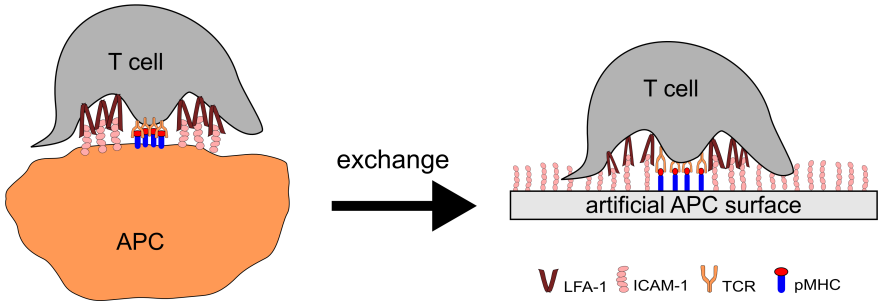

Figure 2.1.: Substituting the APC | A synthetic 2D surface replaces the APC surface by presenting crucial biomolecules and is capable of stimulating T cells.

Until today, 2D synthetic APC substrates have proven to be a fundamental part of research strategies, attempting to gain a deeper comprehension of cellular processes like synapse formation or assessing T cell behavior in terms of proliferation, differentiation, functionality, and activity, among others. With a view to the experimental set-up, 2D model APC surfaces have several advantages over real APCs:

- The contact formation between the T cell and model surface is restricted to a quasi-2D plane, which is important for monitoring events occurring during antigen recognition and IS formation *via* optical microscopy. The variety of high-resolution imaging techniques such as total internal reflection fluorescence microscopy (TIRFM), photo-activated localization microscopy (PALM) or fluorescence microscopy in combination with Förster resonance energy transfer (FRET) require a planar thin surface for imaging. In combination with synthetic stimulating surfaces these techniques have been able to provide exciting new insights into the earliest events of T cell activation, including TCR assembly as well as organization and kinetics of the IS [71, 155, 156].

- Key parameters such as ligand/antigen density and molecular composition or rigidity of the APC can be adjusted in order to systematically examine their effects on IS formation and T cell activation [30, 31, 54, 99, 100, 157].

- Several micro/nano fabrication techniques feature high patterning resolutions and are able to create surfaces allowing for control of the density, orientation and mobility of ligands presented to the T cell [80, 158, 159] and for arrangement of ligands in a structured fashion within sub-cellular dimensions [115, 160–162].

As already mentioned in section 1.4 Grakoui et al. were the first who successfully monitored IS formation of T cells induced through a synthetic 2D surface. They utilized a model of glass-supported lipid bilayer (SLB) featuring mobile pMHC molecules plus

adhesion proteins as surrogate for a live APC. With such an approach they were able to follow the dynamics of receptor clustering and assembly of molecules into the c-SMAC and p-SMAC [30].

Since then SLBs have been widely used to mimic the conditions of an APC membrane as molecules are presented in a quasi-directed manner and are able to diffuse freely within the 2D space [71, 103, 157, 163]. Additional sophisticated lithographic methods enabled to create SLBs featuring physical barriers in the micrometer-scale [80, 158]. Such partitioned bilayers provide locally mobile ligands but at the same time confined to a micrometer-sized area. This strategy of motility in combination with confinement allowed to examine T cell response in terms of local microcluster assembly (see Figure 2.2). Researchers found that multifocal structures are stable connections since clusters remained for the whole time period of cell-surface contact within their spatially-restricted area and were not able to cross obstacles and migrate towards the center. They report the minimal microcluster unit, which is able to induce Ca^{2+} signaling to consist of 4 pMHC molecules. This number was independent of inclusion of non-stimulating pMHC molecules, but co-stimulation by CD28 modulated the threshold lower. The significance of such SLB platforms is emphasized by the various findings gained out of experiments using such APC analogs, as summarized in [54, 157, 164, 165]:

- the typical shape of the IS
- the molecular composition of the IS
- the role of co-stimulatory molecules
- the dynamics of receptor binding and IS formation
- several estimations of minimal molecular requirements for stimulation of T cells and
- assembly of stable microclusters inducing TCR triggering

A major feature of SLBs is the lateral mobility of presented molecules, which can to a certain extent mimic the condition of diffusing molecules in a real cell's membrane. However, SLBs, even in combination with lithographic methods, fail to provide insight into nanoscale organization of clusters and the IS. Questions regarding spatial arrangement of proteins or minimal/maximal dimensions of the synaptic pattern are therefore, difficult to address. Recently, another strategy came up, which directly patterns molecules on solid substrates and utilizes such pre-defined patterns as substitute for the APC. Dimensions and molecular arrangement can be precisely defined prior to the activation and cells are not able to change the conformation of ligands during the experiment. In 2006 Doh and Irvine were the first who pre-patterned the shape of

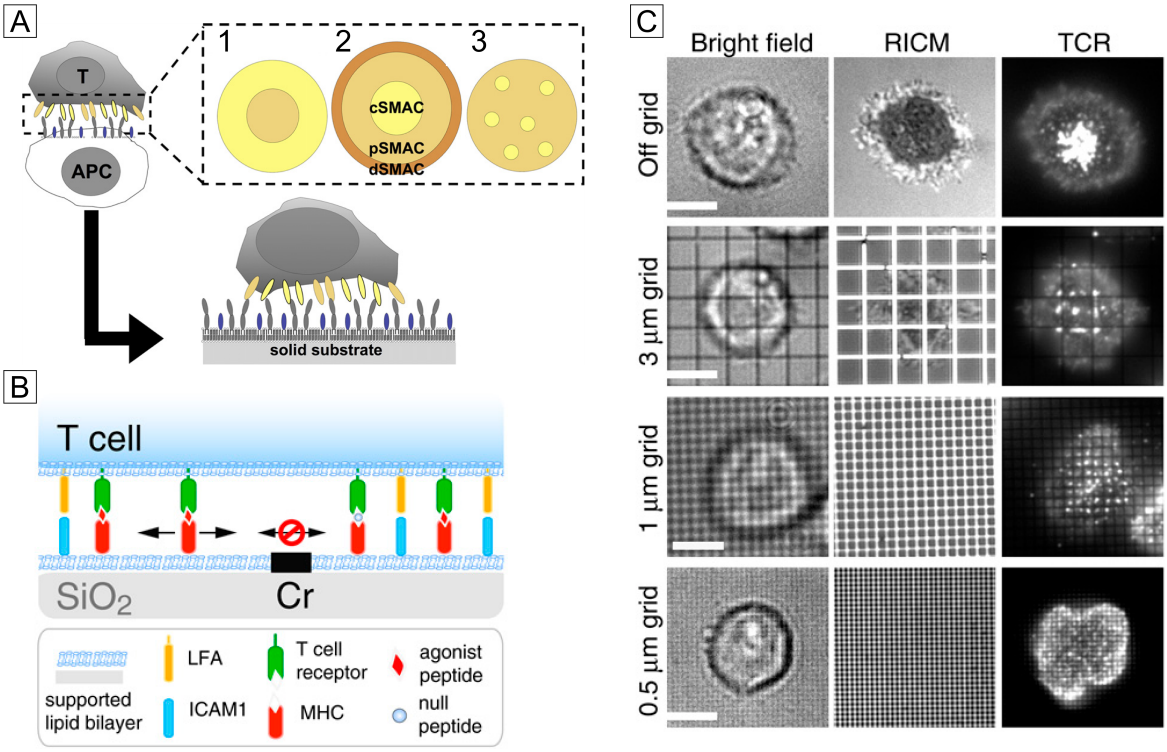

Figure 2.2.: Synapse formation on supported lipid bilayers | A) Replacing the real APC by a lipid bilayer featuring laterally mobile stimulating molecules. The immature (1) inverts into a mature (2) synapse composed of the different spatially confined supramolecular activation clusters (SMACs). Depending on the status of the T cell and type of APC other patterns such as multifocal clusters (3) may form (*en face* view). B) Schematic of experimental strategy: MHC and ICAM- 1 are presented to the T cell through functionalized patterned SLB membrane. MHC is preloaded with an appropriate ratio of null (non-stimulating) and agonist peptide. Chromium (Cr) lines prefabricated on the glass function as diffusion barriers to all lipids and lipid-tethered proteins. C) Bright field, reflection interference contrast microscopy, and TCR distribution on lipid bilayers bearing metal lines (5 nm high, 100 nm wide) forming a grid with different dimensions (off grid, 3.0, 1.0, and 0.5 µm side partition grids) after 5 – 10 min of contact with the surface. The number of pMHCs per corral is restricted and determines the number within a cluster, whereas the number of TCR per cluster is not limited. Four pMHC molecules per grid box was found to be the minimum number of pMHCs necessary to induce TCR clustering. (Scale bar: 5 µm) (adapted from [54, 80]).

the synapse in micrometer dimensions on solid substrates [159]. They applied a photolithographic method to create different shapes of activation sites presenting anti-CD3 surrounded by the adhesive ligand ICAM-1 (see Figure 2.3) and primarily focused on the influence of shape and dimensions of the synapse disregarding number and density of molecules. T cells stably interacted with these focal activation sites, proliferated,

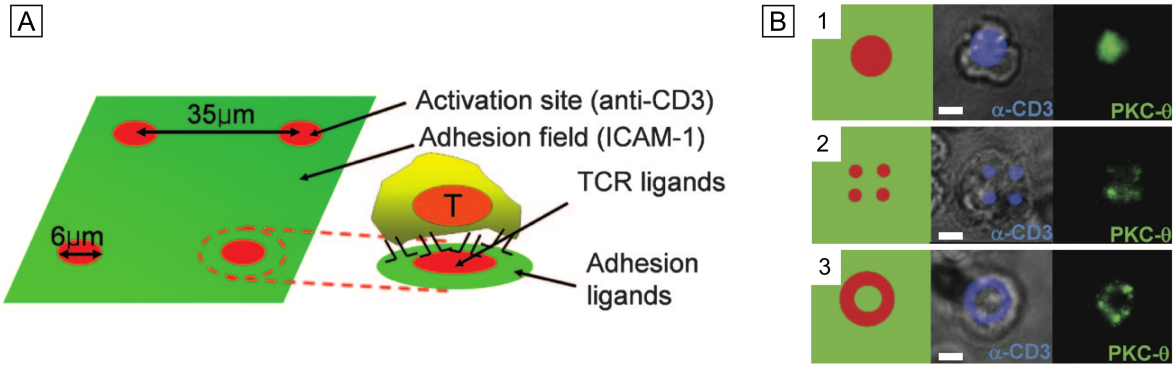

Figure 2.3.: Stimulation of T cells by synapse array patterns | A) Schematic drawing of immunological synapse array surface pattern. Different shapes of activation sites (anti-CD3) surrounded by adhesive ligands (ICAM-1); B) Schematics of different anti-CD3 substrate patterns and representative immunofluorescence images of anti-CD3 (blue) and of PKC-θ (green) at the cell-substrate contact plane. PKC-θ assembles according to the activation sites and represents the underlying anti-CD3 pattern (taken and adapted from [159]); (Scale bars 5 µm).

and secreted cytokines. In contrast, T cells interacting with activation sites patterned to preclude centralized clustering of TCR ligand failed to form stable contacts with activation sites, exhibited aberrant PKC-θ clustering, and had significantly reduced production of the cytokine IFN-γ. As a consequence, the authors concluded that centralized TCR clustering may be required for full T cell activation. With this first trial in which researcher used inalterable "synapse-like" patterns, they could show the high potential of such an approach. However, they were not able to provide insight into the nanoscale organization of receptors and their corresponding ligands, either.

In the next part a high-precision surface patterning technique will be introduced. This intriguing approach is capable of precisely arranging functional biomolecules with nanometer accuracy and can create biomimetic substrates for T cell activation studies at the sub-cellular level. There is lot of evidence that, due to their role during the immune response, T cells are extremely sensitive in terms of arrangement and density of stimulating biomolecules. Having control over molecular densities and their arrangement is therefore, a very important requirement and a major step towards a better understanding of this rather new field of research. Especially with regard to future medical therapies artificial cell environments, and in this case artificial APCs will be of

great importance during *ex vivo* expansion and activation of immune cells in order to eventually have control over the immune system, hereby supporting or even creating intended immune responses while at the same time inhibiting unwanted reactions.

Part II.

Substrate Fabrication

Chapter

3

Micro- and nanopatterned antigen arrays as substitute for the APC

Since the APC plays a key role in terms of T cell activation, a synthetic APC, or in general, a synthetic cellular environment whose parameters are well controllable, is an essential requirement for the success of cellular research. This chapter focuses on the micro- and nano fabrication of APC analogs which can serve as model system to activate T cells in a controlled manner. The organization of receptors in the cell membrane during activation occurs at the molecular level. Therefore, an activation platform which is able to present stimulating ligands with nanometer accuracy is a valuable tool in order to gain information about the complex process of receptor organization, cluster formation and requirements in terms of ligand arrangement. As the recognition of antigen is probably the most essential step for the subsequent activation, we aimed to present the T cells defined stimulatory arrays of pMHC featuring nanometer resolution. Moreover, we focused on presenting TCR ligands only within micro-domains, in order to provide a platform for investigating TCR cluster formation in detail.

All processes, which fabricate nanoscale structures, i.e. patterns with at least one lateral dimension between the size of an individual atom and approximately 100 nm, are collectively denoted as nanolithography. There are two major concepts scientists follow to create structured micro- and nanometer-sized features, the top-down and bottom-up approach. Top-down technologies structure the surface from above by an external device while the bottom-up procedure takes advantage of molecules which self-assemble or grow self-organized on the surface into preassigned patterns. In this work, both methods are part of the fabrication procedure, which was applied in order to create arrays of antigens featuring sub-cellular resolution. We employed a nanolithographic technique based on self-assembly of macromolecules to create periodic patterns of nanometer-sized elemental gold (Au) particles and additionally, a standard photolithography technique to add a superior structure to the self-assembled pattern. Such nanoparticle arrays serve as template in which each individual particle functions as an anchor point for the

selective binding of biomolecules. The final substrates feature periodic antigen patterns with structural dimensions in the micro- as well as nanometer regime. These patterns were employed as synthetic APC analogs, with which ligand distribution could be precisely defined. They constitute an ideal platform, which allows for regulation of the number and nanoscale arrangement of proteins that impact TCR triggering and other aspects of T cell activation.

3.1. Block copolymer micelle nanolithography

The technique used for creating structures in nanometer regime is a bottom-up technique, the so-called block copolymer micelle lithography (BCML). In general, bottom-up approaches utilize molecular components, which build-up into a complex assembly due to single-molecule interactions. The final desired structure is already programmed in the shape and functional groups of the molecules [166, 167]. Bottom-up techniques are usually able to produce devices in parallel processes in contrast to most top-down approaches which apply serial processing steps. Consequently, patterning of surfaces by self-assembly of molecules is generally much cheaper and faster than any top-down method, but could potentially be over-strained as the size and complexity of the desired assembly increases [168]. Nevertheless, a large variety of different patterns were reported [127, 169] and in the notional vision of molecular nano-technology, microchips of the future might be made by molecular self-assembly [170].

The method presented in this work utilizes the self-organization of micelles (see subsection 3.1.2) formed out of diblock copolymers (see subsection 3.1.1). Such micelles are deposited on the surface of solid substrates by dip- or spin-coating creating highly ordered, periodic patterns in the nanometer regime [171].

3.1.1. Block copolymers

Block copolymers are derived from at least two different blocks of polymerized monomeric species[1]. The monomers cluster together and form blocks of repeating units featuring different chemical and physical properties. Due to the distinct blocks, they can have several interesting characteristics, which can be amphiphile[2] or high-temperature resilience and at the same time low-temperature flexibility, among others [172, 173]. Furthermore, their shape and size are easy to tune by changing the molecular weight

[1] A monomer denominates a small molecule that may become chemically bonded to other monomers to form a polymer.

[2] Amphiphile describes a characteristic of a chemical compound, which has both hydrophilic (water-loving; polar) and lipophilic (fat-loving; non-polar) properties.

and composition of the building blocks that lead to a variety of block copolymers varying in architecture, solubility and functionality [174]. Due to their size, they are particularly suitable for creating periodic structures in the nanometer space since final pattern-dimensions correlate one-to-one with the dimensions of the block copolymers.

In this project, amphiphilic diblock copolymers consisting of two covalently bound and chemically distinct polymer coils, a polar and a non-polar, were used. As the chemistry of the two blocks is distinct, in polar/non-polar solutions the two blocks tend two segregate into two micro-domains, held together by a covalent bond [175]. The segregation occurs as a consequence of the reduction of the area between the two phases to minimize the interfacial energy. The length scale of this micro-separation is restricted to the molecular dimension of the blocks. In our case, amphiphilic characteristics of a non-polar poly(styrene) (PS) and a polar poly(2-vinylpyridine) (P2VP) block were utilized to induce aggregation into uniform inverted micelles in organic, non-polar solvents [176]. For details regarding the different diblock copolymers which were used in this study see Table 3.1 in the experimental section (section 3.4.1) of this chapter.

3.1.2. Micelle formation

Micelles are aggregates of surfactants[3] consisting of a hydrophilic head and a hydrophobic tail group, which form in colloidal dispersions. Micelle formation is initiated above a certain concentration of surfactants, the so-called critical micelle concentration (CMC). In polar, aqueous solutions surfactants form an aggregate with the hydrophilic head regions in contact with the surrounding solvent, sequestering the hydrophobic tails in the micelle center, whereas in non-polar solvents the situation is reverse resulting in the formation of so-called inverse micelles.

For our purpose, the diblock copolymers were dissolved in the non-polar solvent toluene resulting in the formation of spherical inverse micelles above a certain concentration threshold. As shown in Figure 3.1 the PS blocks (indicated in blue) form a shell around the less soluble P2VP blocks (indicated in red) facing into the middle of the spherical micelle [176]. The reason behind this behavior is the minimization of the system's free energy [175]; the hydrophobic part tends to stay in contact with the toluene, whereas the hydrophilic part minimizes the contact area with the environment in order to reduce energetically unfavorable interactions with the solvent. The diameter of micelles is mainly determined by the molecular weight of the block copolymers and additionally, but to a lower extent, by the interactions between the individual polymer blocks and the blocks with the solvent [176, 177].

[3]Surfactant is a coinage and means surface active reagent.

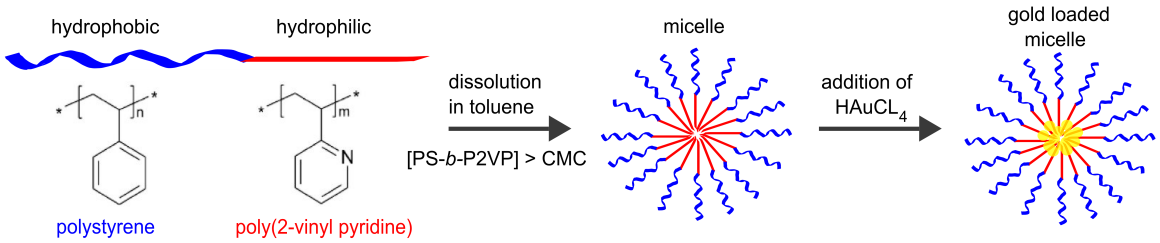

Figure 3.1.: Process of micelle formation | From left to right: Linear diblock copolymer consisting of a polystyrene and a poly(2-vinyl pyridine) block; above a certain CMC polymers assemble into inverse micelles; a metal precursor hydrogen tetrachlroaurate(III)trihydrate ($HAuCl_4$), which is added to the micelle solution accumulates in the center of the micelles (adapted from [178]).

If a metal precursor salt, such as $HAuCl_4$, is added to an inverse micelle solution the compound accumulates in the polar P2VP core due to its low solubility in the toluene and the interaction with the P2VP blocks. The amount of Au in the micelles is of interest for the following work, since it determines the final size of the Au nanoparticles on the substrates [171] (see subsection 3.1.3). The size of nanoparticles determines the success of binding strategies since we aimed to present approximately one biomolecule per particle. If size of particles is too high, more than one molecules are able to bind, and in contrast, if size is too small, binding of molecules is inhibited.

Quantification of the Au "loading" can be done according to Equation 3.1:

$$L = \frac{n}{m} \tag{3.1}$$

The loading parameter L denominates a theoretical measure of the nominal number of precursor salt molecules per vinyl-pyridine (VP) unit. It is defined as the ratio of neutralized (due to the addition of $HAuCl_4$) VP units (n) versus the total number of VP units (m) [176]. Such an incorporation of metal precursor salt shifts the thermodynamic equilibrium between free polymer chains and assembled micelles towards the latter and decreases the CMC at the same time [179].

3.1.3. Fabrication of nanopatterns by the self-assembly of micelles

Micelle organization on flat substrates can be used as a bottom-up approach to obtain small structured features. Coating of a surface with a micelle solution results in evaporation of the solvent, and a subsequent assembly of micelles into a hexagonally arranged monolayer. In this work conventional glass slides were used as solid support and coating with a monolayer of micelles was achieved through dipping the substrates into the micelle solution and retracting them with a defined velocity (see Figure 3.2). A

previous cleaning procedure with piranha solution[4] hydroxylized[5] the sample surfaces and rendered them extremely hydrophilic. The subsequent coating with a monolayer of micelles was realized by means of a custom made dipping device, featuring a very sensitive stepping motor and therefore, capable of slightly retracting the glass slides out of the solution with a defined velocity v. Upon retraction, capillary forces create a meniscus at the solvent-air interface. The solvent starts to evaporate leaving behind sole micelles which assemble on the surface into a hexagonal pattern [176, 179].

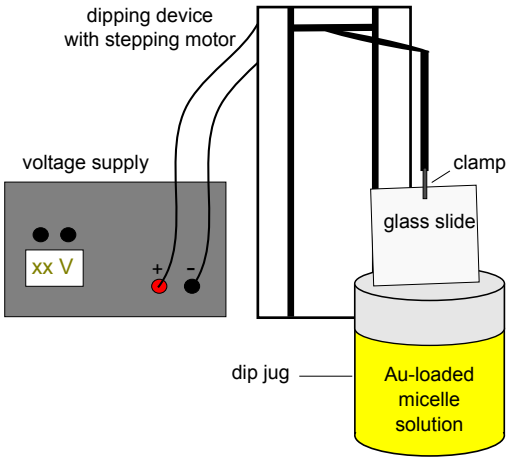

Figure 3.2: Dipping device | A clean and hydroxilized glass slide is dipped into a micelle solution and upon retraction micelles assemble on the surface. The clamp is driven by a stepper motor allowing for the precise adjustment of the retraction speed.

In general such an assembly can be described as a two step process: (i) nucleus formation governed by attractive lateral capillary forces appearing between particles which are partially immersed in a liquid layer and (ii) crystal growth through convective particle flux caused by the solvent evaporation [180–182]. Likewise, the spherical micelles show such a behavior: The 2D crystallization is achieved by solvent evaporation at the interface and capillary forces pack the micelles into a hexagonally arranged mono-micellar film on the surface [177]. These reasons eventually result in the assembly of micelles into a quasi-hexagonal pattern (see Figure 3.3). The density of such a micelle monolayer on the substrate depends on several factors:

- the molecular weight of the polymer shell [171]
- retraction velocity
- velocity gradient [183, 184]
- concentration of polymer in solution [185]
- the solvent properties such as polarity, viscosity, surface tension and temperature [186].

[4]Piranha solution is a mixture of sulfuric acid (H_2SO_4) and hydrogen (H_2) peroxide (H_2O_2). It is a strong oxidizing agent and therefore, removes most organic matter very efficiently.
[5]Hydroxilization means the addition of OH^- groups onto the surface.

Since the size of the Au nanoparticles is mainly determined by the amount of precursor salt per micelle it can be slightly adjusted by the amount of $HAuCl_4$, thus the loading paramter L. However, it is restricted by the size of the hydrophilic part of the block copolymer. By using polymers with different chain lengths the distance between the particles can be varied [171, 177]. In addition, the retracting speed impacts the density of the micelle monolayer, and thus, the interparticle spacing. A higher density (lower particle distance) follows from a higher speed and vice versa [182, 187], since a greater retraction velocity results in the retraction of more fluid and consequently, more micelles assemble on the surface.

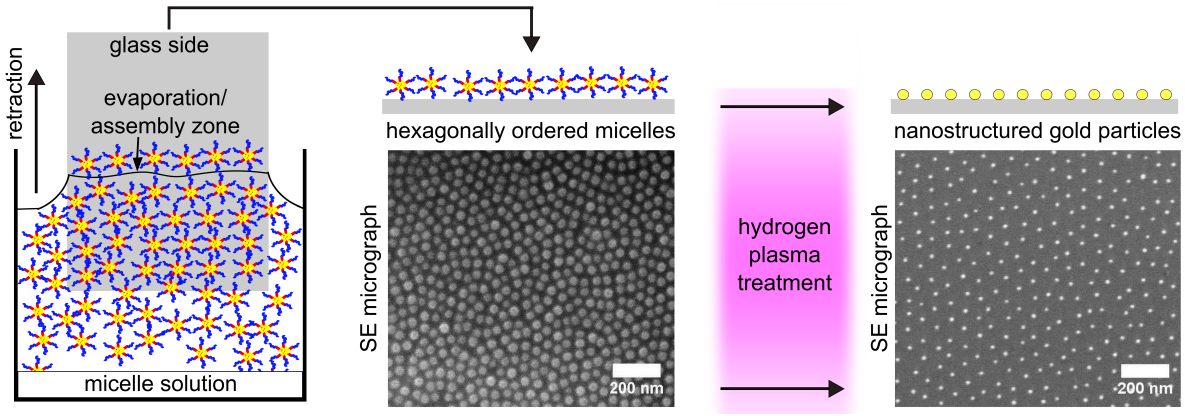

Figure 3.3.: Nanopatterning process | From left to right: A hydrophilic glass slide is retracted from a micelle solution. Micelles assemble into a hexagonal pattern at the solvent/air interface on the surface. A subsequent H_2 plasma removes the polymer shell and leaves pure Au nanoparticles on the surface. The nanoparticles are arranged in a quasi-hexagonal pattern. The average distance of particles depends on the diameter of the micelles, the concentration of micelles in solution and the retraction speed.

Finally, a H_2 plasma treatment removes the polymer shell of the micelles and at the same time $HAuCl_4$ becomes reduced to Au generating spherical Au nanoparticles.

3.1.4. Pattern analysis

Likewise the nanoparticle distance, the quality of the resulting hexagonal pattern, in terms of regularity, including degree of distance variation between individual Au particles, depends on several factors:

- the molecular weight of the polymers [188]
- the retraction velocity [182, 183]
- concentration of the polymer (micelles) in solution [188]

- properties of the solvent like polarity, surface tension, viscosity and temperature [186].

As the lateral structure dimensions of the patterns are in the nanometer range, advanced characterization methods such as scanning electron microscopy (SEM) or scanning probe microscopy (SPM) are required. Two parameters are of major interest: (i) the inter-particle distance and (ii) the particle size. The particle distance and the variety of the pattern regularity was determined by SEM, whereas the particle size by SPM.

Analyzing patterns with the scanning electron microscope

SEM is able to visualize surface topography and even chemical composition with submicrometer resolution and moreover, provides insights into other properties such as electrical conductivity. The surface of a sample is raster-scanned with a focused high-energy beam of electrons. The measured signals result from interactions of the electrons with atoms at or near the surface of the sample surface. Similarly to light microscopy the radiation generates a signal contrast between an object and the surrounding surface. The advantage of SEM is that the wavelength of electrons is much smaller than that of visible light, entailing a much better resolution since the wavelength correlates with the resolution. The wavelength of an electron depends on the acceleration voltage: For example when assuming a typical acceleration voltage of $U = 3000\,V$, the wavelength of the electron is approximately 22.4 pm. Even higher acceleration voltages up to 30 kV are possible and the theoretically resolution achieved with electrons is at least four orders of magnitude higher than the resolution of visible light.

The interaction of the beam with the substrate generates a variety of different signals depending on the nature of the sample and the energy of the electrons affecting the penetration depth. Primary electrons hitting the surface can be reflected by elastic scattering (backscattered electrons) or they can cause ionization of atoms on the surface resulting in low energetic secondary electrons. The secondary electrons originate from the outer shell of an atom hit by either a primary or a backscattered electron. Depending on their energy electrons are classified either as a primary or a backscattered ones and in general, electrons with an energy less than 50 eV are considered as secondary electrons. In most cases electrons are generated by a field emission cathode and then become accelerated by a strong electron field. A set of magnetic and electrostatic lenses focuses the beam to a diameter between 5 and 0.5 nm, before hitting the sample.

The average particle distance and their respective deviations were quantified by ana-

lyzing scanning electron (SE) micrographs with ImageJ[6] an image processing software and a special plugin[7]. In principal this works as follows:

1. image processing enhances the contrast of the Au nanoparticles
2. the image is transformed into a 8 bit grayscale binary image
3. a minimal pixel threshold processing neglects all irregularities
4. the positions of the Au nanoparticles are localized
5. the pattern is compared with an ideal hexagonal pattern (six nearest neighbors are determined)
6. distances between adjacent particles are determined and
7. mean inter-particle distances and deviations are calculated.

In Figure 3.4 pattern images of the different procedural steps are shown.

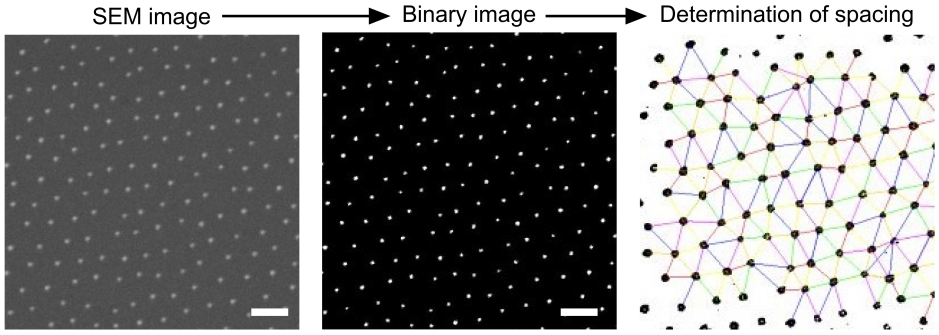

Figure 3.4.: Determination of inter-particle distances | From left to right: A SE micrograph becomes transferred into a binary image and then the software determines the distances between adjacent nanoparticles through delaunay triangulation (for details see subsection 3.4.2; Scale bar: 100 nm).

In addition to the average particle distance, the so called global bond-orientation order parameter $0 \leq \Phi \leq 1$ was determined. Originally, this parameter was introduced to characterize structural order in two dimensional systems such as crystallites melting in colloidal suspensions [189]. This parameter enables to quickly assess the quality of the lattice: a value of 1.0 indicates an ideal hexagonal pattern and the smaller Φ becomes, the more the arrangement deviates from such a perfect hexagonal pattern. This, in turn means, the smaller Φ the larger is the error of the mean interparticle distance (for further explanations of pattern analysis see subsection 3.4.2 in experimental section).

In Figure 3.5 SE micrographs of Au nanopatterns featuring different average inter particle distances are shown. Using different polymers and distinct retraction velocities we were able to cover distances ranging from approximately 30 nm to 300 nm.

[6]Rasband, W.S., ImageJ, U. S. National Institutes of Health, Bethesda, Maryland, USA; http://rsbweb.nih.gov/ij/

[7]by courtesy of Philipp Girard

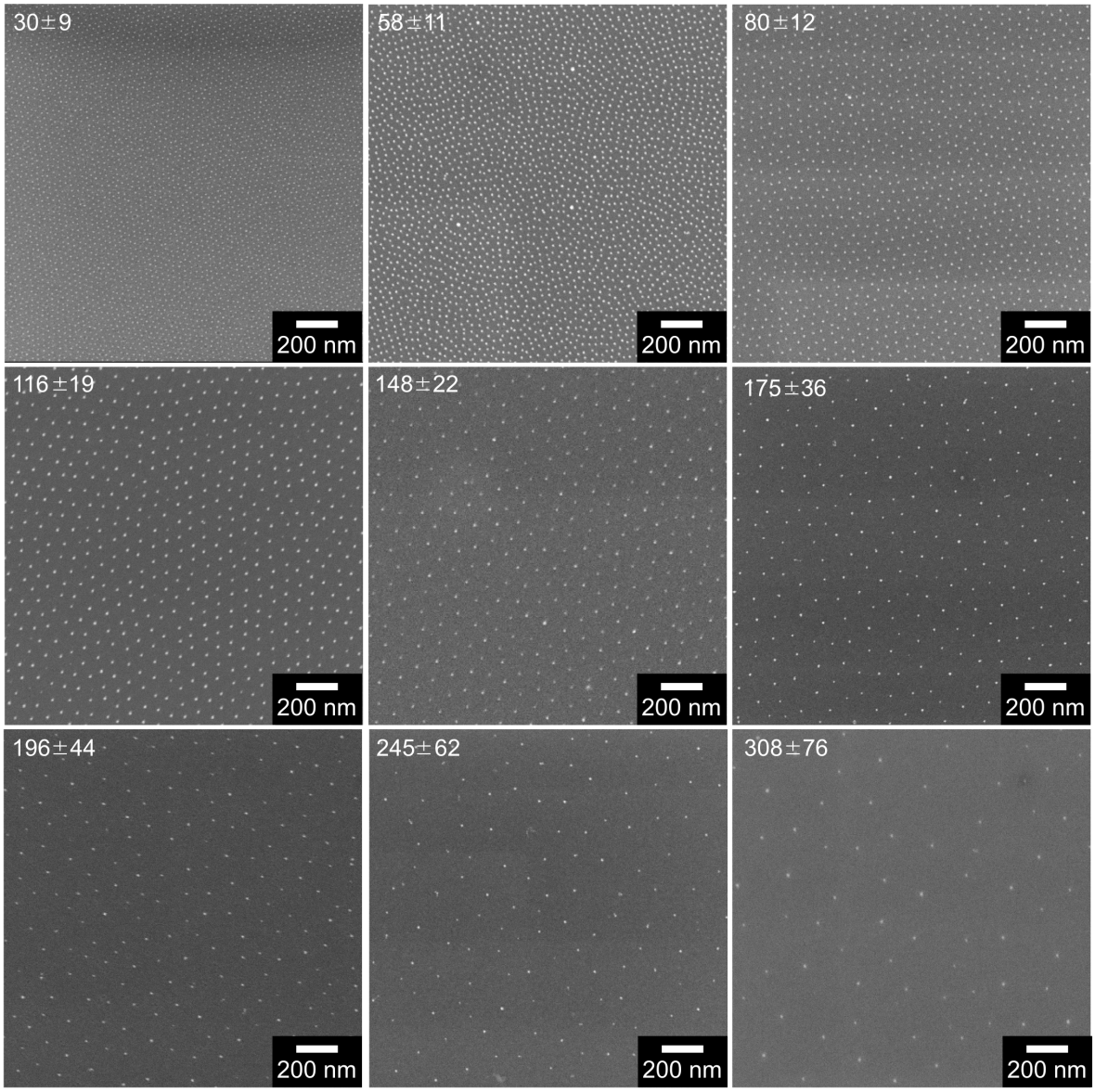

Figure 3.5.: Nanopatterns with different inter-particle spacing | SE micrographs of nanopatterned Au particles featuring different inter-particle distances from approximately 30 – 300 nm (Numbers in each image indicate mean spacing of adjacent particles and corresponding standard deviation for the single value in nm).

SEM imaging is indeed a suitable method to determine pattern quality and homogeneity of pattern, even in terms of particle size distribution, however, our conventional SEM set-up reaches its resolution limit in the one digit nanometer regime. Absolute Au nanoparticle sizes could only be estimated to lie between 5 – 15 nm. Therefore, another high-precision method, SPM, also known as atomic force microscope (AFM), was applied [190].

Determination of particle size by the atomic force microscope

The operating principle of an AFM is based on attractive and repulsive interaction forces of a very sharp tip (see Figure 3.6 C) and a sample surface, including dipole-dipole interaction, *van der Waals* and electrostatic forces. The tip, is situated on a flexible cantilever (see Figure 3.6 B) and when brought into close proximity to the sample surface, forces between the tip and the sample result in a deflection of the cantilever according to Hooke's law[8]. A laser beam which is focused onto and reflected from the backside of the cantilever serves as an optical lever (see Figure 3.6 A). Due to the position of the laser beam on a photodiode the movement of the cantilever and in turn the height profile of the surface as well as the forces acting between the tip and the sample surface can be determined. The advantage over the SEM is that the AFM provides a three-dimensional (3D) surface profile, albeit with significantly slower scan rates than the SEM. In Figure 3.6 D two quasi 3D images of the height profiles acquired with an AFM are shown. The average particle height was determined to be 8 – 10 nm (for details see experimental section 3.4.2).

3.2. Hierarchically structured patterns

The idea behind introducing a superior structure to the nanopatterns is to confine the nanopatterns into micrometer-scaled regions. Such pattern configurations feature dimensions with different length scales: nanoparticles spaced in the nanometer regime and arranged within laterally separated micrometer-scaled islands. It is known that cellular processes can depend on nano- as well as microscale structures. For example, during the adhesion process fibroblasts are sensitive to ligand distances in the nanometer range as well as additional topographical structures in the micrometer range [101]. Furthermore, combinations of micro- and as nanostructures have been used to study how cellular behavior like adhesion depends on local (nanoscale) or global (microscale) features of the artificial cellular environment [191].

[8]The extension of a spring is proportional to the load exposed to it.

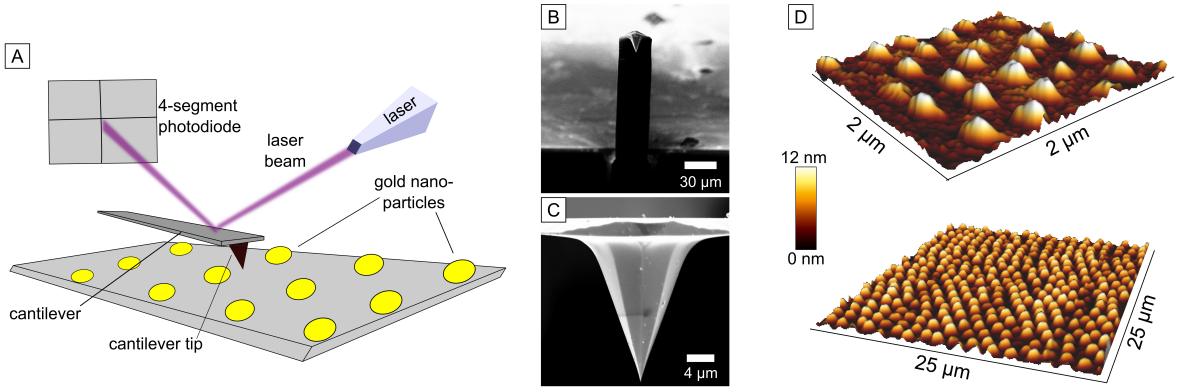

Figure 3.6.: Determination of particle size *via* AFM | A) Scheme of the operating principle of an AFM. A cantilever with a sharp tip (tens of nm) rasters the surface and a laser beam, detected by a photo diode is used to follow the movement of the cantilever. B) SE micrograph of the whole cantilever with tip. C) SE micrographs of a cantilever tip. D) Color-coded topographical information (height signal) of quasi hexagonally ordered Au nanoparticles determined by an AFM. The height (diameter) of particles was determined to lie between 8 and 10 nm.

During activation T cells do temporarily adhere and the contact formation process also depends on environmental parameters of both lengthscales since initial antigen detection and microcluster formation happens on the nanoscale while the activation clusters of the IS are microscale features [159, 192].

The introduction of an additional length scale or superior structure cannot be achieved by pure self-assembly. However, conventional photolithography or electron beam lithography approaches are able to further structure the nanopattern within the microscale [191, 193]. A lithographic structuring results in nanopatterned Au nanoparticles arranged in separate micro-domains described in detail in the following paragraph.

3.2.1. Combination of photolithography and BCML

Photolithography employs light (generally UV light) to transfer a geometric pattern from a photo mask to a light-sensitive chemical photo resist on a substrate. The technique is based on changes of solubility of a photo-sensitive resist material in a specific solvent (developer) upon illumination with light. There are two different types of resist materials: (i) negative and (ii) positive resist. While the negative photoresist, becomes resistant to a specific developer when irradiated, the positive photoresist becomes soluble only upon irradiation.

Basically, two different modes of operation can be distinguished:

- contact mode lithograph
- microscope projection lithography

The contact approach establishes physical contact between the substrate and the photo mask. The projection approach projects the desired structure onto the substrate through a lens system and is technically more demanding. The theoretical resolution limit of projection systems is given by Rayleigh diffraction

$$W_{min} = \frac{k_1 \lambda}{N_A} \tag{3.2}$$

where W_{min} is the width of the smallest feature (also called critical dimension), k_1 a proportionality factor which is process dependent, λ the wavelength of the utilized light source and N_A the numerical aperture of the lens system. The formula exemplifies that the size of the feature is determined by the wavelength of the light. Accordingly, efforts are made to decrease the wavelength in order to fabricate smaller feature sizes. Methods applying deep ultraviolet (DUV) light, with $\lambda < 300$ nm using state-of-the-art excimer laser ArF (193 nm) have pushed far beyond the Rayleigh-Abbe diffraction limit [194] and current progress is made even towards smaller wavelengths. The so called extreme ultraviolet (EUV) light uses 13.5 nm wavelength and is considered as the next generation of lithography [195, 196]. However, moving to such short wavelengths comes along with immense challenges. For instance, free electrons are generated, blurring the produced structures, and air begins to absorb significantly below 200 nm wavelength [197].

In this project, a contact mode lithography technique in combination with a negative resist was applied. The combination of the bottom-up and bottom-down approaches took advantage of the very precise nanoscale patterning capabilities of BCML and the quick and very simple parallel photolithographic process creating additional structures in the micrometer range [193]. In Figure 3.7 A the set-up is schematically displayed. The resist-coated sample becomes pushed either with gas pressure from below, through a vacuum environment or only mechanically (as applied in this study) onto the mask in order to minimize the gap between both. The remaining gap limits the practical resolution of contact mode lithography normally to 0.5 – 0.8 µm, in case of a standard UV wavelengths between 360 – 460 nm.

The combined procedure was as follows (Figure 3.7 C):

1. fabrication of nanopatterns as previously described
2. spin-coating of the nanopatterns with a thin (1.1 – 1.3 µm) resist layer
3. transfer of a certain structure to the resist by illumination with UV light through a photomask
4. development of the structure by means of a developer solution
5. removal of nanoparticles, which are not covered by resist and

6. removal of the polymerized resist structure.

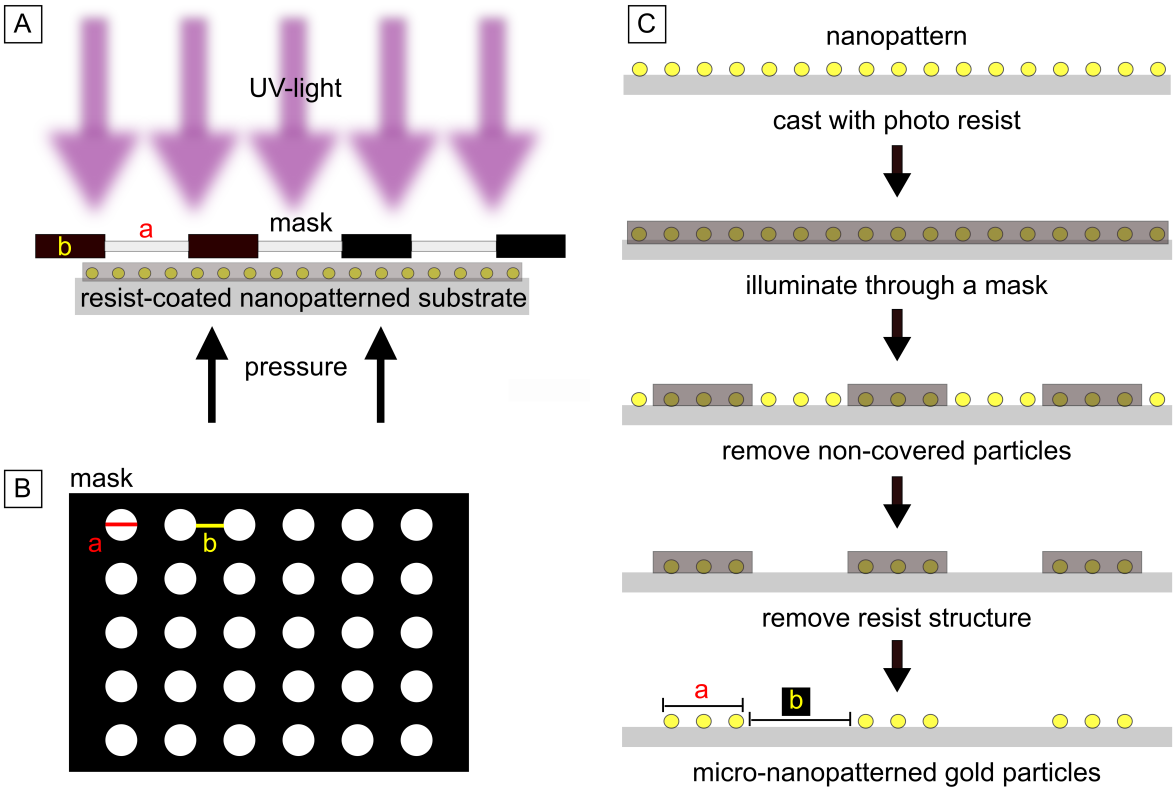

Figure 3.7.: Combination of Photolithography with BCML | A) The resist-covered nanopattern is in direct physical contact with the mask and becomes illuminated with UV light through the mask. B) Scheme of the mask used in this work: Circular transparent areas with a diameter a and a distance b are separated by non-transparent regions. C) Fabrication of micro-nanopatterns: A nanopatterned glass substrate is spin-coated with an irradiation sensitive resist. Illumination (as displayed in A) with ultraviolet (UV) light results in crosslinking of the exposed areas and leaves them non-soluble in the developer solution (this is true for negative resist as used in this work). Non-covered particles are detached followed by a removal of the crosslinked resist pattern. A micro-nanostructured pattern consists of separate particle islands (adapted from [178]).

For the photolithographic patterning we employed commercially available epoxy-based SU-8 negative resist taking advantage of its high aspect ratio[9] (> 20). SU-8 photoresist was developed by IBM for applications in the microchip industry. Due to its remarkable mechanical stability, it has become a widespread resist material which is utilized for a broad variety of applications such as microelectronics, micro-machining or micro-moulding. SU-8 is a very viscous polymer that can be spun or spread over a thickness ranging from one micro- up to two millimeters, achieved by adaptation of the solvent ratio within the resist, and still be processed with standard contact lithography. Its maximum absorption is for UV light around a wavelength of 365 nm. It turned out that

[9]The aspect ratio is the ratio of the width of a structure to its height.

for our purpose this type of resist was ideal, since it allowed to minimize lateral dimensions to the one digit micrometer regime (see also [191]). Samples were spin-coated with an approximately 1.1 – 1.3 µm thick layer of the resist [191]. Before irradiation samples were pre-baked on a hot plate in order to evaporate the solvent of the resist and densify the film. A so-called mask aligner was used to precisely adjust the position of the mask above the sample's surface. Irradiation with a standard UV lamp transferred the pattern of the photomask to the resist layer by rendering the exposed portions of the film insoluble to liquid developers. In detail, upon light exposure the long molecular chains of the resist densely crosslink, causing the solidification of the material. This process is initiated trough a photosensitive acid generator, which releases protons upon the interaction with photons. Now, the free protons serve as catalyst for the cationic polymerization of the resist's epoxy subunits. Such a reaction process is thermally driven, and was therefore, supported through a post baking of the samples. Eventually, non-crosslinked areas were dissolved in developer solution resulting in a micrometer-sized resist pattern over the nanostructured particles. Non-protected particles were removed by a soft ultrasound treatment in an aqueous cysteamine[10] solution. Cysteamine dissolves the Au particles while the highly robust resist remains unaffected. Due to its stability the removal of the SU-8 resist is very challenging to implement and can not be achieved with organic solvents. In this case resist detachment was done by an extensive treatment with reactive H_2 plasma [191, 193]. The resulting patterns feature micro-domains of nanopatterns surrounded by areas without any particles for detailed procedural steps and optimal experimental parameters see section 3.4.1).

In Figure 3.8, resist patterns and micro-nanopatterned Au particles with different patterns are shown. In general, the smaller the feature the more likely are irregularities of the pattern, i.e. structures become vulnerable to disruption. In detail, in our case patterns of high quality over a extended centimeter sized area were only achieved for pattern dimensions of patch diameter $a \geq 1.0\,\mu m$ and patch distance $b \geq 2.0\,\mu m$. However, the resulting pattern does not exactly match the pattern dimensions set by the photomask. The diameter of the particle micro domains is in general larger as the diameter of the transparent circular areas of the mask. The first reason is that crosslinking is not restricted only to illuminated parts, but depending on the illumination dose also parts of the bordering resist crosslink leading to an enlargement of the non-soluble resist patches. The second reason is that removal of Au nanoparticles adjacent to resist patches is inefficient. A possible reason of the latter is that the protective effect of the resist was not restricted to covered particles but also affected non-covered particles in very close proximity. Since the resulting pattern did not exactly

[10]Cysteamine is a chemical compound with the formula $HSCH_2CH_2NH_2$.

match the dimensions set by the mask, the final dimensions of the pattern of the micro-nanostructures were always determined *via* analysis of SE micrographs.

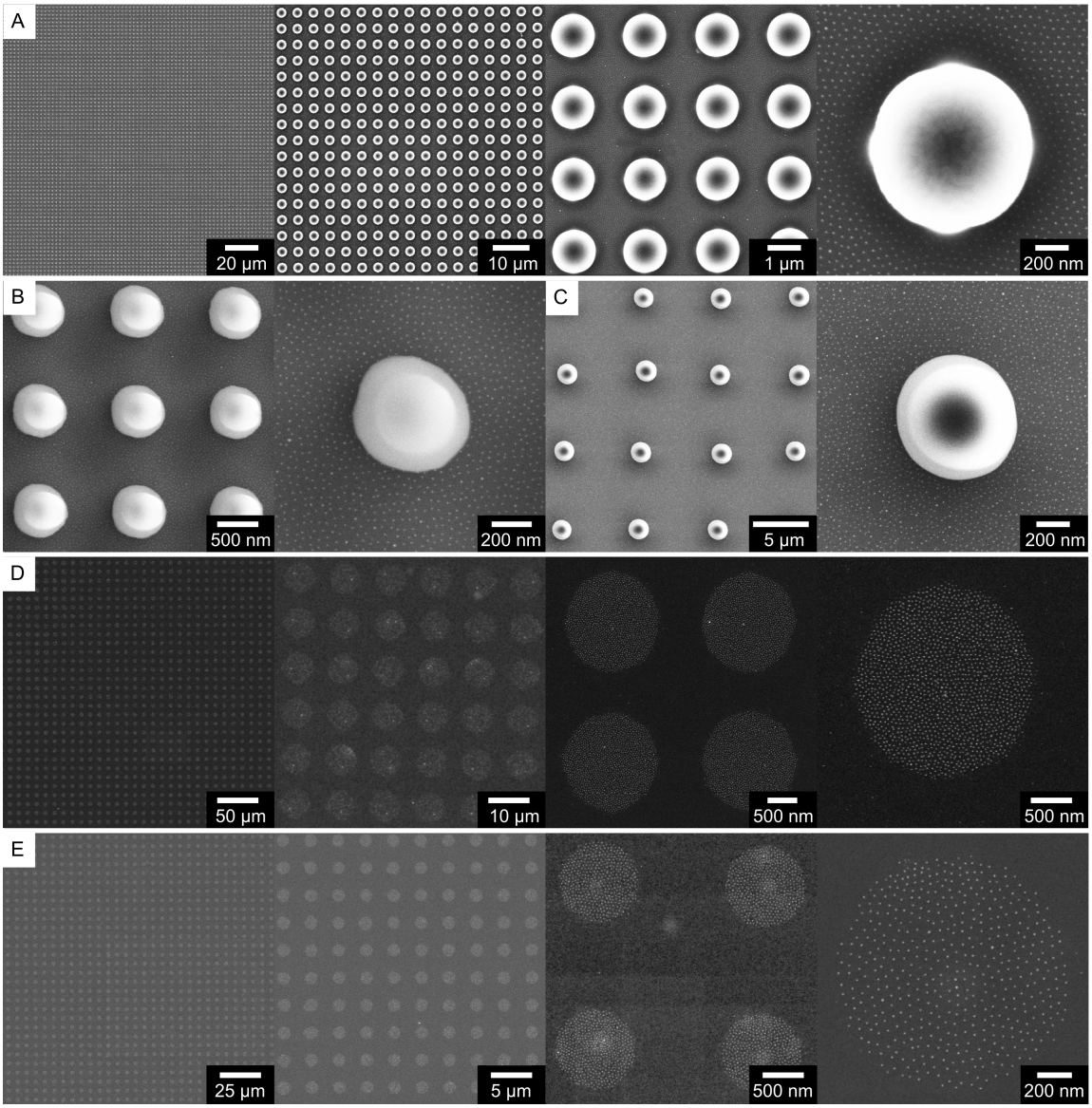

Figure 3.8.: SE micrographs of micropatterned resist on the nanopatterned Au particles(A - C) and micro-nanopatterned Au particles (D - E) | A) Different magnifications of resist patterns on nanostructures; B, C) Like A) only with different dimensions of resist patches; D, E) Different micro-nanopatterns of Au particles.

3.3. Biofunctionalization of substrates

In order to function as surrogate for the APC surface, biomolecules of interest have to be immobilized on the substrate surface. For this purpose, the nanoparticles serve as anchor points for site-selective immobilization and controlled separation of proteins, which play a role during the adhesion process. The area in between the individual particles has to be prepared in a way that non-specific interactions such as electrostatic protein adsorption or cellular adhesion are prevented. This strategy allows for a precise control over the number and density of stimulation-mediating molecules and therefore, enables to study T cell activation as a function of these parameters.

3.3.1. Background passivation

In order to ensure prevention of any type of non-specific cell-surface and protein-surface interactions a so-called passivation of the background was performed. Obviously, unspecific adsorption of biomolecules between the Au nanoparticles or any non-specific cellular interaction with the background would thwart the advantage of BCML. Therefore, the glass area in between the particles was covered with a thin protein repellent polymer layer rendering the background bio-inert. To this end we used the polymer polyethylene glycol (PEG) which has widespread applications in industry, medicine as well as biological research because of its low toxicity and the very low probability to induce specific or unspecific interactions with any biological substance [198]. The non-adhesive properties of PEG originate from a number of factors including the very low interfacial free energy with water, high steric stabilization by volume restriction and excluded volume effects as well as the geometrical structure of PEG in the water lattice [199].

In order to guarantee high stability, PEG was equipped with a silane group (SiH_4)and could therefore, be immobilized on the glass surface through covalent bonds [184] (see Figure 3.9 and for experimental details section 3.4.3). With this strategy we were able to minimize any unwanted interaction of proteins or cells with the background of the substrate. Moreover, the covalent bonds created very stable PEG layers and thus, the method is suitable also for experiments running for longer time periods (days).

3.3.2. Immobilization of proteins on nanoparticles

The hexagonally ordered Au nanoparticles serve as anchor points for the attachment of linker molecules to which the proteins of interest can then be conjugated. We chose complexes of nitrilotriacetic acid (NTA) with the divalent transition metal ion Nickel

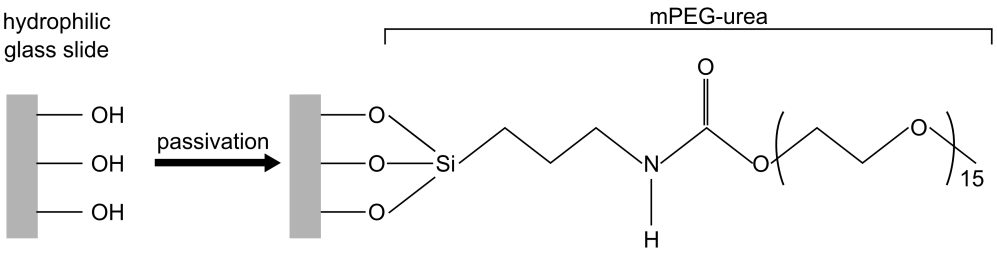

Figure 3.9.: Coating the hydrophilic background with PEG | The mPEG-triethoxysilan-2000-urea covalently binds *via* a silane end group to the OH^- groups presented by an activated glass surface.

(Ni^{2+}) to serve as target for any protein with a terminal poly-histidine (His) tag[11] [193, 200, 201] and has been routinely used for purification of re-combinantly expressed histidine-tagged proteins for decades [202]. A His-tag consists of an amino acid motif in proteins composed of at least six His residues, often at its N- or C-terminus[12] of the protein. In order to ensure binding to Au of the NTA reagents, they were in our case equipped with a terminal thiol group (HS-$(CH_2)_{11}$-EG_3-NTA), which has a high affinity to Au[13] and guaranteed a stable (semi-covalent) connection of the NTA linker to the nanoparticle (see Figure 3.10A)). This coupling approach enabled us to directly address His-tagged proteins to the Au particles and specifically immobilize them on the surface in a highly ordered manner.

In order to investigate the specificity of the NTA-His-tag immobilization strategy we performed conventional fluorescence microscopy. In general, fluorescence microscopy techniques are often applied to allow for visualization of only a certain component of interest within a specimen. This particular component has to be specifically labeled with a fluorescent molecule, a so-called fluorophore. Upon irradiation with a specific wavelength the fluorophore absorbs photons (excitation) and again re-emits photons with a different, longer but also specific wavelength (emission) [203]. Fluorescence microscopy is a widespread tool in biological research since it allows the observation of many biological components; for example, cellular structures and even single proteins can be visualized and tracked in real time [204–206].

In this project, analysis of the fluorescent signal of proteins, which were labeled with a fluorophore, provides evidence for the site-specificity of protein binding to the Au nanoparticles. At the same time this strategy proves the full preservation of protein repellent properties of the coupled PEG after the particle modification process. In detail,

[11] His-tag is a trademarked name registered by EMD Biosciences and was originally invented by Roche.
[12] The N- or C-terminus refers to the part of a protein or polypeptide terminated by an amino acid with a free amine group (-NH_2) or a free carboxyl group (-COOH), respectively.
[13] The sulfur of the thiol group (-SH) has a strong affinity to noble metals, especially to Au, with an interaction strength of approximately 188 kJ/mol.

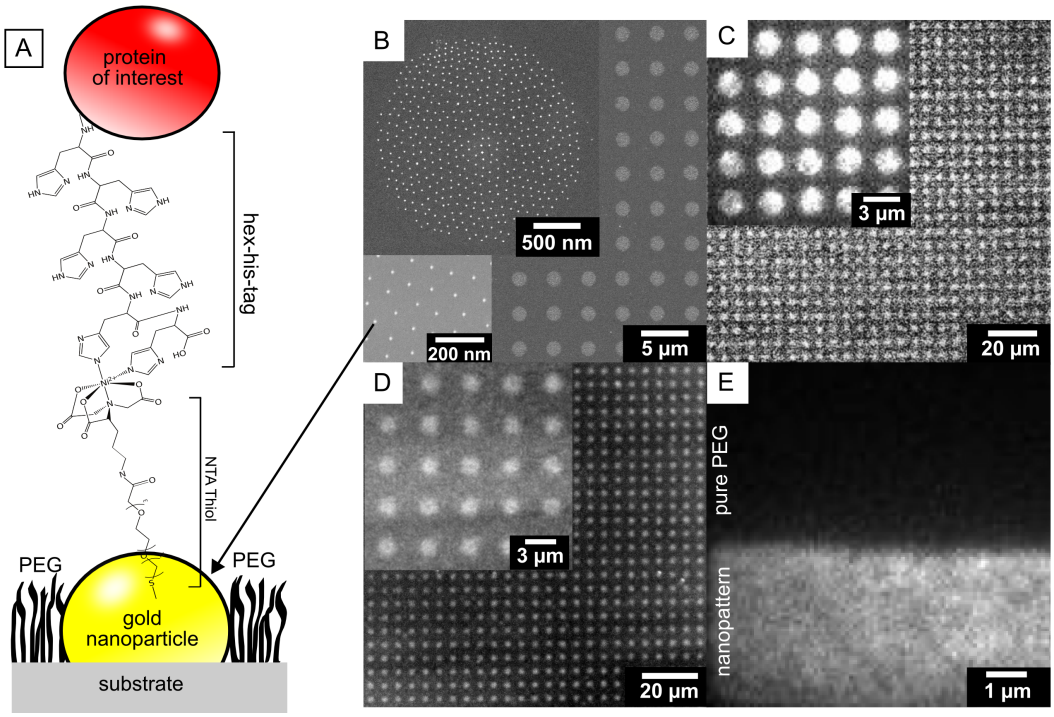

Figure 3.10.: Specific binding of proteins to nanoparticles | Fluorescent microscopy of proteins labeled with a fluorescent dye and immobilized on nanostructures and micro-nanostructures proves the specificity of the NTA-Ni^{2+} His-tag bond. A) Scheme of the bond: Any His-tagged protein of interest can bind to the NTA-Ni^{2+} (Note: Not drawn to scale.). B) Different magnifications of SE-micrographs of micro-nanopatterned Au particles. C) The fluorescent signal of pMHC labelled with a Atto655 represents the micrometer-sized particle islands. D) Same as C) for immobilized ICAM-1 labelled with Cy-5. E) The fluorescent signal shows the border between PEG area and particle region. pMHC only binds on the side presenting Au nanoparticles.

we immobilized pMHC and ICAM-1 equipped with Atto 655[14] and Cy-5[15], respectively on the Au nanoparticles, which were arranged in micro-domains (micro-nanopatterns; see Figure 3.10B)). Both dyes feature a high brightness and in a fluorescence microscope, the micro-nanopatterned substrates with attached fluorescent pMHC/ICAM-1 look like a regular pattern of large bright polka-dots (made up of minuscule fluorescent spots), surrounded by a dark background, consisting of PEG, with practically no proteins bound to it (see Figure 3.10 C),D)). Although the resolution of conventional fluorescence microscopy is limited to visualizing the photolithographic micro-structure and, therefore, is unable to resolve the underlying nanopattern, proof of function – that is specific binding of pMHC and ICAM-1 to Au particles – was observed.

[14] Atto dyes are derivatives of coumarins, rhodamines, carbopyronins and oxazines. For detailed description see http://www.atto-tec.com/.
[15] Cy-5 is a dye of the cyanine dye family belonging to the polymethine group.

3.3.3. Determination of proteins per particle

In order to optically visualize how many molecules are occupying a single Au nanoparticles, methods, which have overcome the barrier set by the diffraction limit of light, would be required. Recently, a variety of super resolution microscopy techniques have arisen [206]. For instance, stimulated emission depletion (STED) selectively deactivates fluorophores in order to enhance resolution in this area and achieving spatial resolutions of 70 nm [207, 208]. Other techniques like PALM and stochastic optical reconstruction microscopy (STORM) collect a large number of images of the same area during many emission cycles. Each image contains only a low density of active fluorophores, so that the chance of overlapping signals from adjacent fluorophores is very low. The image sequence can then be used to determine the position of single fluorophores achieving resolutions down to 10 nm [209–212]. However, all these methods need state of the art equipment and depend on altered optical set-ups and come along with difficult sample preparation such as requirement of unique fluorescent probes or proteins, or the need of extensive post-imaging analysis. At the same time the statistic output is not very high.

To clarify, in our case we intended to know the number of molecules sitting on one individual Au nanoparticle. In order to get sufficient values to provide good statistics we would have to measure many different spots (particles) of different surfaces (> 100). Hence, a more simple and convenient method is to determine the fluorescent signal intensity of several micrometer-sized areas and calculate the amount of fluorophores in this region by comparing it with the signal obtained from a single fluorophore. According to the particle density the absolute amount of fluorophores yields to an average pMHC/particle ratio. This approach comes along with much better statistics since within every single fluorescence image thousands of particles or fluorophores, respectively, are taken into account. Moreover, the set-up is not as demanding as for high resolution microscopy and the measurements are easier to perform. In Figure 3.11 a scheme shows how we "scanned" the surface: Images of different sample areas ($n = 5-9$) separated within the millimeter range were collected. In turn, within such spatially distinct areas images of different spots ($n = 10-15$), of which each was analyzed regarding the total intensity I_{tot}, were acquired. By determining the signal intensity of a single fluorophore (I_{single}) we were able to calculate the absolute number of fluorophores per area (A). Knowing the particle density ($\rho_{particle}$) the average number of fluorophores per particle, the so-called occupation rate (OR) [molecules/particle] could be determined:

$$OR = \frac{I_{tot}}{I_{single} \cdot A \cdot \rho_{particle}} \tag{3.3}$$

We found the average occupation rate to be 1.6 ± 0.4 molecules per particle (see subsection 3.4.4 for experimental details).

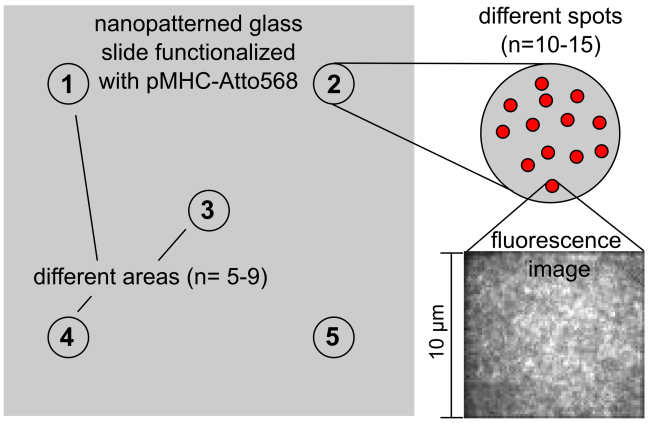

Figure 3.11: Determination of occupation rate by fluorescence microscopy | Several images within different areas (millimeter range) of the surface were acquired in order to cover the whole surface and to determine possible deviations of separated areas. The total fluorescence signal of the eventual microscopy image was used to determine the fluorophores per area, which finally led to a value for the occupation rate (proteins per particle).

3.3.4. Rendering the background bio-adhesive

The motivation of providing a bio-adhesive background is caused by the molecular composition found in a real APC. Adhesive molecules are believed to play a key role during IS formation, therefore, we attempted to better adapt our system to the natural case. To this end, we used a modified PEG, whose exposed ends were equipped with an alkyne group[16] in order to serve as binding site for biomolecules exhibiting an azide group[17]. The binding of alkyne to azide is based on cycloaddition[18] between an azide and a terminal/internal alkyne to give a 1,2,3-triazole (see Figure 3.12) [213]. The reaction requires elevated temperatures and produces mixtures of 1,4 and 1,5 regioisomers[19] (see Figure 3.12 A, B).

In our case we applied the copper(I)-catalyzed azide-alkyne cycloaddition (CuAAC), which can be conducted at room temperature and under aqueous conditions. Moreover, in contrast to the classic so called "Huisgen" version these catalyzed reaction allows the synthesis of the 1,4-disubstituted regioisomers specifically and therefore, comply fully with the definition of click chemistry[20]. CuAAC has come to be regarded as a prototype click reaction and is nowadays, a commonly employed method for the

[16] An alkyne group is a triple bond between two carbon atoms.
[17] Azide denominates the anion with the formula N_3^-.
[18] Cycloaddition is a pericyclic chemical reaction, in which at least two unsaturated systems combine with the formation of a cyclic adduct. Usually, a particular cycloaddition is specified with a two part number code, referring to the π-electrons of both binding partners being part of the reaction.
[19] Regioisomerism denominates the changes of position of a functional group or other substituent on a parent structure.
[20] Click chemistry denominates reactions that are high yielding, wide in scope, stereospecific, physiologically stable, simple to perform, that use only benign solvents, have high atom economy and create only inoffensive byproducts.

synthesis of complex molecular architectures, especially in polymer science and for surface immobilization/modification techniques [214–217]. Using this click chemistry strategy we could easily introduce a stable adhesive background instead of a bio-inert. Moreover, by varying the ratio of PEG with alkyne group and PEG without we were able to adjust the density of the alkyne groups, thus, the availability of binding domains for molecules with an azide group. In our case we used arginine-glycine-aspartate

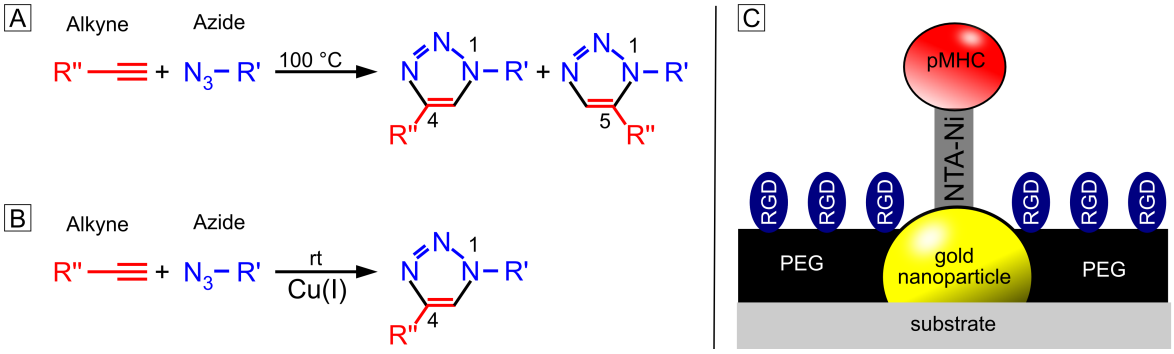

Figure 3.12.: Azide-alkyne cycloaddition/Rendering the background adhesive A) Standard azide-alkyne Huisgen cycloaddition: Alkyne reacts with azide at temperatures around 100 °C to the 1,2,3 triazole as a mixture of 1,4-adduct and 1,5-adduct. B) The copper(I)-catalyzed azide-alkyne cycloaddition can be conducted at room temperature (rt) and synthesizes the 1,4 regioisomer specifically. C) Scheme of the surface functionalization presenting stimulating pMHC on the Au particles and adhesive RGD sequences in the background. RGD is immobilized *via* an azide group to the PEG-alkyne.

(RGD) expressing an azide group to render the background adhesive. RGD is an amino acid sequence consisting of the three amino acids arginine, glycine and aspartate and can be found in the extracellular environment of cells. Particular cell surface receptors, the integrins, are able to bind the RGD sequences and mediate adhesion of the cell to its surrounding. T cells express the $\alpha_4\beta_1$ type of integrin, which is better known as vascular cell adhesion molecule 1 (VCAM-1). Expression of this receptor makes T cells capable of binding to the RGD sequence [218] supporting the adhesion of T cells. In Figure 3.12 C) it is schematically shown how the functionalized nanopatterned surfaces are set-up.

3.3.5. Generation of protein islands on nanopatterns by an external device

In contrast to the method previously mentioned, the idea behind creating separate protein islands is, to have confined nanopatterend structures, which could be activating pMHC islands, surrounded by adhesive, also nanopatterned molecules, for example ICAM-1. The adhesive molecules would not be immobilized to the PEG background

but to the surrounding non-occupied Au nanoparticles (see Figure 3.13). Such types of arrays would be binary nanopatterns featuring two distinct biomolecules within spatially separated areas and a bio-inert background. They would allow for investigating nanoscale spacing effects of two distinct biomolecules.

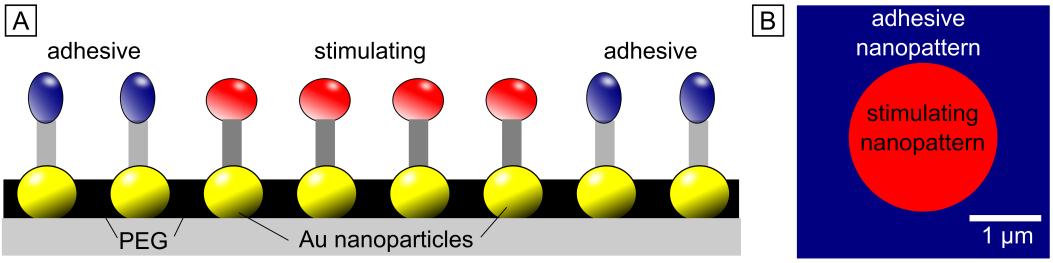

Figure 3.13.: Scheme of nanopatterned stimulating island in adhesive nanopatterened background | A) Initially stimulating proteins are immobilized to Au nanoparticles only to confined regions followed by binding of adhesive protein to the surrounding free particles within a bio-inert PEG background. B) This strategy attempts to better mimic the protein distribution on the APC side in the IS; nanopatterened stimulating islands corresponding in size to the lateral dimensions (1 – 2 µm) of the c-SMAC surrounded by nanopatterned adhesive proteins simulating the d-SMAC (Note: Image represents a schematic top-view of the desired arrangement.).

We used a direct liquid spotting device[21] to dispense attoliter to femtoliter volumes of protein solution onto the surface. This is achieved *via* a thin cantilever, which shortly touches the surface with its tip thereby leaving a tiny droplet (1.0 µm to 100 µm spot diameter) of liquid on the surface. The cantilever tip is connected through a microchannel to a micro-reservoir which becomes filled with solution of interest prior to patterning. A laser is focused on the cantilever and the reflected beam is detected with a photodiode. Likewise to the working principle of the AFM (see also subsection 3.1.4), this set-up enables to control the deflection of the cantilever/interaction force of surface and cantilever, respectively, since the deflection of the laser reflects the movement of the cantilever. Therefore, by controlling the contact time as well as the contact force a precise adjustment of the amount of liquid leaving the cantilever channel is possible. This in turn, enables to control spot size in the micrometer regime.

Using the described top-down approach we created arrays of micrometer-sized droplets on the nanopatterns. PBS containing pMHC in desired concentration was deposited on defined spots and then started to bind to the underlying Au particles since particles were already functionalized with the NTA-Ni^{2+} linker in advance. In (see Figure 3.14) different arrays of micrometer-sized spots created with the Nanoenabler system are shown.

[21] (NanoeNabler^{TM} system), for further details see section 3.4.3

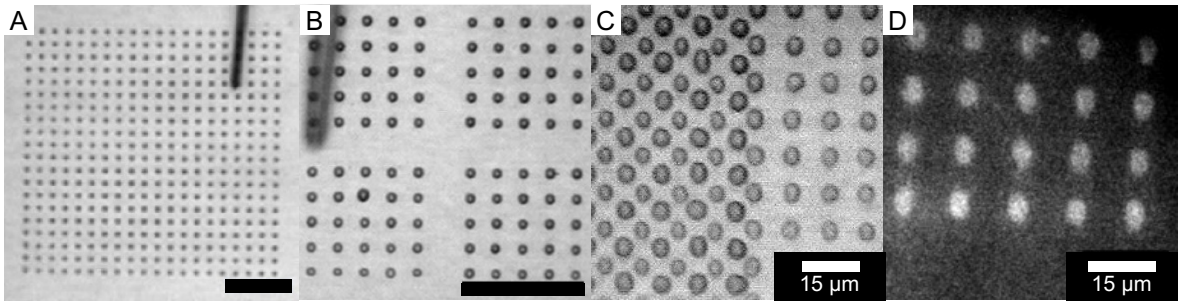

Figure 3.14.: Protein deposition by an external device | A), B) A lever which is connected to a reservoir through a channel is employed to deposit small droplets on the surface. Patterns can be pre-designed and then transferred to the substrate surface (Scale bar: 100 µm). C) Two different proteins can be deposited on the surface by a two step process. On the left side of the image there is a secondary protein solution in between the original protein droplet pattern. D) Fluorescence image of I-E^k-2xHis$_6$-MCC-Atto655 micropattern on Au-nanoarray created with the NanoeNabler system

Herewith, we again demonstrated the creation of nanostructured pMHC islands. The difference compared to micro-nanopatterened pMHC islands is that the surrounding still presents "free" nanoparticles. In a subsequent binding step, they can be used to immobilize adhesive biomolecules in a controlled fashion. This strategy creates patches of stimulating pMHC, corresponding in size to the diameter of the c-SMAC surrounded by nanopatterned adhesive ICAM-1 supporting the formation of a stabilizing peripheral region mimicking shape and composition of the IS. However until now, we did not fully reach to optimize the binding strategy, which appeared to be essential (see subsection 7.1.1 for further information).

3.4. Experimental details and analyses

3.4.1. Preparation of nanopatterns and micro-nanopatterns

Cleaning of substrates and glass containers

Conventional glass slides (Menzel, 24 x 24 mm,) and glass containers for preparing the micellar solution were cleaned in a freshly prepared piranha solution for 1 – 2 h. This solution consisted of a 3:1 mixture of concentrated sulfuric acid (H_2SO_4; p. a.; Sigma-Aldrich, Germany) and H_2 peroxide (H_2O_2 p. a.; AppliChem, Germany). Finally, substrates and containers were extensively rinsed with deionized water and blown dry with pure nitrogen.

Table 3.1.: Types of diblock copolymers

Polymer PS(g/Mol)-*b*-P2VP(g/mol)	PS units	PVP units	PDI† M_W/M_n	particle spacing [nm]
PS(16000)-*b*-P2VP(3500)	154	33	1.05	20 – 35
PS(25000)-*b*-P2VP(15000)	240	143	1.04	35 – 50
PS(110000)-*b*-P2VP(52000)	1056	495	1.15	50 – 100
PS(190000)-*b*-P2VP(55000)	1824	523	1.10	70 – 140
PS(276000)-*b*-P2VP(216000)	2074	571	1.05	90 – 160
PS(557000)-*b*-P2VP(75000)	5355	714	1.07	150 – 300

† The polydispersity index (PDI) is the weight average molecular weight M_W divided by the number average molecular weight M_n. It indicates the distribution of individual molecular masses in a batch of polymers.

Preparation of micelle solution

A weighed portion of the PS-*b*-PVP diblock copolymer (Polymer Source Inc., Montreal, Canada) was placed into a cleaned glass container, filled up with the respective amount of toluene (p. a., Merck, Darmstadt, Germany) and stirred for 24 h. Depending on the desired loading rate a stoichiometric amount of $HAuCl_4$ was added and stirred again 24 h until $HAuCl_4$ was completely dissolved. The solutions used in this thesis featured loading parameters ranging from 0.3 to 0.5. With the following relationship the exact amount of $HAuCl_4$, which is required to obtain a particular loading rate can be calculated:

$$m_{HAuCl_4} = m_{PS-b-PVP} \frac{M_{HAuCl_4} n_{VP-units}}{M_{PS-b-PVP}} L \qquad \text{with } L < 1 \tag{3.4}$$

with $M_{HAuCl_4} = 339,79\,\text{g/mol}$ for $HAuCl_4 \cdot (H_2O)$ (Sigma Aldrich), as used in this thesis. The molecular weight $M_{PS-b-PVP}$ of the different used polymers are summarized in Table 3.1.

Fabrication of nanopatterns

The piranha-cleaned glass substrates were dipped into glass containers filled with micelle solution. They were then retracted with a defined velocity by a custom made device (see Figure 3.2). The voltage supply covers a range from 0 V to 32 V and the voltage-velocity dependence is linear (see Table 3.2). In this work voltages between 5 V

and 20 V were applied to fabricate the nanopatterns.

Table 3.2.: Calibration of dipping device

Voltage U [V]	6	8	10	12	14	16	18
Velocity v [mm/min]	11.1	15.5	19.9	24.3	28.7	33.1	37.5

Upon retraction the micelles assembled on the surface into a monolayer. Substrates were then air-dried and subsequently treated with an isotropic microwave induced H_2 plasma (PS 210, PVA TePla America, Inc.) for 45 min, at 600 W and 0.3 mbar to remove the polymer shell of the micelles.

Fabrication of micro-nanopatterns

The entire fabrication process was performed under clean room conditions with dust filtered air, temperature and humidity control and yellow light in order to prevent unintended illumination of the photoresist.

Nanoparticle arrays on glass substrates were coated with 170 µl of SU-8-2 negative resist (Micro Resist Technology GmbH, Berlin, Germany) by means of a spinning disk. Initial rotation speed was 500 rpm lasting for 5.0 s followed by an acceleration within 5.0 s to 3500 rpm and maintaining this speed for another 30 s. This resulted in a homogeneous layer thickness of 1.1 –1.3 µm (see below for the determination method). Subsequently, in order to evaporate solvent and densify the film the samples were soft-

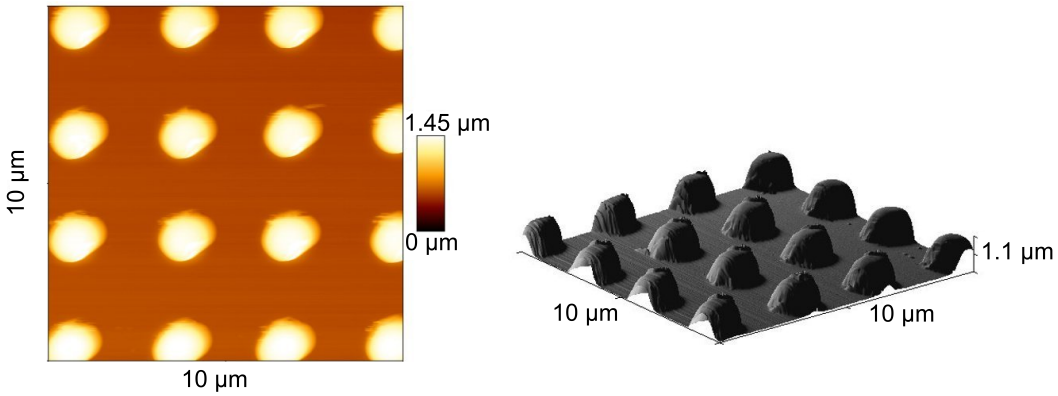

Figure 3.15.: Atomic force micrographs of structured SU-8 resist | Left: AFM image of color coded height signal; Right: quasi three dimensional topography reconstruction (adapted from [178]).

baked on hotplates for 1.0 min at 65 °C followed by 1.0 min at 95 °C. The stepwise heating prevents resist film damages due to distinct expansion of resist film and wafer.

Resist-coated and soft-baked substrates were transferred to a mask-aligner (MJB3; SÜSS MicroTec, Germany), which allows for a precise adjustment and positioning of mask and sample. The illumination with UV light in order to transfer the mask pattern to the sample was done by a HBO 350 mercury lamp at a dose of 50 mJ/cm^2. Post baking in order to selectively crosslink the exposed portions of the film, was equally performed as the soft bake. The structure was developed using the appropriate developer (MR-Dev600, Micro Resist Technology GmbH, Berlin, Germany) and then shortly rinsed with isopropanol, before dried with pure nitrogen. In order to determine the height of the resist layer the topography of the developed resist pattern (height of resist patches) was determined with an AFM (NanoWizard I, JPK, Germany) (see Figure 3.15) [178]. The height of the resist micro-domains was found to be 1.1 –1.3 µm. To detach the unprotected particles the samples were sonicated in a 1 % solution of cysteamine in ultra-pure water for 2.0 min. Lastly, the highly crosslinked resist was removed by a 180 min lasting reactive H_2 plasma treatment at 150 W and 0.4 mbar (100-E, PVA TePla America, Inc.). The values of parameters for the photolithographic procedure generating the best results in terms of pattern homogeneity and quality are summarized in Table 3.3.

Table 3.3.: Parameter values for photolithography

Structures	v_{spin}	$t_{prebake}$	$t_{exposure}$	$t_{postbake}$	$t_{develop}$
1.0 – 5.0 µm	3500 rpm	60 s	2 s	60 s	12 s

3.4.2. Analysis of patterns

Scanning electron microscopy

Samples were coated with a carbon layer by means of a sputter coater (Med020 modular High Vacuum Coating system, BalTec, Witte, Germany) to prevent charging of the surface during image acquisition of the surface with the SEM. The SE micrographs were acquired using a Zeiss LEO 1530 (ZeissSMT, Oberkochen, Germany) with acceleration voltages of about 5 keV and working distances between 5 and 10 mm using in-lens detector or secondary electron detector (see section 3.1.4 for details of the method).

Calculation of particle spacing and density of nanopatterns

In order to determine the quality and spacing of the pattern an image processing analysis of SE micrographs was performed. The software routine provided the mean

distance of the particles, its deviation and the order parameter Φ. The idea of the method is to select the six closest particles for each individual particle and quantify their distances. This works as follows: If r_{jk} denotes the distance of the particle j to other particles k then the six smallest values for each particle are determined. The average spacing then is given by

$$d = \frac{1}{6N} \sum_{j=1}^{N} \sum_{k=1}^{6} r_{jk} \tag{3.5}$$

where d is calculated for every individual particle j and its six closest neighbors and then averaged over all particles. The standard deviation follows as:

$$stdev(d) = \sqrt{\frac{1}{6N} \sum_{j=1}^{N} \sum_{k=1}^{6} [r_{jk}^2 - 6Nd^2]} \tag{3.6}$$

and the standard error as:

$$stdev(d)/\sqrt{N} \tag{3.7}$$

The global bond-orientational order parameter Φ_6 is defined as:

$$\Phi_6 = \left| \frac{1}{N} \sum_{j=1}^{N} \Psi_6(r_j) \right| \tag{3.8}$$

where N is the number of particles in the analyzed area and $\Psi_6(r_j)$ is the local order parameter for a particle j located at r(x,y). It is given by:

$$\Psi_6(r_j) = \frac{1}{n_j} \sum_{k=1}^{n_j} exp(6i\Theta_{jk}) \tag{3.9}$$

where i is the imaginary unit and n_j is the number of nearest neighbors. Θ_{jk} denotes the angle between the straight connecting the particle j and one of its nearest neighbors k and a arbitrary fixed reference axis. In the six nearest neighbor model n_j is equal six and the plugin measures the six angles Θ_{j1} until Θ_{j6} for each particle j and calculates the real and imaginary components of Ψ_6. The so-called Delaunay model is a slight improvement over the described method since it does not necessarily define six neighbors for each particle. This is in so far an advantage over the first model since defects do not result in "wrong" neighbors (due to missing particles) with too large distances. Adjacent particles are only defined as neighbors if they are connected by the

Delaunay triangulation[22]. Hence, the difference is that n_j is not necessarily equal six, however the calculation of the parameters remains equal. Moreover, values of different models only slightly differ since defects in the patterns are not common. Nevertheless, the second method was chosen to be applied in this work.

The described method allowed to determine the average distances $\bar{d}$ and the corresponding standard deviations s_d and error $s_{\bar{d}}$ out of individual images. In order to improve statistics, we evaluated different SE micrographs of different sites of the same sample. In turn, the weighted average D for the particle spacing can be determined. The weight g_i is $\frac{1}{\sigma_i^2}$ where σ_i corresponds to the the error $s_{\bar{d}}$ of each analyzed site i:

$$D = \frac{\sum_i \bar{d}_i g_i}{\sum_i g_i} \tag{3.10}$$

and the weighted error is given by:

$$\sigma_D = \frac{\sqrt{\sum_i g_i^2 \sigma_i^2}}{\sum_i g_i} = \left(\sum_i \frac{1}{\sigma_i^2} \right)^{-\frac{1}{2}} \tag{3.11}$$

Since our intention was to employ nanopatterns for cell experiments, we evaluated the surfaces regarding their consistency of distances between different areas on the surface. However, for cell experiments we finally provided the deviation of the single value for the mean particle distance and not the standard error of the mean neither the weighted error. We decided to do so, since cells are in contact with a micrometer- and not with a centimeter-sized area. According to Equation 3.7 it would be possible to make the standard error of the mean arbitrarily small since it depends on N, the number of particles taken into account. In case of nanopatterns, N can be chosen to be almost "unlimited" high. However, such a deviation for "large" areas does not match the conditions a single cell is confronted with. The cell does not sense average spacings, but instead, possibly even single inter-particle distances. Therefore, we chose to provide the deviation of the single value of a micrometer-sized (tens of squared micrometer) area in order not to underestimate the error of particle spacing.

The global density ρ_{global} (particles per area) and its error $s_{\rho_{global}}$ was determined with regard to the average distance D and its corresponding $stdev(d)$:

$$\rho_{global} = \frac{2}{\sqrt{3}} \frac{particles}{D^2} \tag{3.12}$$

[22] A Delaunay triangulation for a set P of points in the plane is a triangulation such that no point in P is inside the circumcircle of any triangle in the triangulation. Mathematically, this means that it maximizes the minimum angle of all the angles of the triangles.

and by means of Gaussian error propagation

$$s_{\rho_{global}} = \frac{4}{\sqrt{3}} \frac{stdev(d)}{D^3} \tag{3.13}$$

Calculation of global particle density on micro-nanopatterened surfaces

In the case of micro-nanopatterned substrates we distinguish between "local" and "global" density. The local particle density within the micro-domains can be determined using Equation 3.12, the global particle density, on the other hand, refers to the particle density of an area significantly larger than the micro-domains. In contrast to continuos nanopatterns where the global density equals the local particle density, on micro-nanopatterns the global particle density is lower than the local.

Within one circular nanoparticle domain A the number of particles (n_A) can be calculated by

$$n_A = \rho_{global_{extended}} \cdot A \tag{3.14}$$

where A is the area of one single patch. n_A has now to be referred to a greater area. One can imagine identical squares surrounding each circular island and thus, covering the whole area. Each square features an edge length of $(a+b)$ when a is the diameter or edge length of a single patch and b is the distance between to adjacent micro domains [191] (see Figure 3.16).

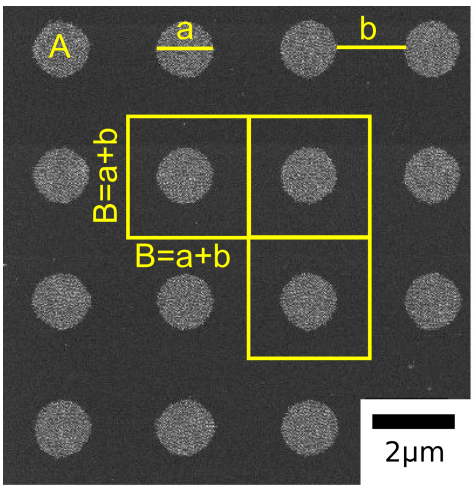

Figure 3.16: Illustration of density calculations Each circular patch A is surrounded by a square with edge length $B = (a + b)$. In order to calculate the global density the number of particles in A is referred to the area of a single square $(a+b)^2$.

Then the particles per area are given in the following way:

$$\rho_{global} = \frac{n_{particles}}{(a+b)^2} = \frac{2}{\sqrt{3} \cdot D^2} \cdot \frac{A}{(a+b)^2} \tag{3.15}$$

Where $A = \pi(\frac{a}{2})^2$ for circular shaped patches. a was determined by means of SE micrographs and the error s_a was estimated to be in the range of 0.1 µm. $(a + b)$

is a fixed value and does not change even if pattern dimensions (a, b) on the surface are slightly different than the dimensions (a, b) set by the mask. The sum of both parameters always stays the same. The error for the particle density is then given by Gaussian error propagation:

$$s_{\rho_{global}} = \frac{2}{\sqrt{3}D^2B^2} \cdot \sqrt{\left(\frac{2A}{D} \cdot s_D\right)^2 + s_A^2} \tag{3.16}$$

with $a + b = B$. In case that the area A of the patch is significantly smaller than the surrounding square, meaning many particles have been removed, then the part with s_D can be disregarded since $s_A >> s_D$. Disregarding yields to:

$$s_{\rho_{global}} = \frac{2}{\sqrt{3}D^2B^2} \cdot s_A \tag{3.17}$$

For a circular shape s_A is given by:

$$s_A = \frac{\pi a}{2} \cdot s_a \tag{3.18}$$

Topographic AFM measurements

The atomic force micrographs presented in this work were recorded with a "NanoWizard I' AFM commercially provided by JPK instruments AG, Germany. The instrument is mounted on an optical microscope (Zeiss Axiovert 200) and is suitable for simultaneous phase contrast or fluorescence imaging. Sharp tip cantilevers (CSC 38, no Al, µMasch) with spring constants ranging from (0.03 – 0.08) N/m were used to scan the surface in liquid (PBS) in intermittent contact mode. Intermittent mode denominates an operating mode in which the cantilever oscillates with a particular drive frequency above the surface, touching it only for a short period in case of maximal deflection towards the sample [219, 220]. Line rate was set to be 0.5 Hz (2 x 2 µm) and 0.3 Hz (25 x 25 µm).

The drive frequency was approximately 30 kHz and drive amplitudes between (0.50 – 0.65) V. In Figure 3.17 color-coded topographical atomic force micrographs ("measured height") of nanopatterned Au particles on glass surfaces are shown. In the lower row, height profiles of particular areas (indicated with white lines) are displayed in order to visualize the quasi uniform height of particles. Note: The AFM is not able to resolve the lateral dimensions of the particles because of tip dimensions. The lateral particle dimension becomes broaden arising from the tip radius of curvature which is larger as the feature to be visualized. Moreover, particle shape reflects tip shape.

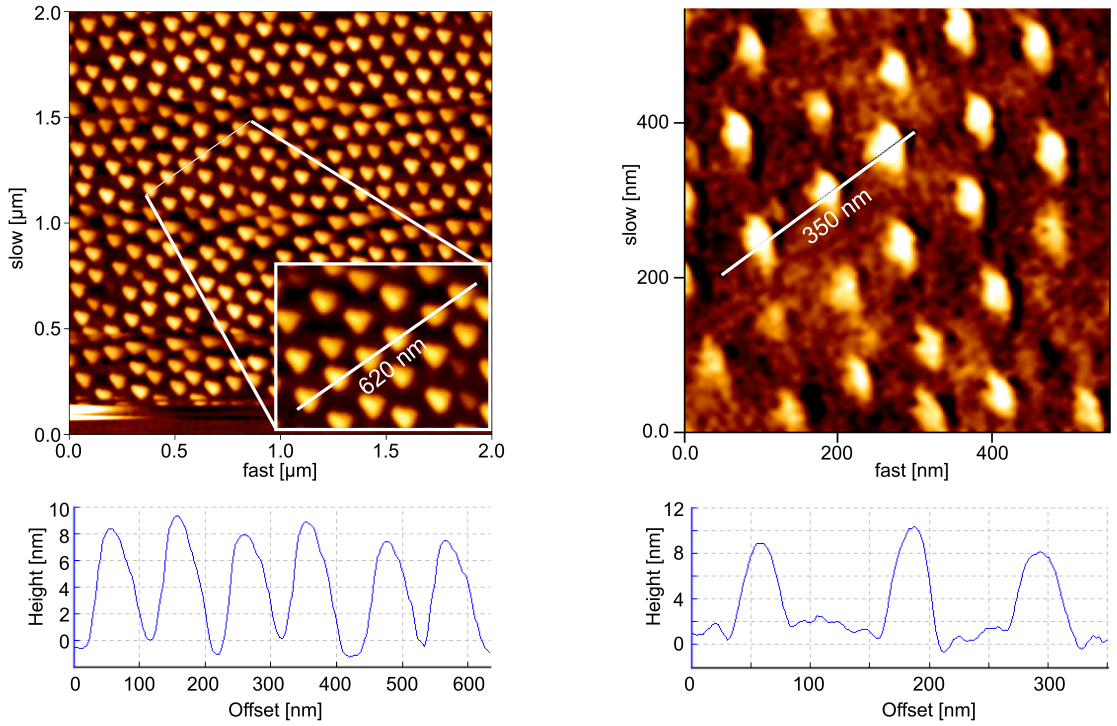

Figure 3.17.: Topographical atomic force micrographs and corresponding height profiles | Upper row: Color-coded topographical AFM images (height signal) of different scan size regions of nanopatterned Au particles on glass surfaces. Lower row: Height profiles of particular areas indicated with a white line in the images above. Particle height lies between 8 – 10 nm.

3.4.3. Functionalization of patterns

Purification of pMHC (IE^k-MCC-Cys)[23]

IE^k-MCC-Cys-producing S2 cells were grown in Sf-900 IIITMSFM medium (Invitrogen) at 27 °C , 90 rpm shaker incubator, and induced for three days at 20 million/ml with 0.5 mM $CuSO_4$. The supernatant was collected by centrifuging the cells down at 3000 rpm for 10 min and filtered through 0.22 µm Millipore Stericup filters (Millipore). 1 mM EDTA and 0.05 % azide was added to the supernatant to prevent protein degradation. The purification of IE^k-MCC-Cys was carried out following standard cobalt column affinity purification at 4 °C . His PurTM resin (Thermo scientific) was washed with equilibration buffer (50 mM sodium phosphate, 300 mM Sodium chloride, 10 mM Imidazole, pH 7.4) and the equilibrated resin was stirred overnight slowly with the filtered supernatant at 4 °C . The resin was then transferred into an empty column cartridge (Thermo scientific) and washed with five resin-bed volume of equilibration buffer three times. The protein was eluted with elution buffer (50 mM sodium phos-

[23] Purification of protein was performed by David Depoil, Skirball Institute of Biomolecular Medicine and Department of Pathology, University School of Medicine, New York.

phate, 300 mM Sodium chloride, 150 mM Imidazole, pH 7.4). The absorbance of the eluted fractions was measured at 280 nm and run in SDS-PAGE gel for protein detection. All cobalt fractions containing IE^k-MCC-Cys (molecular weight 65 KDa) were pooled and further purified through a gel filtration column, HiLoad 16/600 Superdex 200 prep grade (GE healthcare) in AKTA xpress.

Background passivation and immobilization of his-tagged proteins on Au nanoparticles

Substrates were rendered hydrophilic by a reactive H_2 plasma (6 min, 0.4 mbar, 150 W, TePla 100-E, Wettenberg, Germany) before being placed into a custom-made glass rack and transferred into a clean glass flask containing a 1 mM solution of the linear poly-(ethylene glycol) mPEG2000-urea (CH_2-O-(CH_2-CH_2-O)$_{43}$-NH-CdO-NH-CH_2-CH_2-CH_2-Si(OEt)$_3$) in dry toluene (Merck) and 0,05 % triethylamine (99,5 %, Sigma Aldrich). Samples were kept at 80 °C under nitrogen atmosphere for at least 12 h to guarantee the formation of a covalently coupled homogeneous PEG layer. Slides were then removed from the flask and sonicated three times for 5 min in ethylacetate (p. A., Merck) and three times in methanol (p. A., Sigma Aldrich) in order to remove the PEG residues, which only had adsorbed non-specifically and then dried. The glass slides were immediately placed upon a droplet of NTA-thiol (1 mM, SuSoS AG, Switzerland) in pure ethanol (Sigma-Aldrich) and incubated for at least one hour at 4 °C , then rinsed with pure ethanol and dried with pure nitrogen. Glass bottoms of 8 well Lab-Tek Chambers (Sigma-Aldrich) had been removed and were now replaced by the bio-functionalized surfaces. Eventually, chambers were incubated for at least 20 min in a 100 mM aqueous solution of nickel-chloride ($NiCl_2$), rinsed with PBS, followed by an incubation with his-tagged pMHC (5 µg/ml) over night at 4 °C . Before seeding of cells samples were intensively rinsed with PBS. Additionally, several types of control surfaces were used. For positive controls proper Lab-Tek-chambered glass slides were incubated with pMHC or entirely Au-coated glass slides were biofunctionalized with NTA-Ni and His-tagged pMHC as described above. Negative controls were either (i) glass slides without Au nanoparticles, passivated with PEG and then functionalized the same way as the structured surfaces or (ii) conventional Lab-Tek chambered glass slides without any treatment.

In order to present adhesive RGD in the background instead of PEG the protocol was slightly adjusted: Background passivation was done as described above but only with a different type of PEG[24], which was equipped with an alkyne group providing the

[24]The PEG and also the cRGD-N_3 were kindly provided by Seraphine Wegener and Franziska Schenk.

possibility of binding to an azide group. Dry passivated surfaces were then incubated for two hours in an aqueous solution of 150 µM cyclic RGD exhibiting an azide group (cRGD-N_3), 1 mM copper(II) sulfate, 100 mM ascorbic acid and 100 mM buffer (TRIS) at room temperature. Then substrates were rinsed with Milli-Q water before further processed as described above (except for the NTA, which was not only dissolved in pure ethanol but also water in a ratio of 1:1 in order to prevent damaging of pMHC).

Creating pMHC islands with the NanoeNabler™ system

Samples were passivated and functionalized with NTA-Ni as described in the previous section 3.4.3. Protein solutions were prepared at a concentration of 5 µg/ml in PBS with 10 % glycerol in order to prevent evaporation. The scanning patterning tool (SPT) (SPT-S-C10S, BioForce Nanosciences, Inc., USA) was loaded with approximately 1.0 µl of protein solution. Spotting with the NanoeNabler™ system (BioForce Nanosciences, Inc., USA) was done with a force set point of 0.01 V (indicated in Volt since it refers to the deflected signal of the laser on a photodiode), a withdrawal distance of 40 – 50 µm and a spotting velocity of 0.5 µm/s.

3.4.4. Molecular occupation rate of particles

Determination of number of molecules per individual particle

Samples were prepared, processed and evaluated as described in the fabrication, bio-functionalization and image analysis section. The background was bio-inert due to the covalently bound PEG layer and particles served as anchor for the pMHC, I-E^k-2xHis_6-MCC-Atto655 (ATTO-TEC, Siegen, Germany; purification and labeling of the pMHC molecule was performed by Dr. Markus Axmann). The concentration of the pMHC was 5 µg/ml for the bulk measurements and was decreased by a factor of 100 to determine the single molecule signal. All experiments were performed on a modified Axiovert 200M epi-fluorescence microscope (Zeiss, Germany) at 37 °C (Incubator XL S1, Heating Stage P Lab-Tek S1, Objective Heater S1, Zeiss). For excitation of the fluorophore, a diode laser (iBeam smart 640, Toptica, Germany), which was directly modulated in time, was applied. The laser light was coupled into the microscope *via* its rear port using a custom-build free-beam-path optical system. The field of sample excitation was limited using a rectangular aperture in the optical pathway. The sample was excited *via* a 100 x, NA = 1.46 Apochromat objective (Zeiss) for an illumination time $t_{ill} = 1.0$ ms at 640 nm with an intensity of 5 kW/cm^2 (measured at the sample). The excitation wavelength was separated from the fluorescence using a dichroic mirror

(z405/515/647/1064rpc, Chroma, USA) in the filter wheel of the microscope. The fluorescence itself was split in the detection pathway using the Optosplit-II-device (Cairn Research, UK) and a custom filter combination (HC Beamsplitter 662 imaging, Brightline HC 685/40, Semrock). Images were recorded on a back-illuminated, liquid-cooled EMCDD camera (iXon Ultra 897, Andor, UK) operated at 17 MHz read-out speed with a varying electron multiplying (EM) gain. A self-written software (Labview, National Instruments, USA) generated the timing protocol for the diode lasers / camera and recorded the images. Images were analyzed using self-written algorithms in Matlab (Mathworks, USA). The position of individual diffraction-limited fluorescence signals as well as its width σ, its intensity and the level of background noise was determined using a Bayesian estimation algorithm. Bayes Rule gives the probability $\rho(D/H)$ of an experimentally obtained intensity distribution D for a hypothesis H as:

$$\rho(D/H) = \rho(H/D) \cdot \frac{\rho(D)}{\rho(H)} \tag{3.19}$$

with H being a Gaussian intensity distribution with the 5 parameters x-position, y-position, width, intensity and noise level (standard deviation of the background signal). Given that $\rho(D)$ is independent of the hypothesis-parameters and equal to 1, yields to:

$$\rho(D/H) = \frac{\rho(H/D)}{\rho(H)} \tag{3.20}$$

The algorithm determines the maximum of the probability $\rho(D/H)$ by variation of the hypothesis-parameters within the prescriptive, theoretical limits for individual and diffraction limited fluorescence signals. Depending on the actual hypothesis-parameters, the expectancy value of the intensity for each pixel is estimated from the underlying Poisson statistics. $\rho(D/H)$ for a whole 5 x 5 pixel sub-image area is calculated as the product of the 25 individual pixel probabilities (for background noise level a 7 x 7 pixel area was used). After localization of the maximum intensity value in the sub-image, a recursive, and for each parameter independent (because of the convex function characteristics of the intensity), a iterative line search method was applied in order to determine the values of all parameters for the maximized probability value. Now, the fluorescence intensity was determined of areas sized 110 µm^2 and compared with the average intensity value of one single pMHC protein. Knowing now the number of pMHC proteins per area this value could be related to the amount of particles within such an area. After correction for the background signal obtained from a sample incubated with unlabeled protein, this value was divided by the calculated average single molecule intensity ($N > 300$). Since we realized that every parameter, like incubation

time and concentration of protein, washing steps and so on, influences the signal intensity, we always followed a strict protocol (see above) and used the chambers which were used for cell experiments. In Figure 3.18 the data is shown for surfaces with particle spacings between 100 – 150 nm. We chose this particular distance range, since this was the critical regime regarding T cell stimulation and we intended to determine the corresponding critical density. It should be noted that the signal from a sample incubated with unlabeled protein did not significantly differ from a sample without protein. A negative control without Au nanoparticles or without the linker molecule yielded similar, negligible results. After correction for the labeling degree of the protein itself (here 40 % and 60 %), the obtained protein density was compared with the Au nanoparticle intensity to calculate the average protein/particle ratio, which is 1.6 ± 0.4 molecules per particle[25]. For a discussion of the distribution of the occupation rate values see section 5.1.

[25] The microscope was set-up by Dr. Markus Axmann and experiments were performed with great support from him.

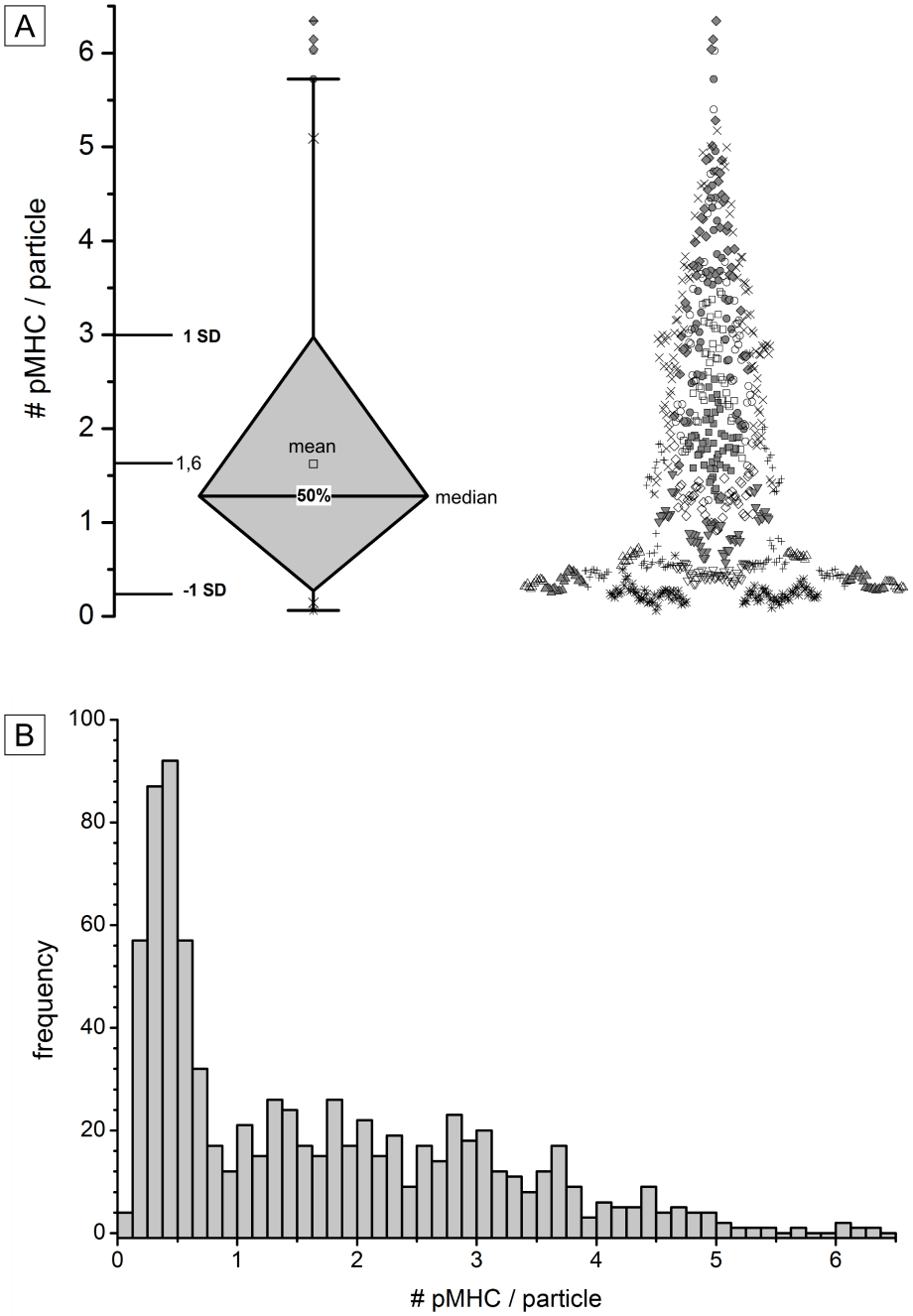

Figure 3.18.: Particle occupation rate | Occupation rate of pMHC molecules per Au particle for surfaces with distances between 100 – 150 nm (For each evaluated surface the distance was determined individually). A) Right side: Box Plot of the data.The mean ratio of molecules to particles was determined to be 1.6 ± 0.4 and the standard deviation (SD) of the single value to be 1.4. Left side: Symbols represent data points of the different surfaces. Same symbols but filled and non-filled, respectively, represent data points from the same surface but out of different chambers. B) Histogram of the occupation rate values.

Part III.

Cell Experiments

Chapter

4

T cell activation experiments

In this chapter we address fundamental questions in TCR triggering and other aspects of T cell activation using the engineered substrates presented in the previous chapter 3. In particular, we aimed at understanding the influence of:

1. number and nanoscale arrangement of pMHC molecules
2. micrometer-scaled and spatially separated activating islands and
3. additional adhesive molecules, such as ICAM-1 and RGD on the process of T cell activation.

As discussed, the detection of antigen and the subsequent appearance of TCR microclusters correlates with very early activation events such as the elevation of intracellular Ca^{2+} level (within seconds) and cell spreading, which comes along with the polarization of the MTOC (within minutes) [90, 221]. On a longer time scale, the T cell starts to secrete signaling molecules (e.g. IL-2 [3]) and to up-regulate activation markers (e.g. CD69 [222]) on the cell surface (within hours), to proliferate [223] and differentiate [224, 225] (within days).

We monitored early as well as late responses, such as intracellular Ca^{2+} level, cell spreading, MTOC polarization and cytokine release of T cells in contact with our substrates. This approach allowed for exploration of nanopatterned antigen arrays regarding their potential to activate T cells and to determine particular requirements for successful activation in terms of nanoscale arrangement of TCR ligands. In the following the influence of different surface parameters on such activation related events are described and evaluated.

4.1. Monitoring activation events

The first signal for the T cell is provided by a specific antigen, loaded on a MHC class II molecule, which becomes recognized by the TCR. Usually, some additional stimulatory

signals are required at least for primary T cells. Co-stimulation for these cells comes from the CD80 and CD86 proteins on the surface of the APC, which can trigger the CD28 receptor. In contrast, T cells which have already been in contact with antigen do not necessarily need some additional co-stimulatory signals.

In our studies we used the well characterized antigen-specific transgenic AND-TCR system in mouse $CD4^+$ T cells[1] [226]. T cells were spleen derived blasts of such AND transgenic mouse expressing a cognate TCR for the MHC class II antigen IE^k complexed with a moth cytochrome C (MCC) peptide[2]. For test reasons a murine T cell hybridoma[3] (3B11; recognizing the $HEL_{34\text{-}45}$ peptide)[4] was used since primary T cells are very sensitive and handling must be done very carefully. In contrast to naive T cells, our primary T cells had already been primed for a specific antigen (T cell blasts) and hence, co-stimulation turned out not to be necessary (see further paragraphs for additional information).

Upon recognition of antigen the intracellular Ca^{2+} level of the T cells raises [26, 31]. Consequently, in order to show very early signaling we attempted to follow the Ca^{2+} influx events. The T cell-APC interface becomes initially organized in multiple of tiny microclusters [81]. These microclusters translocate with time and transform the interface into the highly structured IS [227]. This translocation comes along with spreading and MTOC polarization of the T cell [85, 221]. Obviously, movement of microclusters in the case of immobilized ligands is very restricted. Nevertheless, we investigated to what extent cells were able to spread and polarize their MTOC. Moreover, we monitored the IL-2 secretion after one day of culture time on our substrates serving as a long term indicator for the degree of activation.

4.1.1. Calcium influx events

Elevation of intracellular Ca^{2+} level is a very early activation related event, which happens within seconds upon detection of the specific antigen by the TCR, and is an essential step for the full activation of the T cell [228, 229]. Resting T cells maintain a low concentration of Ca^{2+}, however, antigen detection induces a Ca^{2+} influx from the extracellular space by several routes [230]. It has been reported that such a Ca^{2+} mobilization can be mediated by engagement of a single pMHC on an APC [79] and it

[1] AND mice are alpha/beta TCR transgenic mice produced using the alpha and beta chain genes that encode a receptor specific for pigeon cytochrome c in association with IE^k class II MHC molecules. The TCR expressed in these mice is composed of alpha and beta chains derived from the cytochrome-c specific T cell clones AN6.2 and 5C.c7, respectively. This TCR is termed "AND".
[2] by courtesy of Michael Dustin, New York School of Medicine, New York
[3] Hybridomas are hybrid cell lines created by fusing healthy cells with cancer cells.
[4] by courtesy of Günther Hämmerling, DKFZ, University of Heidelberg

is known that Ca^{2+} signaling activates a plethora of responses within T cells, including secretion, motility, growth and differentiation [231–233].

In order to monitor such an immediate Ca^{2+} influx, Ca^{2+} indicators which photochemically respond to the binding of intracellular Ca^{2+}-ions by changing the spectral properties can be used to determine Ca^{2+} concentrations inside living cells [234]. Since the amount of available primary cells was limited we tested this imaging technique using the T cell line. T cells were loaded with the Ca^{2+} indicator Fluo-4[5] before a small amount of ionomycin was added in order to raise the intracellular level of Ca^{2+}while imaged with a fluorescence microscope. Ionomycin increases Ca^{2+} influx *via* activation of endogenous entry pathways [235] and activates PKCθ to mediate T cell activation [236]. In Figure 4.1 a single T cell is shown for different time points after adding ionomycin. The increased fluorescence signal after 224 seconds indicates the raised intracellular level of Ca^{2+} which has completely decreased after 736 seconds. Hence, we were able to follow the elevation of the intracellular Ca^{2+} concentration; however, we barely achieved to image several cells within one and the same experiment.

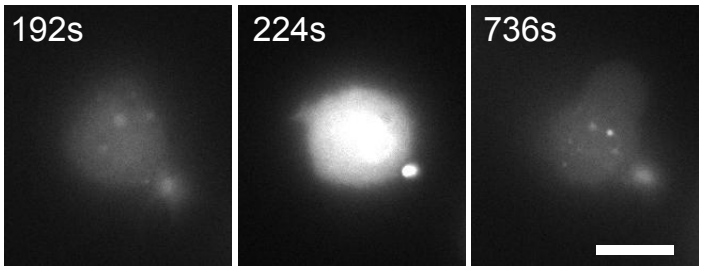

Figure 4.1: Fluorescence microscopy imaging of a Ca^{2+} influx event of a T cell | Ionomycin induces Ca^{2+} influx of a T cell. The level of intracellular Ca^{2+}-ions is visualized by fluorescence intensity (Scale bar: 10 µm).

In summary, the method turned out to be very challenging and time consuming, as the quantitative outcome of single Ca^{2+} influx events is very low. Because of the limited availability of cells we decided that determination of Ca^{2+} influx events are not a suitable method to quantify to what extent nanopatterned antigen arrays are able to activate T cells. We concentrated on other methods which were more promising, since they provided a higher outcome and consequently, much better statistics.

4.1.2. Spreading area

In contrast to adherent cells such as fibroblasts, T cells are characterized through high motility since they constantly patrol the body always scanning the environment. Their key function is not to establish stable long-term contacts to their surrounding but to

[5]Fluo-4 is a green-fluorescent Ca^{2+} indicator used as non-fluorescent acetoxymethyl ester which is cleaved inside the cell to give the free, fluorescent Fluo-4. Fluo-4 is commercially distributed by Invitrogen.

maintain flexibility and motility. However, as previously described, they feature the ability to make transient intercellular junctions. *In vivo* as soon as the T cell's TCR detects foreign antigen the T cell obtains a stop signal and starts to increase its contact area with the APC surface [25, 30]. So far, it is not clear to what extent initial spreading contributes to subsequent downstream signals during the process of T cell activation. There is evidence that T cells need to physically contact APCs over a prolonged period of time (up to several hours) in order to get activated [31]. Observations of T cell – APC interactions, both *in vitro* as well as *in vivo* suggest that the contact time can influence effector functions, qualitatively and also quantitatively. Hence, the cell – cell contact time seems to be a key correlate for establishing an appropriate immune response [237]. In the first instance, integrin-mediated adhesiveness is a key paradigm regulating contact formation of cells to the ECM however, integrins are also involved in intercellular contact formation such as the formation of the IS between T cells and APCs [238–240]. Gathering this information, the initial spreading of T cells crucially contributes to the final activation of the T cell. Therefore, we decided to monitor spreading behavior of T cells on our artificial APC surrogates.

Interference reflection microscopy

The microscopy technique reflection interference contrast microscopy (RICM) also referred to interference reflection microscopy (IRM) is a very suitable method to assess the size of the cellular contact area of a cell to an underlying glass surface. The intensity of the signal is dependent on the proximity of the object to the substrate and therefore, the actual regions of tight contact can be very precisely determined. The microscopy method is based on the interference pattern of reflected linearly polarized light. Reflection happens at the glass surface as well as at the specimen itself and in dependency of the membrane-surface distance, basically three different interference situations for the reflected beams can be distinguished (for further experimental details of the method see section 4.2.2):

1. The membrane is attached (in close proximity) to the glass surface. Destructive interference occurs due to a phase shift of 180° of the beam reflected by the glass compared to that reflected by the membrane and results in a dark pixel in the image.

2. The membrane is not attached to the surface. The phase shift between both reflected beams is no longer 180° and they do not cancel each other out resulting in a brighter pixel in the resulting image.

3. There is no specimen and the reflected light from the glass generates a bright pixel.

As a start and for qualitative testing cells were seeded on different surfaces for 45 minutes in order to assess which conditions are able to induce spreading of primary mouse $CD4^+$ T cell blasts. In Table 4.1 the different surfaces presenting different coatings are listed. Coating of glass surfaces with pMHC and ICAM-1 was done by simple physisorption[6]. Nanopatterns or bare glass surface were passivated by covalently attaching PEG, as described in the surface section (subsection 3.3.1) before the pMHC and/or ICAM-1 were immobilized on the Au nanoparticles. In case of functionalization with both, pMHC and ICAM-1, molecules in suspension were mixed in advance and then randomly immobilized on the Au nanoparticles. By means of IRM imaging it was qualitatively investigated, what kind of surface type supports (✓) or inhibits (-) the formation of tight cell – surface contacts.

Table 4.1.: Induction/inhibition of spreading on different surfaces (Note: "α" stands for "anti-").

Coating	Glass	Nanopattern
nothing	-	-
PEG	-	-
pMHC	✓	✓
ICAM-1	-	-
pMHC + ICAM-1	✓	✓
αCD3	✓	not tested
αCD3 + αCD28	✓	not tested

As expected, antibody coated surfaces (anti-CD3 and anti-CD28), which are routinely used to stimulate T cells by triggering the TCR, were able to induce spreading and adhesion of T cells. Also in agreement with our previous expectations, T cells seeded on bare glass surfaces or coated with PEG were not able to induce spreading. However, even the adhesive ICAM-1 alone, which is the corresponding ligand for the integrin LFA-1, was not enough to initiate spreading, either on glass nor on nanopatterned surfaces. This preliminary test revealed that an adhesive coating alone was not sufficient for T cells to stop and start spreading. Instead, it turned out that T cells in fact, need a stimulatory signal from a specific antigen triggering the TCR to

[6]Physisorption denominates the absorption by physical binding forces primarily the *van der Waals* forces.

start adhesion, which is in agreement with literature [25]. Moreover, we found that any co-stimulatory signal or adhesive molecule, such as ICAM-1 was not crucial for T cells to successfully attach to the surface. Surfaces homogeneously coated with pMHC and even nanopatterns functionalized solely with pMHC were able to induce T cell adhesion. For this preliminary test we only used nanopatterns with rather small inter-particle spacings between 50 and 70 nm. Summarized, the qualitative assay revealed that in our system the only requirement for successful spreading turned out to be a biomolecule which is able to trigger the TCR such as anti-CD3 or pMHC.

Image (A) in Figure 4.2 shows adherent cells as extended dark patches next to non-adherent cells (bright patches). (B) shows T cells, which are either in contact with a nanopatterned or an non-patterned part of the substrate. The left side lacks Au nanoparticles, and subsequently pMHC, thus preventing T cells from initiating cell spreading. On the right side the surface is nanostructured with Au particles and biofunctionalized with pMHC, which allows cells to adhere. Both areas are divided by the so-called dipping edge which is a characteristic of the coating procedure. Within the dipping edge an uncontrolled assembly of micelles and therefore also of particles presenting pMHC is common. The image further demonstrates that T cells selectively adhere to the pMHC functionalized nanostructured area and that non-structured areas are sufficiently passivated that they are unable to induce spreading and adhesion.

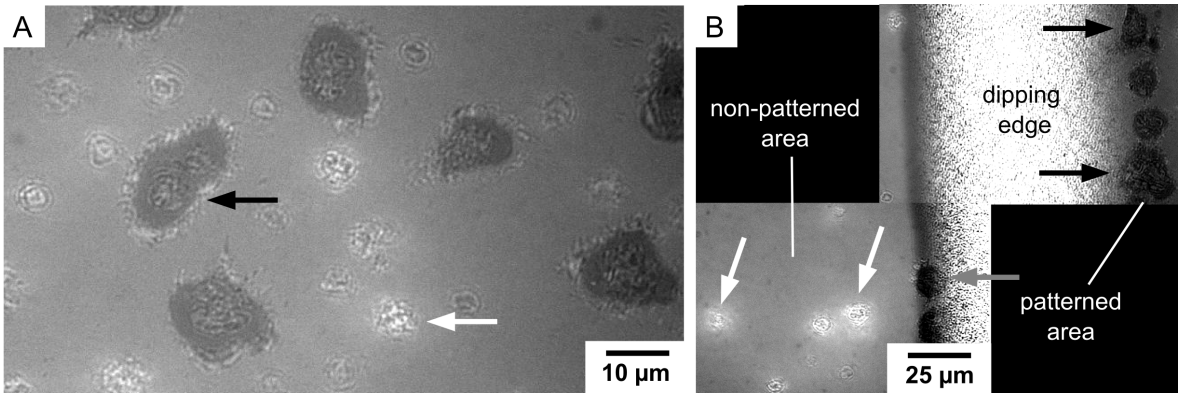

Figure 4.2.: IRM images of T cells on pMHC-presenting nanostructures | Spacing of nanopatterns was 64 ± 9 nm and time of image acquisition was 45 min after initial seeding. (A) IRM images of adherent (dark, black arrow) and non-adherent (bright, white arrow) T cells; (B) Non-adherent T cells on an unpatterned area (left) and adherent T cells on a nanopatterned and pMHC functionalized area (right). The two regions are divided by the dipping edge – where an uncontrolled assembly of nanoparticles is common - which is a characteristic of the fabrication process. The grey arrow indicates a cell adhering to the dipping edge. (Note: B consist of two separate images since due to high magnification (63 x) it was impossible to capture both sides of the dipping edge within one image); (adapted from [160]).

Scanning electron microscopy

Since IRM is not capable of high resolution imaging and, therefore, not able to resolve the nanoscale features, we additionally applied SEM. SEM provides the opportunity of significantly higher magnifications and is therefore suitable to verify the contact formation of T cells and at the same time visualize the underlying Au nanoparticle array.

T cells were seeded and cultured on substrates for 45 minutes similarly as described above, albeit in order to perform SEM an additional treatment of cells was necessary. SEM only works under an highly evacuated environment, and such ambient conditions would cause the cells to be destroyed due to the evaporation of the liquid (mainly water) within the cells. Water evaporates quickly as soon as the ambient pressure decreases. This in turn, generates high surface tensions and alters the structure of the cells. The dehydration in advance guarantees the absence of liquid within the cells. However, the pre-desiccation must be performed in a controlled manner, too, since even under ambient air, drying of cells harms their structure.

The dehydration of cells was done by critical point drying, which is a well-established method to remove liquid out of biological specimen in a precise and controlled manner [241–243]. Critical point drying is based on 'the continuity of state', a thermodynamical condition where a medium's density in the liquid state equals the density of the gas state. Such conditions are reached for a specific temperature T_c, pressure p_c and an according particular density ρ_c, and is known as the critical point P_c. Removal of liquid at P_c causes the surface tension forces between the interfaces to be reduced to almost zero. Hence, evaporation of liquid at the critical point occurs without any force generation at the interfaces and keeps the biological specimen intact.

In practice, after being in contact with the substrate for 45 minutes, the cell's water was first replaced by ethanol during extensive replacement cycles. In the critical point dryer the ethanol was again substituted by liquid carbon dioxide (CO_2) (for experimental details see section 4.2.2). T_c and P_c for CO_2 is 31 °C and 73.8 bar, at which liquid CO_2 becomes hypercritical and the evaporation leaves the cell structures unscathed.

In Figure 4.3 SE micrographs of T cells exemplify how T cells adhere to nanopatterns featuring spacings of 100 – 120 nm between the pMHC anchorage points. T cells spread and some develop extensive filopodial structures. The images prove that T cells adhere to nanopatterns and that pMHC alone seems to be enough if presented in a sufficient density.

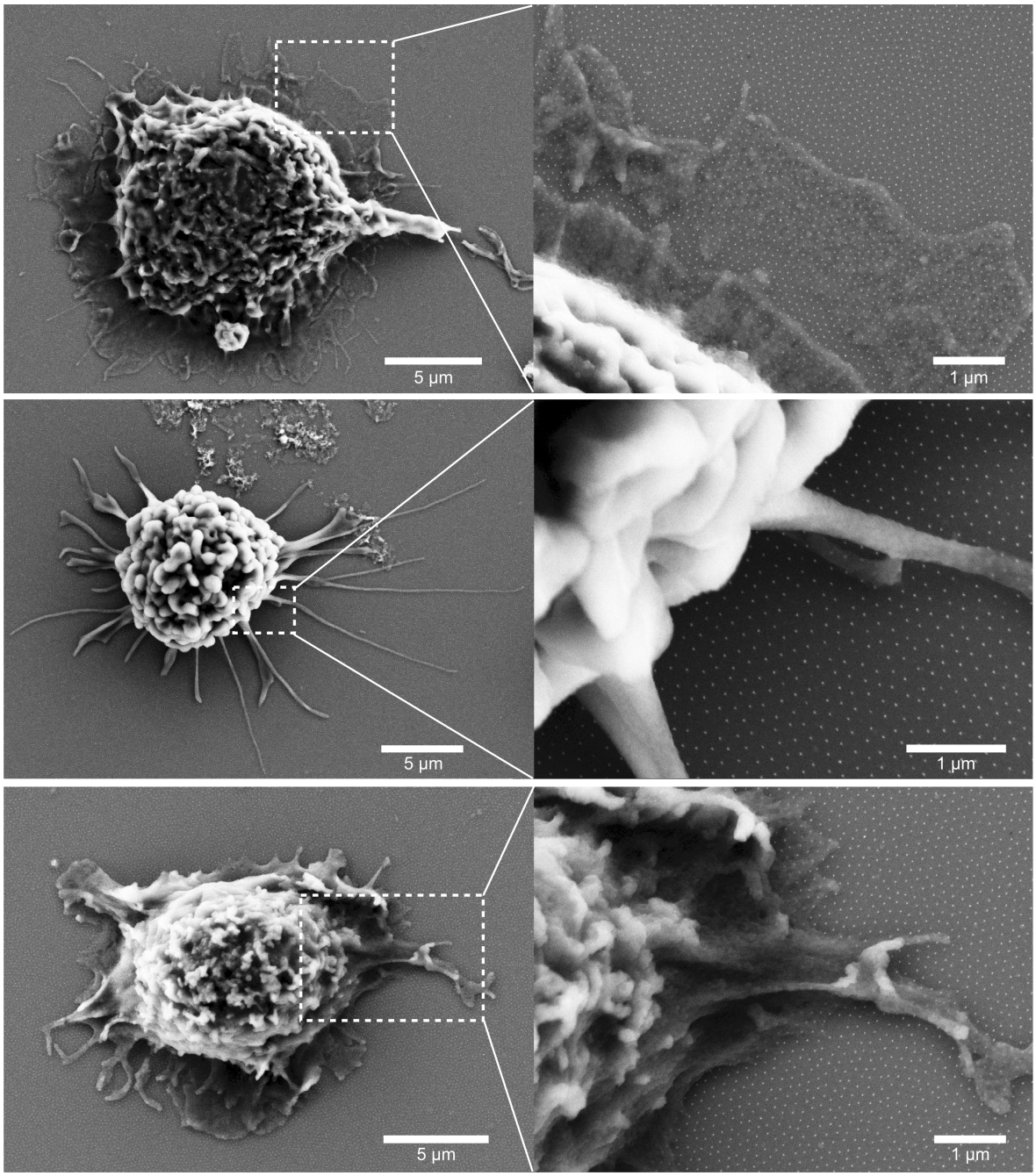

Figure 4.3.: SEM images of T cells on pMHC-presenting nanostructures | Examples of T cells adhering to nanopatterns (100 nm – 120 nm particle spacing) presenting pMHC. Pictures in left column show the entire cells while the right column enlargements of a particular area in order to visualize the underlying nanopatterned Au particles. The T cell in the middle row exhibits many filopodial structures while the other two T cells are well spread. For imaging T cells were fixed and critical point dried in advance (for details see section 4.1.7).

Quantitative analysis of adhesion behavior

Since qualitative analysis revealed that presence of pMHC induces initial spreading and adhesion we then quantitatively evaluated the adhesion behavior of T cells. We seeded cells on nanopatterned functionalized surfaces and assessed the size of contact area as well as the fraction of adherent cells after (45 ± 15) minutes. The choice to start measurements approximately 30 minutes after seeding was based on theoretical background as well as practical experience. The dynamics of IS formation is reported to start initially after antigen detection and to last up to two hours [84]. Once attached, we observed the majority of cells to be adherent for up to two hours and afterwards it was a combination of migrating and to a lower extent spreading. Obviously, we did not start evaluations initially after cell seeding since they had to sink down to the bottom and get in contact with the surface. Once in contact, we found cells to migrate on the surface for some minutes before starting to spread. We estimate that the majority of adherent cells persisted to be attached for up to two hours and afterwards it was a combination of migrating and to a lower extent spreading (For further details regarding the experimental details see section 4.2.1.).

The determination of the amount of spread versus non-adherent cells was done manually since a software-based automated detection routine failed because of the difficulty to distinguish between non-adherent and adherent cells.

As shown in Figure 4.4 (A), we detected the amount of spread cells (dark grey bars) on nanopatterns to strongly decrease with increasing spacing between the adjacent particles, thus low particle densities. Indeed, we even found that most T cells failed to adhere on nanopatterned surfaces with spacing greater that 150 nm. The percentage of adherent T cells was highest (approximately 60 %) on nanopatterned surfaces featuring a short inter-particle distance (30 nm – 80 nm) and a similar amount of spread cells was found on positive control surface (pMHC). On surfaces with more widely separated nanoparticles the percentage of adherent cells continuously decreased down to only approximately 10 % for T cells seeded on surfaces with largest spacings between the protein anchorage points of about 300 nm. Moreover, some of these few adherent cells on low pMHC densities may only have found defects of the pattern, dirt or some unusual protein accumulations. These findings strongly indicate that spreading behavior and the ability to adhere directly correlates with the particle spacing: the higher the spacing, the less adherent cells!

In order to further elucidate the adhesion behavior of T cells we plotted adhesion versus particle density (see Figure 4.4 B), emphasizing the rapid quasi-linear increase in percent adhesion as densities approach 100 μm^{-2}. For greater particle densities, a

plateau is observed suggesting saturation of percentage of adhesion. It seems that in our experimental set-up, if T cells do not discover a sufficient amount of pMHC they fail to establish contact to the underlying substrate. Hence, these data indicate the necessity for a certain minimal density of pMHC molecules for initiation of T cell adhesion and spreading.

Additionally, those cells that even achieved spreading - although they were confronted with inter-particle distances greater than 150 nm - developed only significantly smaller contact areas, compared to cells seeded on surface with particle spacings below 150 nm (see Figure 4.4 A; light grey bars). A Welch's t test[7] yields a p value below 0.0001 which indicates a very significant difference between the mean spreading areas below and above 150 nm. Hence, there is evidence that particle distribution modulates the T cell spreading behavior, both, in terms of successful attachment as well as in terms of the size of the established contact area.

In comparison to the very strong decrease of percentage of adhesion the spreading area does not show such a "collapse" of values. This behavior is due to a simple reason: Each cell that achieves spreading reaches a certain size of contact area, which at least is as large as the projected cell area. Consequently, the contact area cannot converge against zero since for cells failing to spread a contact area cannot be determined.

In summary, we observed that T cells do need a particular amount of pMHC in order to induce spreading, however, it is unclear due to what reason. It might be that a high density of pMHC triggers a high amount of TCRs, which eventually leads to spreading. It is more likely, however, that pMHC molecules additionally serve as anchor points supporting T cell attachment. As soon as enough ligands are in contact with TCRs on the membrane of the T cells, they successfully spread and adhere. In this case the MHC molecules would substitute for adhesive ligands such as ICAM-1. The triggering of the T cell receptor would not be the crucial parameter but the availability of TCR ligands deciding about the success of T cell spreading and adhesion (see subsection 5.2.1 for further discussion).

In the following paragraphs we tested further events, related to the activation of T cells and moreover, we assessed the role of additional adhesive molecules in order to target the unresolved question regarding the role of pMHC – TCR bonds during spreading and adhesion.

[7]The so-called Welch's t test is an adaptation of the Student's t-test designed for testing two samples having possibly unequal variances regarding significant differences of their mean values.

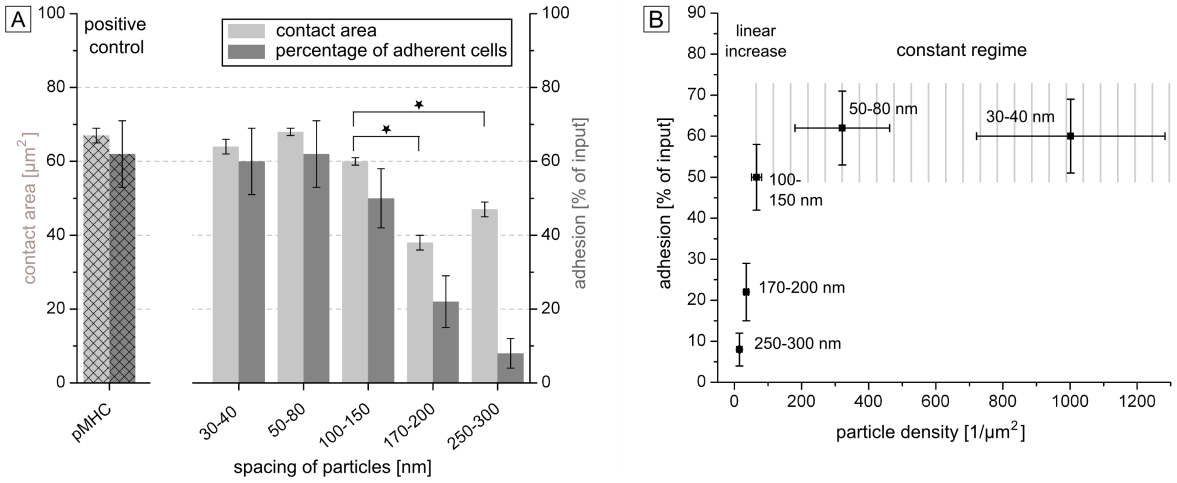

Figure 4.4.: T cell adhesion on nanopatterns | A) Percentage of adherent T cells (dark grey bars) and mean contact cell area (light grey bars) after (45 ± 15) minutes of cell-substrate contact time. (Positive control: pMHC-coated glass surfaces; Star ($\star$) indicates significant differences of mean values according to Welch's t- test: $p < 0.0001$; $n > 100$ spread cells for each mean value, except for cells on surfaces with particle distances greater than 150 nm because of very low cell adhesion numbers). B) Percentage of adherent cells (data presented as in A) plotted as a function of particle density. In both graphs y-error bars correspond to the standard error of the mean while x-error bars in B correspond to the error of the single value.

4.1.3. Polarization of microtubule organizing center

Spreading of T cells comes along with the polarization of the T cell's MTOC. Hence, monitoring the MTOC of T cells allows for verifying that the early activation phase, including the establishment of cell – surface contact was successfully initiated. During formation of the IS between a T cell and a target cell, polarization supports the positioning of the MTOC just beneath the cell-cell interface by remodeling of the MTOC and associated organelles. Secretory organelles inside the T cell become aligned with the IS by such a cytoskeletal reorganization, which enables the directional release of cytokines and/or cytolytic factors towards the target cell [28]. This way, cell polarity modulates the formation of the IS and establishes sustained T cell signaling [221]. In case of $CD8^+$ T cells MTOC polarization is essential for maintaining the specificity of a T cell's cytotoxic responses [244]. For instance, as a cytotoxic T cell prepares to kill its target, it repositions its MTOC to be focused only on the recognized target cell and to prevent harm to any surrounding, healthy tissue [245].

In order to visualize intracellular components immuno-labeling methods are a common and well-known tool [246]. We accessed MTOC polarization by immunofluorescence labeling and imaging of α-tubulin. Immunofluorescence uses the specificity of antibodies against their antigen to bind fluorescent dyes to specific biomolecules (in this

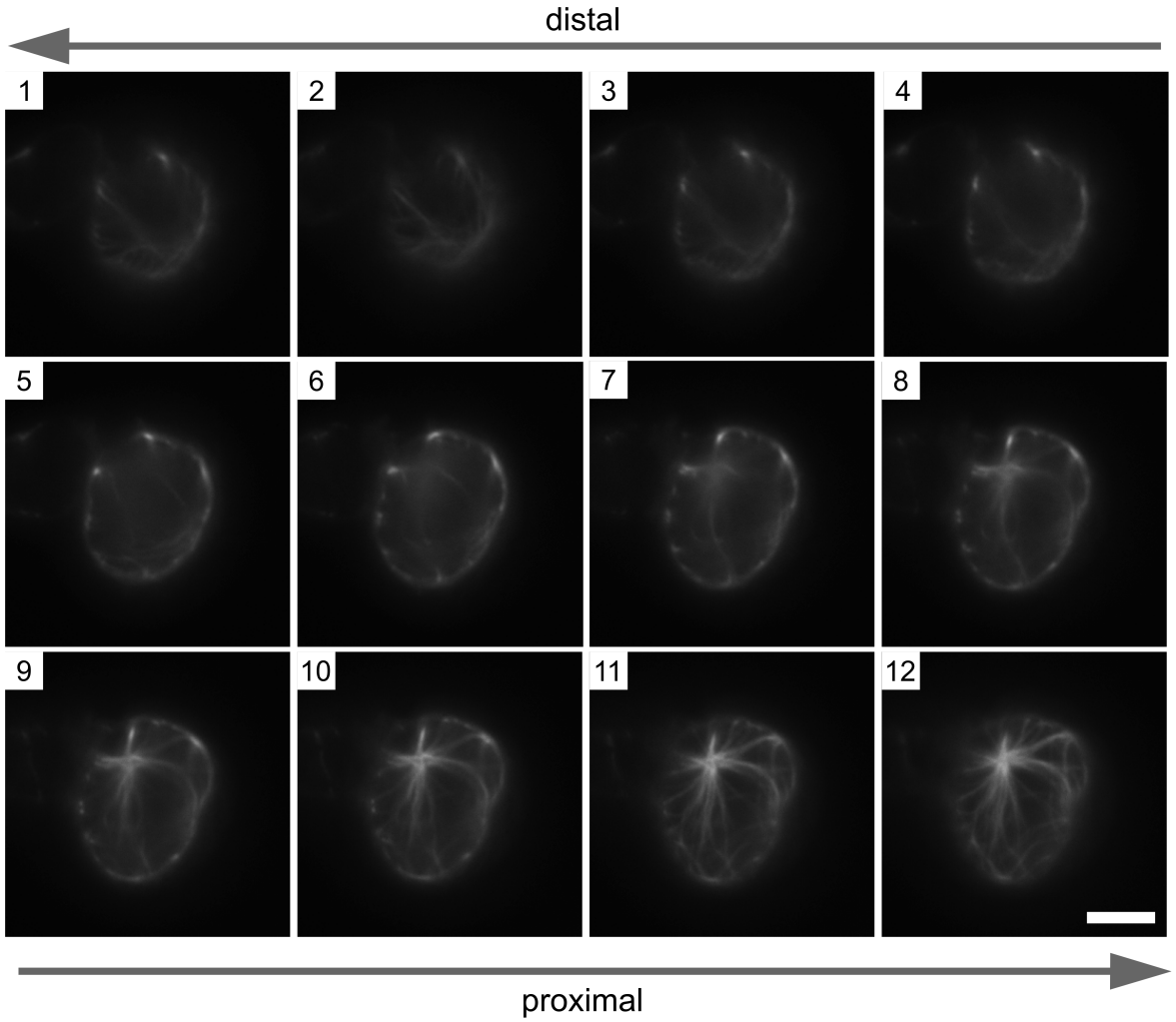

Figure 4.5.: z-stack fluorescent images of a T cell exhibiting a polarized MTOC *En face* view of a T cell on a nanopatterned pMHC surface with polarized MTOC towards the surface. The different pictures were acquired at different z-positions (distinct distances from the substrate surface). From image 1 ($\approx$ 10 µm) to 12 (very close proximity) the focal plane approaches step-wise towards the surface. In image 10 – 12 the polarized α-tubulin is visible as fiber-like structures from the center to the rim proving the polarization of the MTOC (Scale bar: 5 µm).

case α-tubulin). This approach allows visualization of the distribution of the selected molecule throughout the specimen. α-tubulin is one of the most common members of the tubulin[8] family and makes up microtubules[9]. Therefore, visualization of α-tubulin serves as qualitative marker of MTOC polarization and hence, physiological reorganization of the cell as a consequence of early activation events. In Figure 4.5 a cell with polarized MTOC is shown. The images are acquired with *en face* view of the cell at different z-positions. In close proximity to the surface (image 11 + 12) a quasi-radial structure appears from the center to the rim, which indicates the polarization of the centrosome towards the surface.

We again tested different surfaces for their ability to induce cells to polarize. With this assay it was only possible to detect a successful (✓) or non-successful polarization (-). Only cells that adhered could be immunolabeled since non-adherent cells were simply washed away during the labeling procedure, which included several washing steps. Hence, MTOC polarization (see Table 4.2) strongly correlated with attachment of cells to the substrate and results are, logically, the same as in the case of adhesion.

Table 4.2.: Induction/inhibition of MTOC polarization (Note: "α" stands for "anti-")

Coating	Glass	Nanopattern
nothing	-	-
PEG	-	-
pMHC	✓	✓
ICAM	-	-
pMHC+ICAM-1	✓	✓
αCD3	✓	not tested
αCD3 + αCD28	✓	not tested

In Figure 4.6 T cells with polarized α-tubulin are shown. The attachment of cells to the surface came along with the polarization of the centrosome. Hence, we observed on entirely coated pMHC or anti-CD3 surfaces (positive controls) as well as on nanopatterns functionalized with pMHC such a polarization of the α-tubulin. On nanopatterns the attachment and consequently also the cell polarization was dependent on the spacing of adjacent particles. We observed polarized T cells only on nanopatterns with

[8]Tubulins belong to the globular protein class, which are spherical proteins that form colloids in water. Globular, fibrous and membrane proteins are the main protein classes.

[9]Microtubules are highly dynamic protein filaments maintaining the structure of the cell. They are part of the cytoskeleton.

spacings below 150 nm, above it was impossible to detect any polarized cells. The first reason is that the number of adherent cells was very low, and with high resolution fluorescence microscopy, it is generally difficult to detect only very few targets, which are scattered over large areas. Second, we speculate that adhesion forces of T cells on nanopatterns with spacings above 150 nm were lower and T cells were simply detached from the surface during labeling procedure.

We can therefore, conclude that the polarization, similar to spreading of T cells, was dependent on a certain density of pMHC molecules. Above a particular spacing we did not see any polarized α-tubulin, which is in so far obvious since only attached cells can polarize their centrosome. Hence, if cell-substrate connection was successfully achieved by a sufficient amount of T cells, then we could also detect T cells with a polarized MTOC, verifying that T cell spreading comes along with polarization.

4.1.4. Quantification of IL-2 concentration as an index of activation

In vivo, after detection of antigen by the TCR on an APC, the IS starts to form between the T cell-APC pair and results in the activation of the T cell. The IS keeps persisting for some time before the connection is dissolved and the T cell starts to migrate and to secrete chemical messengers which have certain purposes, such as recruitment of other immune cells. IL-2 is such a growth factor, which furthermore acts as an autocrine agent[10], capable of binding to autocrine receptors on the surface of the cell by which it originally became secreted. As soon as the TCR becomes triggered, the cell's former low affinity IL-2 receptors transform into receptors showing strong affinity to IL-2. The secreted IL-2 binds to the high-affinity receptors at the cell membrane, hereby further stimulating the T cell [247, 248].

The IL-2 concentration is a very common indicator providing information about the activation rate of an entire cell population. The higher the IL-2 concentration in the surrounding medium the more cells secrete IL-2 due to a foregoing stimulation. As a consequence, the IL-2 concentration directly provides information about the stimulatory potential of the substrate.

We assessed the amount of IL-2 secreted by T cells activated on nanopatterned substrates after 24 hours in order to investigate the effect of ligand distribution on T-cell activation long term. In each experiment several hundred thousand cells were analyzed on average. We defined the index of activation, $I_{activation}$, as the amount of IL-2 (X_{IL-2}) secreted by around 1.5×10^5 cells after 24 ± 1 hours on the individual

[10] Autocrine signaling denominates a signaling process in which a cell secretes signaling molecules which can then bind to the membrane receptors of the same cell.

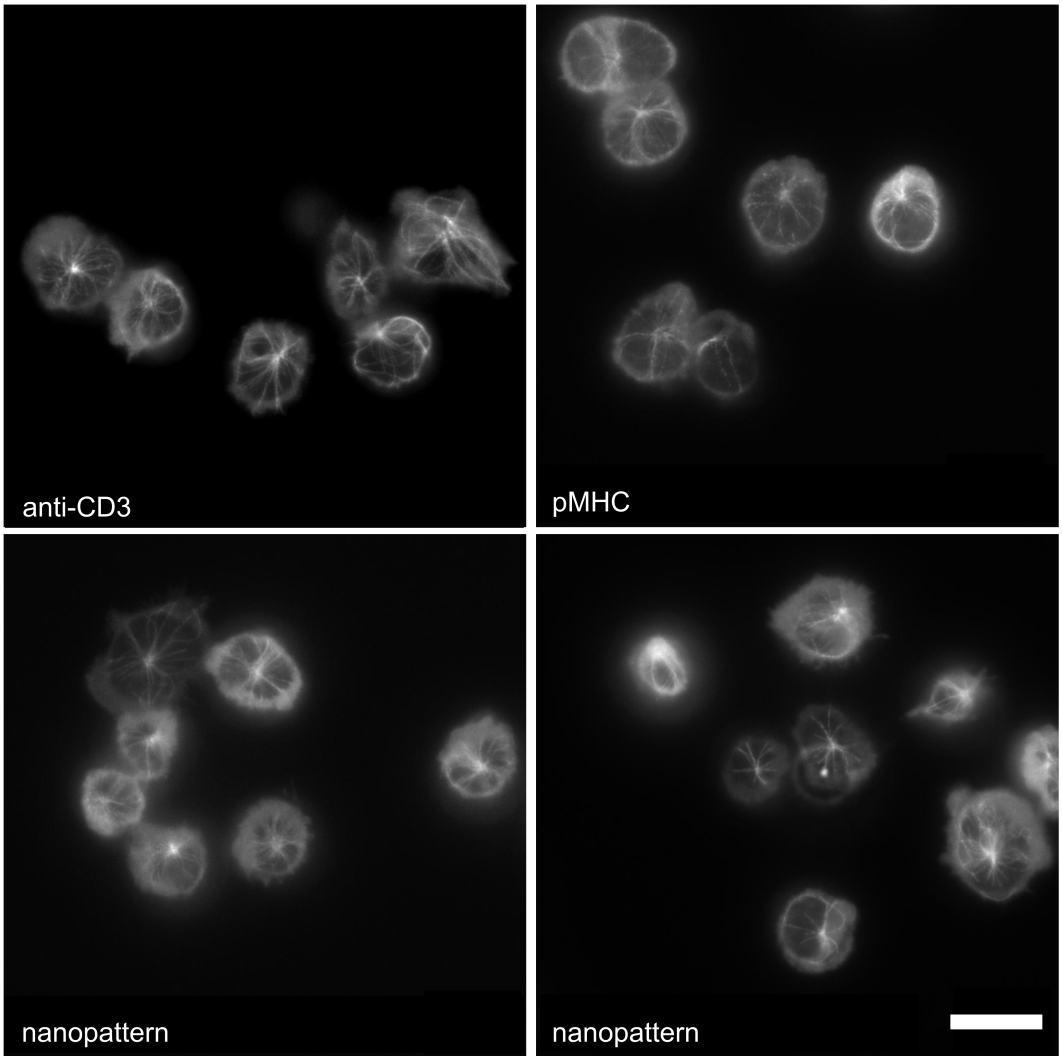

Figure 4.6.: Fluorescent images of T cells exhibiting a polarized MTOC | *En face* view of T cells glass coated with anti-CD3 and pMHC, respectively as well as on nanopatterns functionalized with pMHC. The polarized α-tubulin is clearly visible and proves the polarization of the MTOC (Scale bar: 10 µm).

surfaces related to the amount ($X_{control}$), which was secreted by the same amount of cells on entirely pMHC-coated control surfaces during the same experimental time:

$$I_{activation} = \frac{X_{IL-2}}{X_{control}} \tag{4.1}$$

Such a "normalized" value has the advantage over absolute IL-2 concentrations that values gained at different days, out of different cell batches are better comparable. Cells always behave differently and it can occur that different cell batches show different activation potential. As long as every surface type is included in every individual experiment the fluctuations would average out. However, it was impossible to include

every surface type in each experiment due to many different parameters which were tested. Therefore, relating the absolute values to a standard value was necessary (for further details see also section 4.2.1).

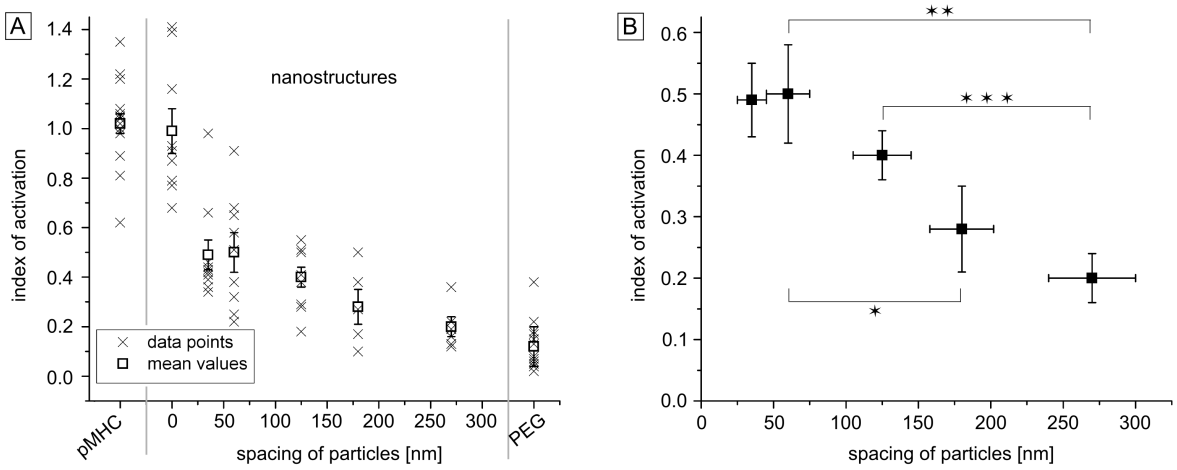

Figure 4.7.: Index of activation over particle spacing | The normalized IL-2 secretion of T cells on different surfaces plotted against the distance between pMHC ligands. (A) shows individual measurements and mean values of the index of activation as a function of the particle distance. On the far left and far right of the graph data from cells on PEG-coated surfaces (negative control) and entirely pMHC-coated surfaces (positive control) are shown. The values for substrates with "0" particle distance were gained on entirely Au-covered surfaces. (B) selectively shows only the mean values gained on the different nanopatterned surfaces (same data as in (A)). (Stars in (B) indicate significant differences of mean values according to Welch's t- test: ($\star$) $p = 0.045$; ($\star\star$) $p = 0.012$; ($\star\star\star$) $p = 0.005$; The y error bars in B correspond to the standard error of the mean, x error bars to the standard deviation of the single value.

In Figure 4.7, $I_{activation}$ is shown as a function of particle spacing. Positive control data were obtained on substrates entirely coated with stimulating pMHC while negative control values on surfaces entirely covered with bio-inert PEG layer, which is known to prevent any cellular interaction. The additional positive control ("0" spacing) was based on surfaces fully covered with Au and functionalized with pMHC, which is similar to substrates routinely used for T cell activation. We did not observe a significant difference of IL-2 secretion between T cells on adsorption-based pMHC-coated glass surfaces and cells on Au-coated surfaces functionalized with NTA-Ni^{2+}-pMHC. Therefore, we conclude that at high pMHC densities the immobilization strategy does not impact IL-2 secretion. As expected, the highest values are obtained from cells on pMHC surfaces, whereas the lowest values are from cells on PEG surfaces, which serve as a negative control. Moreover, we observe a significantly higher $I_{activation}$ for T cells on the positive controls compared to those cultured on nanopatterns, even for low nanoparticle spacings. Since we detected the number of adherent cells to be in the

same range, the reason for this "jump" is presumably not the number of activated cells. Hence, we suppose that, since the pMHC density of continuously coated surfaces is significantly higher, T cells become activated more efficiently resulting in an increased amount of secreted IL-2 (for further discussion see section 5.2).

T cells seeded on nanostructures show a quasi-linear decrease of IL-2 release with increasing particle distance. The mean values of $I_{activation}$ of surfaces featuring spacings above 150 nm are significantly different from those obtained on patterns exhibiting distances below and equal 150 nm (see Figure 4.7 B).

Figure 4.8 shows the $I_{activation}$ plotted as a function of particle density. If $I_{activation}$ is represented in such a manner, we observe a strong decrease of $I_{activation}$ below, and a constant IL-2 secretion above a threshold particle density of approximately 100 – 200 particles per µm^2. In the regime below 100 particles per µm^2 IL-2 secretion depends linearly on the particle density while above saturation is observed. This data suggests that IL-2 secretion seems to be predominantly regulated by the global pMHC concentration. However, we cannot exclude that also the distance between adjacent particles plays a key role and causes the $I_{activation}$ to collapse when T cells are confronted with low pMHC densities.

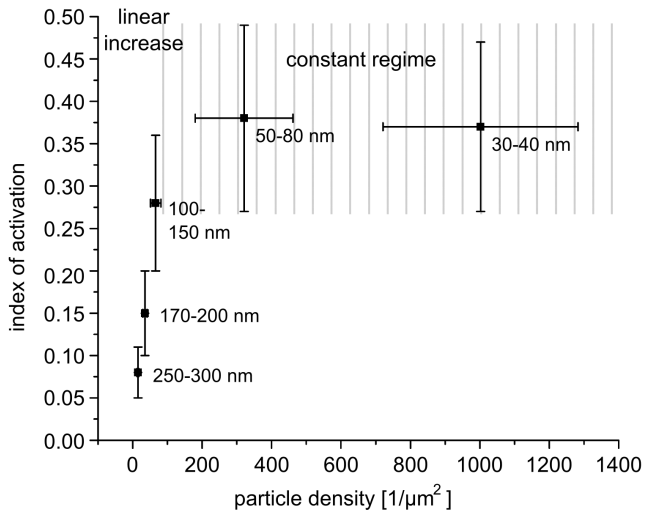

Figure 4.8: Index of activation over particle density | Mean values of the index of activation for T cell populations seeded on nanopatterns as a function of global particle density. The index of activation on surfaces covered entirely with PEG, but processed identically (incubation with the same linker and protein solutions as the nanopatterned surfaces), was set as the background value. This value was subtracted from the IL-2 values measured on the nanopatterned substrates. The error bars were calculated using Gaussian error propagation.

4.1.5. Investigating effects of inter-particle spacing *vs* density of particles

The response of T cells to the continuous nanopatterned pMHC could either reflect the requirement for a certain number of pMHC molecules in the contact area or a critical distance between pMHC molecules. In order to distinguish between the two, we

Table 4.3.: Features of micro-nanopatterns

surface number	1	2	3	4
inter-particle distance [nm]	70 ± 10	70 ± 10	110 ± 15	110 ± 15
diameter of micro-domains (a) [µm]	1.5	1.5	1.5	1.5
micro-domain grid spacing (b) [µm]	3.0	5.0	3.0	5.0
local particle density [particles/µm^2]	236 ± 67	236 ± 67	95 ± 26	95 ± 26
global particle density [particles/µm^2]	46 ± 15	17 ± 5	19 ± 6	7 ± 2
particle spacing of extended nanopattern with respective global particle density [particles/µm^2]	158	261	247	406

compared the effect of local versus global particle density on T cell response. Continuous nanoparticle arrays have identical local and global particle densities. In contrast, micro-nanopatterned particles, can be prepared with the same local density (within their micro-domains), but lower global densities. Conversely, micro-nanopatterned surfaces with the same global particle density as continuous nanopatterned surfaces feature significantly more densely arranged particles within their micro-domains. We prepared four micro-nanopatterned surfaces with a global particle density between 7 and 46 particles per µm^2 (see Table 4.3 for details). The local particle density values within the micro-domains, 236 and 95 particles/µm^2), were chosen based on particle density values that caused spreading, MTOC polarization and IL-2 secretion on continuous nanopatterned surfaces or were within the critical regime, respectively. However, the global particle density of micro-nanopatterned surfaces, was in the range where adhesion and spreading on continuous nanopatterned pMHC was very reduced or prevented. Using this strategy we were able to discern whether spatially confined activating islands are sufficient to induce T cell adhesion, spreading and IL-2 production or whether the over-all availability of pMHC is the critical parameter for T cells to become stimulated.

On micro-nanopatterned substrates we detected very low adhesion ranging between 10 % and 18 % and almost no MTOC polarization. The behavior seemed similar to that of cells seeded on extended nanopatterns exhibiting a spacing above the threshold spacing of 150 nm. Accordingly, IL-2 secretion of cells seeded on micro-nanopatterns was very low. In Figure 4.9 (A) the $I_{activation}$ is plotted as a function of particle density. Red stars indicate data obtained on micro-nanostructured surfaces. The black squares represent the data of cells on nanopatterns as shown in the previous paragraph in Figure 4.8. For each data point the average $I_{activation}$, which was secreted by T cells on

negative control surfaces (PEG) was set as the background value and subtracted from $I_{activation}$ for each nanopatterned substrate.

The $I_{activation}$ of cells on micro-nanopatterns matches the values of cells on continuos nanopatterns with larger spacing but identical global particle density. This means secreted IL-2 levels were in the range of those cells cultured on surfaces with extended patterns featuring a significantly less dense nanopattern (larger spacing) but similar global particle densities. Figure 4.9 (B) depicts an enlargement of the linear increasing section of the $I_{activation}$ plotted over particle density. The linear fit to both, $I_{activation}$ values obtained on micro-nanopatterns (red) as well as on nanopatterns (black), shows the proportionality of IL-2 secretion to the density of particles within a certain regime. The slope of the linear fit for micro-nanopatterns is slightly larger than that of the continuos nanopatterns suggesting that the particle distance influences IL-2 secretion, too, but only as a secondary effect. Summarized, the data indicates that activation of T cells is predominantly regulated by the global pMHC concentration and depends on the local spacing of the pMHC pattern only as a higher order effect. For a detailed discussion of the effects described above, see section 5.2.

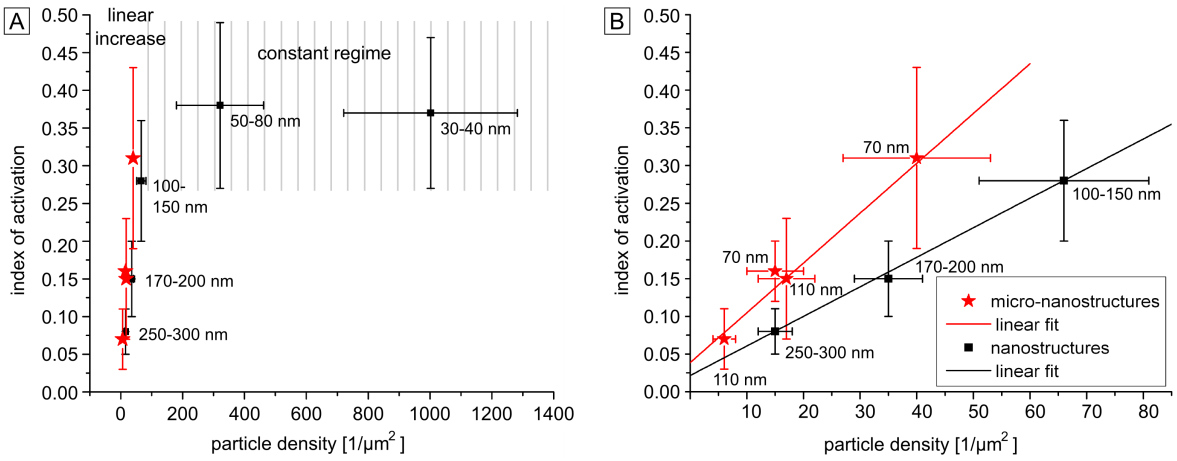

Figure 4.9.: Index of activation over particle spacing - micro-nanopattern *vs* nanopattern | The $I_{activation}$ on different micro-nanopatterned and nanopatterned surfaces plotted against the particle density. A) Mean values of cells cultured on nanopatterned (black data points (squares), $n > 5$, same as shown in Figure 4.8) and micro-nanopatterned (red data points (stars), $n = 4$ for each data point) as a function of global particle density. B) Enlargement of data shown in (A). Within the critical regime the $I_{activation}$ depends linearly on the particle density. The slope of the linear curve for nanopatterns is smaller than that of micro-nanopatterns suggesting that there is also an effect of particle spacing.

4.1.6. Introducing adhesive ICAM-1 molecules to the nanopatterns

The critical TCR ligand density described in subsection 4.1.4 is significantly higher than the previously reported low pMHC thresholds, some of which were determined to be in the one digit range [79, 80]. However, in contrast, to these previous reports where T cell activation was achieved using real APCs or lipid bilayers presenting ICAM-1 together with pMHC, our purely pMHC-based approach did not provide co-stimulation or adhesive support.

In order to investigate the effect of ICAM-1 on the adhesion process in our system we immobilized pMHC and ICAM-1 simultaneously on the nanopattterned particle arrays. We mixed pMHC and ICAM-1 in advance, so that they competed for binding to the NTA linker attached to the Au particles. We started with analyzing the contact area of spread cells. As shown in Figure 4.10, results suggest that additional adhesive ICAM-1 increases in all cases the average contact area about approximately $20-30\,\%$. The strongest increase could be observed for high particle spacings of $250-300\,\mathrm{nm}$ indicating that the ICAM-1 supports adhesion and can, at least in terms of contact area, compensate for the low densities of pMHC. However, we did not detect a significant higher amount of spread cells if additional ICAM-1 was present (data not shown). Cells still were barely able to attach to surfaces featuring nanoparticle spacings larger than $150\,\mathrm{nm}$. Therefore, we assume that the situation remains as described before: The amount of anchor points the T cell is in contact with is not sufficient to induce adhesion. However, given that cells achieve to spread, then apparently spreading is supported by the additional ICAM-1 since contact areas increase. Nevertheless, the results we present are only preliminary and further experiments are required, to specify the exact effect of additional ICAM-1 on the nanoparticles. Furthermore, in our eyes such an approach, which binds two distinct biomolecules randomly to the particles, loses some of its controllability since it is not clear how molecules distribute on the nanoparticles. A more specific strategy to introduce additional adhesive molecules is therefore described in the next subsection 4.1.7.

4.1.7. Introducing an additional adhesive background

Due to the weak adhesion and low IL-2 secretion on pMHC-only nanopatterns and also on pMHC/ICAM-1 nanopatterns within a certain low pMHC density regime we decided to introduce an adhesive background instead of the bio-inert PEG. With this strategy we intended to investigate if the critical regime we found is affected by the presence of a sufficient amount of additional adhesive molecules. We used the previously described click-chemistry system to bind cyclic RGD featuring an azide group (cRGD-N_3), to the

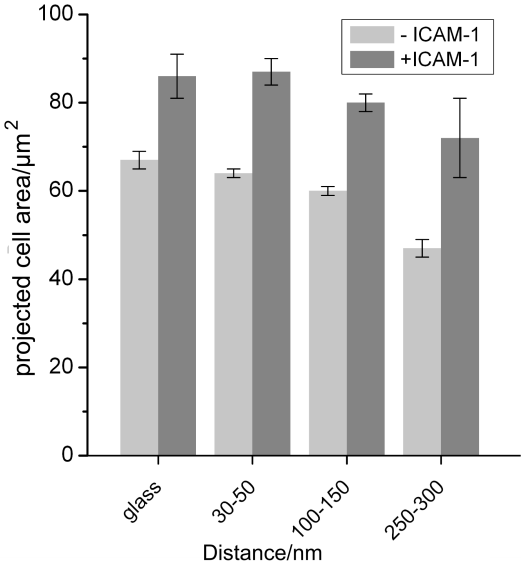

Figure 4.10: Mean contact area of T cells on surfaces presenting ICAM-1 and/or pMHC | Mean contact cell areas on glass/nanopatterns presenting pMHC with (dark grey bars) and without (light grey bars) additional ICAM-1 after (45 ± 15) minutes of cell-substrate contact time.

modified PEG-background. T cells express a type of integrin and thus, the adhesive molecule RGD is expected to support the contact formation process of the T cell to the underlying substrate. The reason why we chose in this case RGD instead of ICAM-1 is due to experimental limitations. The ICAM-1 was, so far, not available with any other end group than the His-tag. However, in order to guarantee the specificity of binding only to particular areas (adhesive molecules to the background *vs* stimulating molecules to the Au particles) a distinct immobilization approach was required.

Qualitative analysis of adhesion behavior

In contrast to the case where ICAM-1 was additionally immobilized on the Au nanoparticles, cells adhered on large spacing patterns as well as on micro-nanopatterns when RGD was present in the background. The adhesion rates were in the range of cells seeded on nanopatterns featuring spacings below the critical spacing of 150 nm. We could show that neither a critical regime or a threshold value for pMHC density nor a critical spacing was still existent. In Figure 4.11 cells on micro-nanopatterns featuring global pMHC densities below the threshold value but an adhesive RGD background are shown. The shape of contact area of T cells obviously represents the underlying micropattern.

This adaptation to the underlying micro-domains hints to the assumption that T cells preferentially adhere or form contacts to those areas presenting stimulating pMHC. It seems that the microcluster formation especially takes place on the particle islands as long as the surrounding provides an adequate environment for cells to settle. Probably, as soon as the background does not consist of a bio-inert molecular layer but instead

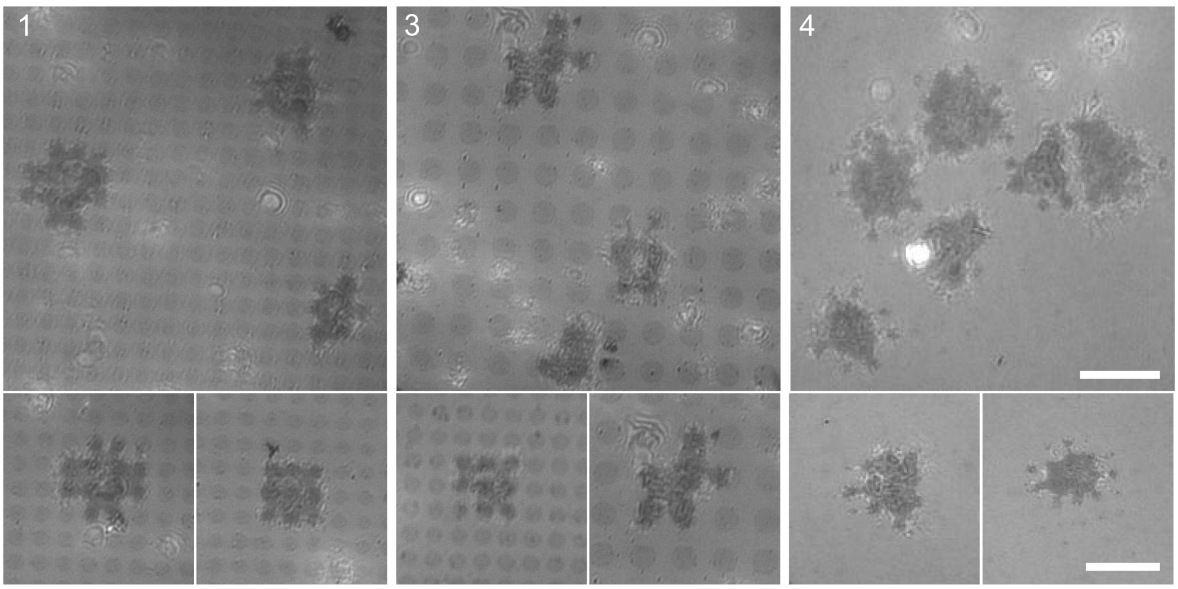

Figure 4.11.: IRM images of T cells on micro-nanopatterns | IRM images of adherent T cells (dark patches) on micro-nanopatterns featuring different particle spacings/microstructure dimensions and an adhesive RGD background (Note: Surface parameters are according to parameters for the specific surface number (**1, 3, 4**) as summarized in Table 4.3. The higher the spacing the less visible is the micropattern, as in the images on the right column). The shape of the T cells adapts to the micro-domains presenting stimulating pMHC. We assume that T cells preferentially adhere and form microclusters at regions where there is pMHC in combination with RGD (Scale bar: 10 µm).

adhesive molecules, T cells are able to attach to the surface and start to scan the surface for pMHC. The tight contact formation seems to happen preferentially in those regions where pMHC is present. We assume that as soon as T cells do not depend on pMHC bound to Au particles as the only possible anchor points to attach, a significantly smaller amount of pMHC, as also reported in literature, is sufficient to support spreading, microcluster formation, and adhesion.

Moreover, as aforementioned, we also detected T cells to be adherent on continuos patterned surfaces featuring up to 300 nm spacing in case of RGD presentation through the background. Since the BCML technique is, so far, limited in the generation of patterns to inter-particle spacings of approximately 300 nm we were not able to test spacing/density limitations in case of homogeneous nanopatterns presenting an adhesive RGD background.

Scanning electron microscopy of T cells on micro-nanopatterns

In order to further elucidate the preferential contact formation on the particle islands we again examined adherent T cells on micro-nanopatterns with the SEM.

We detected cells to be adherent, as already shown by IRM, on micro-nanopatterns

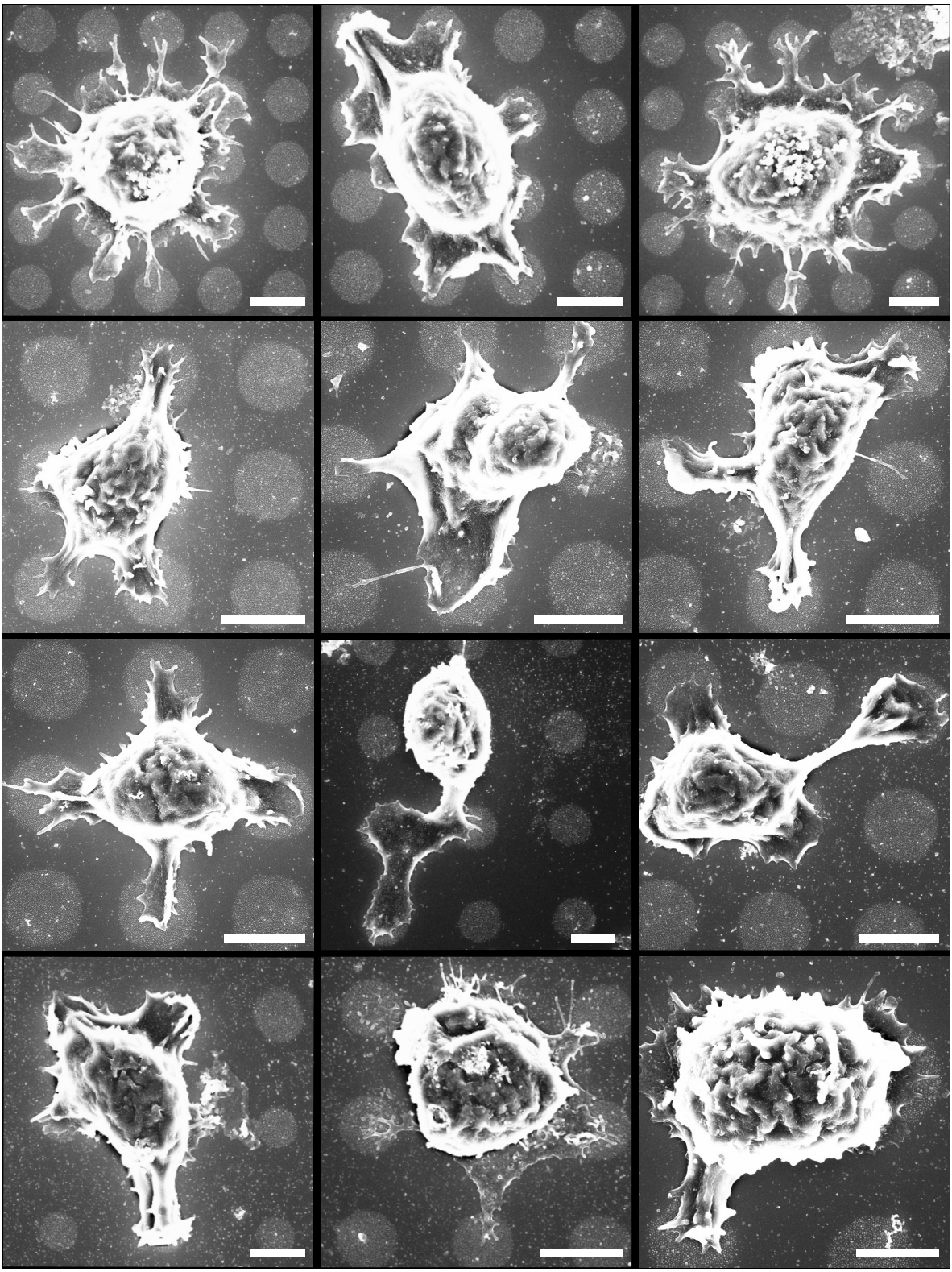

Figure 4.12.: SE micrographs of T cells on micro-nanopatterns | T cells on micro-nanopatterns featuring particle spacings between 60 nm – 80 nm and different microstructure dimensions. Substrates present pMHC bound to the Au nanoparticles and adhesive RGD in the background. The images show how T cells clearly attach preferentially to the micro-domains presenting stimulating pMHC (Scale bars: 2 µm).

as shown in Figure 4.12. The SE micrographs again demonstrate that T cells form tight contacts preferentially at the micro-domains where pMHC is present. Their shapes reflect the pattern they are confronted with. Consequentially, although the entire surface is adhesive and presents biomolecules to which the cells could possibly attach, T cells presumably scan the surface for antigen and form adhesions at those areas where they discover pMHC. This finding is not surprising since *in vivo* scanning the extracellular environment for agonist peptide is a T cell's task within the systemic operating mode of the immune system. As soon as they encounter foreign antigen loaded on MHC molecules they start to form microclusters. It would be conceivable that upon such antigen detection they always start a particular signaling cascade leading to spreading and formation of adhesions irrespective of the arrangement of pMHC. However, it seems that T cells quite strongly react to the conditions they are faced with since they adapt their shape to the lateral distribution of pMHC. Moreover, it demonstrates that T cells are quite deformable and react flexible to uncommon circumstances. It again shows that they do not always form a model synapse like it has already been shown in previous research projects. Instead, it seems that T cells primarily form cell – surface adhesions on the stimulating micro-domains. Up to now we do not know how TCRs are exactly organized on these patterns. Further investigations are necessary to elucidate the molecular assembly and structure formation at the cell – surface contact area.

4.2. Experimental details and analyses

4.2.1. Activation experiments

Preparation of primary T cell blasts[11]

AND TCR transgenic mice were purchased from Jackson Laboratories (Bar Harbor, ME) and were crossed to B10.Cg-Tg (TCR AND) 53Hed/J (B10.AND). AND mice are alpha/beta TCR transgenic mice produced using the alpha and beta chain genes that encode a receptor specific for pigeon cytochrome c in association with IE^k class II MHC molecules. The TCR expressed in these mice is composed of alpha and beta chains derived from the cytochrome-C specific T cell clones AN6.2 and 5C.c7, respectively. All mice were housed in specific pathogen-free conditions and cared for in accordance with protocol approved by Institutional and Animal Care and Use Committee. Experiments were performed on F1 progenies between 8 and 12 weeks of age. AND TCR

[11] Preparation of cells was performed at the Skirball Institute of Biomolecular Medicine and Department of Pathology, New York University School of Medicine, New York, New York 10016, United States.

Tg splenocytes cells were activated in DMEM (Invitrogen) with 10 % FBS (Hyclone) using 1.0 µM MCC peptide (MCC88-103). At 48 h, cells were washed twice in complete medium and were plated at approximately 1×10^6 cells/ml with 50 U/ml of IL-2. The cells were replenished with fresh media and IL-2 every two days. After six days cells were deep-frozen and shipped on dry ice to the laboratory where experiments were performed. Upon arrival cells were immediately transferred to a liquid nitrogen storage tank.

Thawing and culturing of T cells

All cell culture steps were performed under sterile conditions, under a sterile flow hood (Heraeus Kendro; VWR International GmbH, Germany). For activation experiments, cells were thawed about 24 h prior to the experiment. Vials containing 1.0 ml cell suspension with approximately 5.0×10^6 cells were warmed in a water bath at 37 °C until cell suspension was almost completely thawed. Cells were re-suspendend in 10 ml of the appropriate liquid medium (RPMI 1640 with phenol red and glutamine, Invitrogen) supplemented with 10 % fetal bovine serum (Invitrogen) and 1 % penicillin-streptomycin (Invitrogen) in 15 ml falcons, centrifuged, re-suspended in 5 ml complete medium and cultured in conventional cell culture flasks in an incubator (Thermo Scientific, USA) at 37 °C and 5 % CO_2.

After 24 h cell suspension was taken out of the cell culture flask, centrifuged, re-suspended in complete medium (details see above), so that cell density was 0.5×10^6 cells/ml. Cell density including fraction of dead cells was determined using trypan blue and a Neubauer Hemocytometer. Then 0.3 ml (1.5×10^5 cells) of cell suspension was added to each chamber (0.8 cm^2) presenting a bio-functionalized glass surfaces as bottom.

Adhesion/spreading experiments

After (45 ± 15) min cell-substrate contact time at 37 °C and 5 % CO_2, cells were imaged with a custom-made interference reflection microscope (IRM) (details see section 4.2.2). Images were taken randomly and the contact area was determined by manually outlining the edge of cells ($n > 100$ for each data point, except for cells plated on particle distances above 150 nm; here $n > 15$ because of very low adhesion) using ImageJ. The fraction of adherent cells was calculated by manually counting adherent cells *versus* non-adherent cells ($n > 100$ adherent cells for each data point). The fraction of dead cells (usually around 30 – 40 %), which was determined before seeding, was subtracted from non-adherent cells.

Alpha tubulin staining

After 30 min cell-substrate contact at 37 °C and 5 % CO_2, cells were fixed with 4 % PFA (Honey- well Riedel de Haen, Germany) at 37 °C for 10 min before being permeabilized with ice-cold methanol for 1 min and washed three times with PBS and 2 % bovine serum albumin (BSA, MP Biomedicals LLC, France). Next, surfaces were incubated with 10 µg/ml of monoclonal anti-beta tubulin Cy-3 labeled antibody (Sigma-Aldrich) diluted in PBS containing 2 % BSA. Once again, chambers were rinsed with PBS containing 2 % BSA. Stained cells were imaged with an inverted fluorescence microscope (Olympus IX71, HBO lamp, Sony CCD Camera, Delta vision system) using appropriate filters and a 60 x objective (Olympus).

ELISA (IL-2 release)

Supernatant (200 µl) was taken out of the culture chambers after 24 h culture time at 37 °C and 5 % CO_2. The IL-2 concentration within the medium was determined by a high sensitivity ELISA analysis Kit from eBioscience (Mouse IL-2 ELISA Ready-SET-Go!).

The reason for using the index of activation, thus a normalized value instead of absolute IL-2 values is trivial: Every experiment is different. In particular, living cells always behave different depending on cell batch and several other unspecified circumstances. Moreover, cell densities can be slightly different; proteins can be less functional and so on. Hence, the absolute values of IL-2 release for the same experimental conditions can differ quite a lot (up to a factor of two in our case) even when conditions are the same. But we realized that this is not due to the different surface but due to circumstances as described before. In order to eliminate this effect in a statistical examination, every type of surface would have to be included in every individual experiment. This, however, was impossible due to the many different surface parameters we tested. Therefore, an alternative to neglect the effect of differently behaving cell batches (or other unspecified effects) is to perform normalization. We therefore, related every absolute IL-2 value to a control value, which was in our case the amount of IL-2 that cells secreted on entirely coated pMHC surfaces. So, in parallel to every experiment we always had at least two positive control surfaces whose average IL-2 value was set as a standard value equal 1.0.

4.2.2. Microscopy techniques

Critical point dryer

In order to perform scanning electron microscopy cells were dried using a critical point dryer (CPD 030, Bal-Tec). Fixation was done using glutaraldehyde (4 %) (Sigma-Aldrich) in PBS for 15 min, where after the dehydration was achieved by incubating the samples in a series of aqueous solutions of pure ethanol, starting with 50 % and followed by 60 %, 70 %, 80 %, 90 %, 96 % and three times 100 % ethanol, for at least 30 min every time. Samples were then transferred into the chamber of the critical point dryer where the ethanol was substituted by liquid CO_2 by an extensive liquid exchange. The chamber was heated until a certain pressure ($p_c \approx 75$ bar) and temperature ($T_c \approx 31\,^{\circ}C$) were reached were the density of liquid and gas phase were the same (critical point). At these conditions, the CO_2 was very carefully released by a needle valve always paying attention that pressure and temperature remain around p_c and T_c, respectively. This procedure was done until all CO_2 within the chamber had completely disappeared.

Scanning electron microscopy

First, nanopatterns with the critical point-dried T cells were coated with carbon using a sputter coater (Med020 modular High Vacuum Coating system, BalTec, Witte, Germany) to prevent charging of the surface during imaging. SE micrographs of T cells on nanopatterns were acquired using a Zeiss LEO 1530 (ZeissSMT, Oberkochen, Germany) with acceleration voltages of about 5 keV and working distances between 5 and 10 mm using in-lens detector or secondary electron detector. For details of the method see section 3.1.4.

Interference reflection microscopy

The custom-made IRM set-up is based on a inverse microscope (IX71, Olympus, Germany) with a 63x oil objective (Neofluar Antiflex, NA = 1.25; Zeiss, Germany) equipped with a $\lambda/4$ waveplate and is capable of three different wavelengths. It is equipped with a electrical stage (SCAN IM 112 x 74; Märzhäuser Wetzlar, Germany) and an additional piezo stage (P-563.3CD; Physical instruments, Germany) which enable precise movements in the milli- and nanometer range, respectively. The light source is a fiber-coupled (400 µm Ocean Optics, USA) xenon lamp (XBO R 100W/45C OFR; Osram, Germany) providing a quasi continuous spectrum and a high color-rendering index (> 95). In order to minimize light scattering the entire optical beam bath is light-proof covered. For image acquisition a CCD camera (Orca-R2; Hamamatsu, Japan) is

employed. The microscope is surrounded with an incubator box in order to keep the temperature constant at 37 °C and CO_2 concentration at 5%.

4.2.3. Discussing evaluation methods

The choice of 45 min as time point to determine contact area

In theory T cells start to establish contact to the APC surface immediately after detection of antigen by the TCR and can reach their maximal size even after 2 – 10 min.

We are aware that some cells might have had a larger spreading size before images were taken while others had not already reached their maximal size at the time point of image acquisition. Furthermore, probably some cells were still migrating and not adhesive and maybe few were even migrating again after having already spread. However, it is not crucial to always measure exactly peak sizes of spreading area, nor it is even possible. In average the combination of conditions is not crucial since for mean values the different stages of spreading average out.

The method to determine amount of spread cells

As mentioned, quantifying the amount of spread versus non-adherent cells was done manually since a software-based automated detection routine failed. It is very challenging for a software-based edge detection routine to distinguish between non-adherent and adherent cells. While adherent cells (visible as black patches in the IRM picture) could be detected it is very difficult to detect non-adherent cells.

Nevertheless, it was obvious that the spreading behavior of cells crucially depends on the particle distance: We observed many cells spreading on low distances while on high distances it was barely possible to find adhesive cells. The chosen method to quantify this experimental observation is at least a suitable way to put this observation into numbers. Particularly, in combination with the IL-2 data this information becomes very significant since the IL-2 release shows very similar behavior as the cellular spreading data.

Part IV.

Discussion

Chapter

5

Discussion

5.1. Nanopatterned protein arrays as a substitute for the APC surface

We successfully introduced a new engineered platform replacing the APC surface during the T cell activation process. As summarized in chapter 1 in detail, artificial APCs have been commonly used to study T cell activation and have contributed to the understanding of receptor organization during IS formation. For instance, fluid-supported planar bilayers presenting mobile ligands have been applied to mimic the membrane conditions of an APC surface or lithographic methods pre-patterning the stimulating and adhesive molecules on solid substrates provided control over microscale ligand presentation. However, all these systems reported so far, lack the ability to control the nanoscale organization of the molecules involved. In contrast, nanopatterned biointerfaces can be used for a precise control of number and nano-scaled spatial arrangement of APC surface molecules.

In particular, the high lateral resolution of pMHC arrangement makes these substrates a very useful tool for exploring receptor organization within the membrane of T cells. The high precision of antigen presentation comes along with the immobility of ligands, which obviously does not reflect the situation in a live cell's membrane. However, a model system is not supposed to be an exact copy of nature but a simplified version of the very complex original system. Within a model system the focus goes to few but potentially prominent components to be investigated.

The focus of our engineered platform was on the control of a precise nanoscale control of antigen presentation in order to provide new insights about requirements in terms of ligand distribution and receptor organization. We demonstrated that our platform is able to present stimulating ligands with nanometer accuracy and to modulate T cell response. Moreover, it is scalable and should even be sufficiently stable for clinical applications, such as controlled stimulation and expansion of T cells *ex vivo*.

5.1.1. Block copolymer micelle lithography - a simple technique to create periodic nanopatterns

The multiple bio-inspired applications of Au nanopatterns, which has been reported so far emphasize the importance of such a technique capable of organizing biomolecules with high precision, as reviewed in [115]. We again demonstrated that the assembly of micelles on centimeter-sized substrates is a relatively simple and fast bottom-up approach to fabricate highly ordered structures in the nanometer range, as previously reported [115, 171]. We successfully produced arrays of nanopatterned Au particles with inter-particle distances ranging from 30 – 300 nm. Moreover, a photolithographic technique allowed for the addition of a superior structure in the micrometer regime to the nanopatterns. Such a combination of a self-assembly technique and a top-down approach created laterally separated nanopatterned micro-domains and the resulting micro-nanopatterns feature distinct local and global nanoparticle densities.

We demonstrated the specificity of the protein immobilization technique which was using an NTA-Ni^{2+} molecule as linker between Au particle and His-tag proteins. The NTA was equipped with a thiol end group, which guaranteed a very stable connection to the Au particles. The background of these resulting pMHC patterns was either rendered fully bio-inert using a PEG layer or adhesive by addition of RGD to the PEG. We could successfully demonstrate that such a engineered platform, can be used to study T cell adhesion at the single receptor level.

5.1.2. Number of biomolecules per individual particle

Previously reports attempted to assess the occupation number of Au nanoparticles with biomolecules by AFM. The findings of these studies provide evidence that each Au nanoparticle of the pattern is occupied by at least one biomolecule. In detail, Wolfram et al. as well as Aydin et al. used the same binding system as described in this thesis to immobilize His-tagged N-cadherin/His-tagged green fluorescent protein (GFP) on the Au particles. They report a significant increase in height for functionalized Au nanoparticles as compared to sole Au particles [193, 249]. Such a topographical information demonstrates the presence of additional molecules on top of the particles but does not allow for quantification of numbers of molecules per individual particle. Moreover, it is restricted to rather small scan areas (approximately 1.0 μm^2, as reported) and therefore, the statistics of this method is poor.

In order to overcome the obstacle of restriction in terms of providing exact numbers, Wolfram et al. additionally applied immunogold labeling in combination with analysis *via* SEM. A primary antibody followed by a secondary, labeled with Au, was attached

to the N-cadherins presented by the nanoparticles. In the SE micrographs Au dots originating from the labeled secondary antibody could be detected in close proximity to the original Au particles of the nanopattern. Wolfram et al. found 75 % of nanoparticles to be occupied, of which 48 % exhibited a single molecule occupancy and 27 % a double occupancy.

For the first time we applied fluorescence microscopy to determine the average number of biomolecules (in this case pMHC labeled with a fluorescent dye) bound to individual nanopatterned Au particles. This method does not need additional antibody labeling but directly accesses the molecules of interest. Moreover, this approach provides significantly better statistics than previously reported techniques; in every measurements several thousand of particles/molecules were taken into account. Moreover, every individual measurement is much faster than the aforementioned methods and we were therefore, able to investigate many different surfaces.

We found that the numbers of pMHC per particle ranges from almost zero up to almost 7 pMHCs per particle. The peak value was determined to be around 0.5 whereas the mean value to be 1.6 ± 0.4. Hence, we found significantly higher deviations as previously reported, which might be due to the significantly higher amount of data or due to differences of the systems.

We speculate that in case of high occupation ratios, the immobilization of proteins was not restricted to particles but unspecific adsorption to the background took place. A pMHC/particle ratio of 7:1 is very unrealistic due to the length of the pMHC molecule of $7-8$ nm nanometers. Instead, we assume that in such cases binding to the background had happened because of an insufficient PEG layer density. We could verify the large-scale homogeneity of the PEG layer by imaging fluorescently labeled PEG layers. However, we speculate that PEG layer density was, in some cases, insufficient at a smaller length scale (tens of nanometer), which enabled the pMHC to bind non-specifically.

On entirely coated PEG surfaces binding of pMHC was almost completely inhibited and thus, there is evidence that PEG layer formation might be influenced by nanopatterns. This assumption is supported by our observation of a decreased fluorescence signal of the labeled PEG in case of presence of nanoparticles compared to pure PEG surfaces. Nevertheless, the fluorescent signal of the pMHC molecules was in most cases very uniform and we did not detect bright, next to dark spots, again supporting the assumption that large scale defects of the PEG layer allowing for unspecific pMHC assembly did not exist.

In case of small molecule/particle ratios (< 1) the immobilization of pMHC must have been reduced by either a high PEG density or some other experimental details such

as washing steps, although we kept all procedural parameters constant. At this point we cannot provide any theoretical explanation for the effects we observed. The wide distribution of number of pMHCs per particle is a drawback of the nanopatterns, since it does not fully guarantee stable and comparable conditions and might have led to over- or underestimation of particle spacings. Future experiments employing nanopatterns must at best, attempt to determine occupation rates using different approaches in order to gather information from different perspectives.

5.1.3. Generation of nanopatterned synaptic stuctures

On nanopatterns ligands are immobile and the T cell is not able to re-organize ligands in order to form a synaptic pattern. Therefore, we generated patterns better mimicking the molecular arrangement found in a IS *in vivo* where pMHC accumulates in a circular micro-domain. For this purpose we applied a top-down approach depositing protein solution only in micrometer-sized spots corresponding in size to the c-SMAC. The surrounding non-occupied particles can now serve as anchor points for any additional molecules, such as ICAM-1 supporting the formation of an adhesive p-SMAC.

We could demonstrate that the deposition of pMHC in such confined areas is possible. We suggest the immobilization of a secondary protein to happen with a distinct binding strategy. During our attempts we used the same linker system for pMHC and ICAM-1 for binding to the nanoparticles and speculate that exchange of binding partners had happened. Therefore, the incubation with the secondary biomolecule, led to destruction of the pMHC islands (see subsection 7.1.1 for further details).

Such substrates, which exhibit, in addition to the nanoscale arrangement of ligands, pre-defined microscale features mimicking the synaptic pattern, could be used to further study the role and requirement of mature IS formation.

5.2. T cell response to nanopatterned antigen arrays

In this study we successfully showed that nanopatterned antigen arrays can be used to modulate the degree of T cell activation by controlling the number and spatial arrangement of TCR ligands. Once primary $CD4^+$ T cell blasts were seeded on our nanopatterns presenting agonist pMHC, TCRs were triggered, they adhered, polarized the MTOC and on a longer time scale they started to secreted the cytokine IL-2. On the other hand we found no response to pure glass or PEG-coated surfaces. Hence, the presence of pMHC was crucial to initiate such stimulatory events and co-stimulation was not necessary. Additional adhesive molecules turned out to be essential only when

the pMHC density was below a particular threshold range of approximately 90 – 140 pMHC molecules/µm^2. Moreover, for initiation of activation related events such as spreading and MTOC polarization, we found the global density of pMHC to be crucial and not high locally-confined pMHC densities.

In detail, when T cells were seeded on nanopatterns presenting only pMHC, we detected that for T cell adhesion and subsequent spreading to be initiated, T cells require a minimum particle density of approximately 100 particles/µm^2, which corresponds to a particle spacing of approximately 115 nm. At greater particle distances (especially above 150 nm) the amount of spread cells was strongly reduced. Accordingly, the IL-2 secretion was very low for high particle spacings and low densities (below approximately 100 particles per µm^2). At higher particle densities, both cell spreading and IL-2 secretion levels reached a plateau. Additionally, we found that if cells were presented with pMHC densities, which were in fact above the threshold range but only available within separate micro-domains corresponding in size to the lateral dimensions of the c-SMAC, they were not able to induce spreading, MTOC polarization or IL-2 secretion. Instead, it seems that if pMHC is the only ligand available for T cells, then its availability must be guaranteed over the entire cell-surface contact area, otherwise attachment seems to be inhibited. We can therefore conclude that in a pMHC-based system the global availability is crucial, whereas high pMHC densities of locally-confined areas do not provide adequate conditions capable of inducing T cell activation related events.

However, as soon as we introduced an adhesive RGD background we could no longer detect any threshold value regarding adhesion and spreading of T cells. Since the fabrication of nanopatterns is, so far, limited to the fabrication of patterns featuring maximal inter-particle distances of 300 nm we were not able to decrease the particle density further than approximately 14 particles per µm^2. If surfaces presented stimulating pMHC islands in combination with RGD in the background again cells were able to adhere to the substrates even if global pMHC densities were below the threshold value.

The quantification of pMHC/particle ratio allowed for the determination of ligand densities corresponding to particular particle densities. On nanopatterns of hexagonally arranged particles a particle distance of 150 nm is equivalent to a particle density of 70 per µm^2. Assuming an average particle occupation of 1.6 ± 0.4 the pMHC density on these substrates corresponds to 112 ± 28 pMHC molecules/µm^2. Hence, the threshold for adhesion and IL-2 production is approximately at 90 – 140 pMHC molecules per µm^2 when stimulation is based only on pMHC. Relating this pMHC density to an individual T cell's contact area of approximately 50 µm^2 [1] this leads to $(4.5 - 12.6) \times 10^3$

[1] This size of contact area was found to be at the lower end of the entire range of mean T cell spreading

pMHC molecules per cell. Since the initial cell-surface contact area is smaller than the final contact area, the pMHC range required to initiate adhesion is presumably significantly smaller. However, it seems that the amount of pMHC necessary for T cell attachment, is still within the range of 10^3. Establishing such quantitative requirements for providing a TCR-only signal through nanopatterning may provide the possibility to generate substrates that could be used to induce antigen-specific T cell tolerance [250].

5.2.1. The role of adhesion during T cell activation

So far, several studies titrated pMHC and measured adhesion, but generally the density of pMHC was not reported [251, 252]. Immobile pMHC in supported planar bilayers were shown to mediate adhesion of T cell hybridoma's at 1000 molecules/µm^2, but not 50 molecules/µm^2 [253], which is consistent with our current study and the threshold range we found. It seems that on substrates with a sufficient high pMHC density, additional co-stimulatory and adhesion-mediating molecules may function only as signal amplifier and may not be a crucial requirement.

It is known that TCR triggering induces adhesion by transforming the T cell's integrins into high-affinity states supporting the contact formation [254]. However, our results suggest that if no corresponding ligands for the high-affinity integrins are available, spreading and attachment can still occur, if TCR binding/microclustering can happen in a sufficient extent. Given this case any additional receptor interactions seems to become obsolete for T cell adhesion to occur.

The fact that spreading events are determined by the entire number of available pMHCs, rather than the peak density in sub-regions corresponding in size to SMACs, is presumably also due to the restricted availability of anchor points at the T cell-surface contact area. It again seems that T cells require a sufficient amount of anchor points over the entire cell-surface contact area to achieve spreading.

The dynamics of spreading were not investigated in detail in this thesis. However, at the very beginning of cell surface-contact we found cells to migrate or scan the surface before starting to spread. Therefore, we suggest that monitoring spreading and contact formation could help to understand how a T cell's adhesion behavior changes with different ligand distributions.

The critical global TCR ligand density found in this study is significantly higher than the previously reported low pMHC thresholds, some of which were determined to be in the one digit range [79, 80]. However, our threshold range was only detected if stimulation was based on purely pMHC and substrates did not provide neither adhesive

areas determined in this study.

support through integrin ligands [159] nor co-stimulation of the CD28 receptor. CD28 has been reported to be part of microclusters and to be crucial for activation [46, 255, 256]. In agreement with previous reports where T cell activation was achieved using real APCs or lipid bilayers presenting ICAM-1 together with pMHC, the threshold value for the pMHC density disappeared as soon as we included an adhesive RGD background. This means, that in fact effector $CD4^+$ T cells can be stimulated through exposure to pMHC only, if the density is above 90 pMHCs/μm^2, however in case of additional adhesive support (or maybe co-stimulation, not tested) the required amount tends to be significantly lower.

Prior studies on LFA-1 deficient mice suggest that LFA-1 increases the sensitivity of the T cell to antigen [257]. In the absence of LFA-1, up to 100-fold more antigen was required for T cell – APC conjugation and subsequent events of T cell activation, including TCR down-regulation, Ca^{2+} influx and T cell proliferation. The authors suggest that LFA-1 facilitates the functional triggering of TCRs passively by promoting adhesion of T cells to APCs. According to this theory, we speculate that adhesive molecules play a crucial role during T cell activation if the global pMHC density is below 112 ± 28 molecules per μm^2. In such cases adhesive molecules might, for example influence binding kinetics and increase the number of pMHC – TCR binding events by guaranteeing a tight T cell – APC contact.

5.2.2. TCR cluster and IS formation – key events during T cell activation?

The approach, which we introduced to the field of immunology presents immobile ligands and even lacks any additional adhesive molecules. Hence, the system does not allow for the formation of synapse-like patterns and we cannot even guarantee the formation of TCR clusters. However, we could demonstrate, that T cells show activation-related events when confronted with such conditions. This fact again shows that formation of a "model" IS with its bull's eye like appearance seems not necessarily required for the activation of T cells [53, 85, 227]. Instead, it is believed that microclusters are reported to be able to mediate both initial as well as sustained signaling and such incipient clusters rather than the formation of a mature IS seem to play a key role during the activation process [33, 89, 258].

According to our findings, we theorize that for a successful activation, T cells must be able to form ample receptor-ligand bonds linking the cell to the surface. It is not clear to what extent "real" cluster formation is possible on our substrates since they do not allow for lateral ligand re-arrangement. We speculate that, at least on uniformly coated

pMHC surfaces TCR microclustering occurs as previously shown for entirely anti-CD3 coated substrates [259]. This clustering may facilitate adhesion and spreading in the absence of adhesion molecules. On nanopatterns, however, our findings only suggest that TCR engagement must occur over the whole cell-surface interface, but we do not know to what extent TCR assembly is supported.

In literature there is evidence that single pMHC ligands are non-stimulatory as monomers and minimally stimulatory as dimers [260]. Monomeric MHC-peptide complexes engaged T cell receptors but did not induce activation unlike dimers, trimers or tetramers [261]. Others proposed the minimal signaling cluster units to consist of four pMHCs [80]. A study, which used soluble dimers featuring distinct nanoscale spacers between the two MHC molecules revealed an effect of receptor proximity; pMHC molecules linked through shorter crosslinkers showed higher potential to activate T cells [192]. Further, activation studies proposed that the high sensitivity *in vivo* could be accomplished by formation of pseudo-dimers consisting of an agonist and an endogenous peptide. In this model it is theorized that the CD4 coreceptor stabilizes the pMHC – TCR pairs by forming a bridge between both [262] and induces further signaling [263].

According to this gathered evidence, let us suppose that on nanopatterns T cells were able to form, at least, pMHC dimers. Due to the length of pMHC – TCR bonds of about 15 nm [264] we must assume that dimerization was impossible between pMHCs immobilized on adjacent particles; at least not for nanopatterns featuring spacings roughly above 40 nm. Consequently, dimerization would have been occurred only between pMHC pairs bound to the same nanoparticle. Such a situation might have been possible, since according to the distribution of pMHC/particle ratios, there were always some nanoparticles possessing more than one pMHC. Let us assume that the TCR only becomes triggered by such a confirmation of multiple particle occupancy, then only a significant less amount of pMHCs would actually contribute to the stimulation process. However, it is conceivable that the rest of the pMHCs might still have engaged the TCR but did not induce stimulation and only functioned as anchor points.

In addition we observed slightly increased $I_{activation}$ values, as a measure of IL-2 secretion, within and below the critical pMHC density regime for cells seeded on micro-nanopatterns (ligands assembled in micro-domains; lower spacing) compared to those cells seeded on continuos nanopatterns (ligands are uniformly scattered, higher spacing) exhibiting comparable global pMHC densities. If this effect was due to ligand proximity then even adjacent pMHCs with higher distances than 30 nm but below 150 nm would feature higher potential to stimulate T cells. However, the observed effect is not significant and if existent then it seems that TCR triggering/clustering can still, in

most cases, not occur in a sufficient extent to initiate adhesion.

Lastly, we speculate that the quasi-proportional increase of $I_{activation}$ with density of pMHC in the transition regime is due to an increasing probability of successful T cell stimulation including adhesion and IL-2 secretion. As discussed above, the exact reason of higher stimulation rates is unclear and can include higher probability of TCR engagement, triggering and/or clustering. Averaged over a high cell number the development of $I_{activation}$ results in such a linear behavior. At the same time, this data cannot exclude that each cell may act as a digital antigen counter system that needs to detect a certain number of pMHC molecules to initiate activation pathways.

In order to further elucidate the activation state of single cells we related the $I_{activation}$, as an indicator of IL-2 secretion to the amount of adherent cells on the different surface types:

$$\frac{I_{activation}}{[\%] \text{ of adhesion}} \tag{5.1}$$

In Figure 5.1 it is shown that in such cases the "normalized" $I_{activation}$ levels out and there is no decrease for high spacings. Instead, the value for highest particle distances is greatest, however, not significant, since relative deviations are in the 50 % range[2]. These data provide indications that on nanopatterns the IL-2 secretion can be directly traced back to the amount of spread cells since relating $I_{activation}$ to the amount of spread cells yields similar values for different types of nanopatterns. In case of the homogeneous coated surfaces such a normalized value is 1.59 ± 0.53 (data not shown), which is more than double the value calculated for low spacing nanopatterns. In this case, we theorize that either single cells secrete double the value of IL-2 over time (within 24 hours) or that on continuously coated surfaces conditions are such that T cells, which initially did not achieve to adhere, do so with time.

On homogeneously pMHC-coated surfaces, the probability of the formation of pMHC oligomers is significantly increased. Trimeric or tetrameric agonist ligands that engage multiple TCRs for a sustained duration are reported to be significant more potent stimuli than dimers [260]. Therefore, we hypothesize that IL-2 secretion, induced through surfaces entirely coated with pMHC, is much more efficient since the probability of pMHC trimerization or tetramerization is considerably increased compared to nanopatterned surfaces and could explain the significant higher activation potential of uniformly coated pMHC surfaces.

In order to test this hypothesis we propose to apply nanopatterns with larger particle sizes. If the particles size is such that the probability of binding multiple pMHC molecules is significantly increased, then the strength of T cell response would equal

[2]The deviations were calculated by Gaussian error propagation.

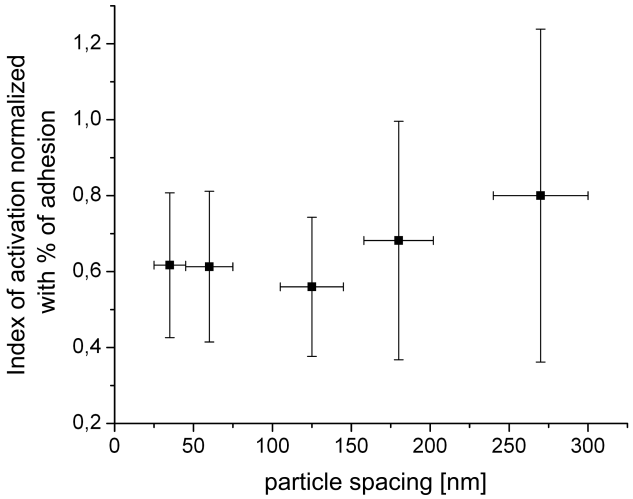

Figure 5.1: Index of activation normalized by the percentage of adhesive cells | The index of activation as a measure for IL-2 secretion levels out if related to the precentage of adherent cells on the different nanopatterns.

that on entirely coated pMHC surfaces, given the hypothesis is true.

5.3. Nanopatterned antigen/antibody arrays and their potential contribution to clinics

The development of culture platforms for *ex vivo* T cell activation and expansion is of particular interest for the adoptive T cell therapy and the investigation of T cell-mediated immunity [265, 266]. APC analog systems provide more general and effective ready-to-use approaches for T cell stimulation than live APCs [165].

So far, efficient *ex vivo* stimulation and expansion of T cells is often done by antibodies to CD3 and CD28 used as mimics of natural APC ligands since antibodies deliver much stronger signals than physiological ligands. The focus commonly lies on increasing the ratio of stimulating surface area to culture volume and therefore, 3D beads coated with antibodies have become a standard method to stimulate T cells *ex vivo* [267]. So far, in such approaches not much attention has been payed on the coupling chemistry and the precise control over ligand arrangement and density.

Recently, we reported the successful immobilization of anti-CD3 to nanopatterns. Activation related events, such as CD69 expression, IL-2 production and proliferation were also - similar to the findings of this study - found to be dependent on the spacing of nanoparticles/density of anti-CD3. In this system, a decrease of T cell response was found above 60 nm spacing. Interestingly, $CD4^+$ T cell response suggests an enhanced stimulation on low-spacing nanopatterned antibody arrays compared to anti-CD3 coated plastic surface [162]. Another study investigated the effect of nanoscale antibody spacing on the extent of membrane-localized phosphotyrosine for T cells as well

as cell-surface contact area for NK cells using anti-CD3 and anti-CD16, respectively. In both cases, researchers report that the strength of response could be modulated by spacing of nanoparticles [161].

Gathering these findings, despite that nanopatterned substrates do only mimic very few biochemical and biophysical properties of the natural APC, they have demonstrated to constitute a ready-to-use approach for exploring the activation of T cells. Whereas pMHC-based nanoarrays are physiologically more relevant and could help to extend knowledge about the stimulation processes between real T cell – APC conjugates, antibody-based nanoarrays could help to better understand the requirements for antibody-based *ex vivo* activation.

It is unlikely that biomimetic nanopatterns, at least in their current state, will be used to expand T cells in clinics. However, the findings gained so far suggest that nanopattern-based research can help to define optimal activation/culture conditions, such as pMHC/antibody densities or presence/absence of additional biomolecule. Depending on the intention, such knowledge would allow for adaptation of the artificial ECM properties and would finally lead to the development of high potential T cell culture platforms.

Part V.

Conclusion & Outlook

Chapter

6

Conclusion

For the first time we successfully achieved to provide an engineered platform substituting for the APC featuring antigen (pMHC) presentation with nanoscale resolution. At the same time the bio-interface was suitable for a wide range of biological investigations and fulfilled requirements like cell culture conditions and suitability for different microscopy techniques.

We successfully demonstrated that the response of $CD4^+$ T cell blasts can be modulated by varying the distance of adjacent nanoparticles (pMHC anchor points) of our antigen nanoarrays. Provided that the global pMHC density of such nanopatterns is high enough, $CD4^+$ T cell blasts can adhere and produce IL-2 without the presence of additional adhesive or co-stimulatory molecules. We assume that pMHC – TCR bonds are able, up to a certain extent, to take on the role of adhesive molecular bonds if the global pMHC density is above 112 ± 28 molecules per μm^2. However, such densities are not able to induce stimulation if confined to micrometer-sized areas. Instead, T cells require pMHC molecules to be available over the whole cell-surface contact area in order to overcome barriers for cell spreading. Once spreading is initiated, further signaling induces cytokine secretion. If pMHC densities are low then adhesive molecules become pivotal. Provided that there is additional RGD in the background, then the required amount of pMHC to induce spreading and IL-2 secretion is significantly lowered. In other words, T cells need to establish a certain amount of cell-surface connections in order to successfully spread and induce further activation related events. If pMHC is not available in a sufficient amount, then additional cell-surface connections, such as integrin-ligand interaction are essential.

Chapter

7

Outlook

7.1. Future directions applying nanopatterned interfaces as APC surrogates

The introduction of nanopatterned arrays to the field of immunology by primarily investigating the effect of nanopatterned MHC molecules loaded with antigen presented on a glass surfaces can only be regarded as a starting point. The presentation of only one type of an immobilized biomolecule by a very stiff material is far away from conditions found in a cell's membrane *in vivo*.

In fact, we have already achieved to introduce a secondary molecules, either the adhesive RGD to the PEG background or the ICAM-1 to the particles. The potential of nanopatterns lies beyond these preliminary demonstrations, since binding and incubation strategies can be improved, binary nanopatterns presenting distinct metal particles can be used or even elastic substrates featuring nanopatterned particles could be applied. Such advancements would introduce additional characteristics, which are similar to the conditions found on a live APC surface and at the same time provide precise control of ligand and receptor organization within the sub-cellular space. In the following subsections we will discuss possible further development of the engineered platform and potential future research.

7.1.1. Towards advanced nanopatterns by upgrading binding strategies

In order to present two distinct biomolecules by the nanoparticles at the same time binding strategies would have to be improved and/or changed. For instance, it is conceivable to create nanopatterns which present pMHC and ICAM-1 simultaneously but only in laterally separated areas mimicking the conformation as found in the IS *in vivo*. So far, we have already achieved to fabricate nanopatterned pMHC micro-domains corresponding in size to the c-SMAC. The surrounding p-SMAC could be established

by coupling ICAM-1 to the non-occupied Au particles encircling the pMHC activation patches. To this end a distinct method of coupling the ICAM-1 compared to the His-tag binding strategy of the pMHC would be required. One method, which has already been successfully applied, is the use of a biotin tag linking biomolecules to Au. If using such distinct immobilization techniques then exchange of binding partners would be minimized. In detail, in a first step the NTA-linker would be directly deposited on the particles followed by an incubation with $NiCl_2$, which then allows for conjugation of pMHC only to defined circular and micrometer sized patches. Now, in a second step a biotin-tag with a thiol end group could be immobilized to the free nanoparticles, while streptavidin would then link biotinylated ICAM-1 to the biotin-tag coupled to the particles. Such a proceeding would guarantee that molecules only become immobilized on the nanoparticles within defined regions.

Recently, another strategy was introduced in order to address different linker systems; binary nanoarrays consisting of uniformly quasi-ordered Au and titanium dioxide (TiO_2) particles featuring different physicochemical properties [268]. Such patterns would also allow for a site-specific coupling of two distinct biomolecules.

All these additional options improving the nanometerscale presentation of molecules would finally allow for a very precise control over receptor organization during antigen recognition, IS formation and T cell activation.

7.1.2. Combining nanopatterns with compliant supports

Regarding cellular research the advantage of gels over inorganic solid materials such as glass is their capability to better mimic a cell's biomechanical environment. So far, a variety of different elastic supports consisting of polyacrylamide (PA) [269], poly(dimethylsiloxane) (PDMS) [270], hyaluronic acid (HA) [271] and PEG [272] have been applied to study cellular behavior in dependence of substrate rigidity. In the field of immunology PA gels have for example shown that T cell activation is dependent on the elasticity of the support, on which they are cultured [99, 100].

In our laboratory the combination of nanopatterns with elastic PEG hydrogels has already been achieved [124, 128]. PEG hydrogels are composed out of a network of crosslinked polymer chains and can contain up to 99 % of water. They are non-toxic and permeable for nutrients as well as gases and thus, very biocompatible. Due to different water ratios and polymer lengths the elasticity of such substrates spans a wide, very physiological range from kPa to MPa. Hydrogels with a significant water content possess a degree of flexibility very similar to natural tissue, whereas hydrogels with low water contents can almost be as stiff as bone or solid glass substrates. These

characteristics are responsible for the widespread usage in many biologic and medical applications [273, 274].

In order to bring the advantages of hydrogels together with those of nanopatterned surfaces a transfer method has been developed. The procedure is schematically displayed in Figure 7.1 [115, 128]. Briefly, a transfer linker is covalently coupled to the Au particles on solid surfaces and subsequently, substrates are coated with an aqueous pre-polymer solution, containing the PEG-DA macromers and a photo-initiator, which builds radicals upon irradiation with UV light initiating the polymerization process of PEG-DA. The unsaturated transfer linkers co-polymerize with the respective PEG-DA macromers into a polymer network. The addition of water causes the gel to swell producing high lateral forces that detach the Au nanoparticles from the solid substrate.

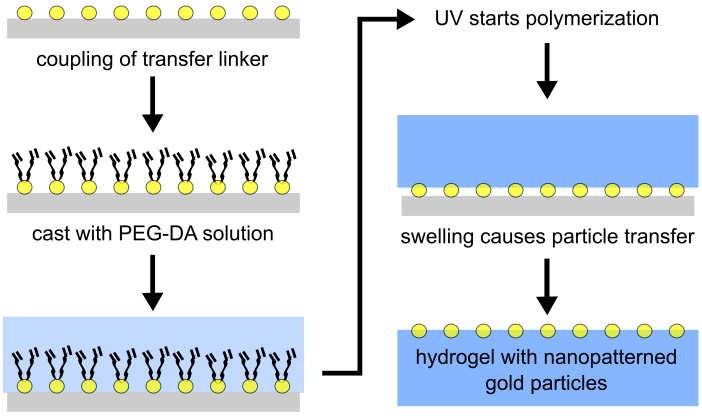

Figure 7.1: Transfer of Au nanopatterns to PEG hydrogels | First, a transfer linker is coupled to the Au nanoparticles. The surface is coated with PEG-DA initiator solution and exposed to UV light causing the polymerization process, whereby the linker becomes crosslinked with the polymer network. Addition of water causes the hydrogel to swell and high lateral forces lift the particles off the surface and separate the gel from the glass support [115, 178].

These substrates have been successfully employed to investigate effects of substrate rigidity in combination with ligand arrangement on the process of the adhesion process of fibroblasts [272]. Within this project, we have already tested if nanopatterned hydrogels functionalized with pMHC are able to stimulate T cells. We could successfully show that IL-2 secretion was induced, verifying the potential of nanopatterned hydrogels regarding T cell activation. In detail, we tested different gels exhibiting nanopatterns with 60 and 100 nm spacing and Young's moduli of 9 kPA, 39 kPA, 90 kPa and also a very stiff one with approximately 6000 – 7000 kPa. Cells on all types of hydrogels secreted IL-2, however, these are only preliminary results. Nevertheless, these initial tests can be regarded as a proof of principle showing that such substrates can be applied to function as APC surrogate. For future experiments nanopatterned hydrogels can serve as platform allowing for control over nanoscale antigen arrangement and at

the same time providing the ability to tune the compliance of the substrate. Such an extended platform could shed light on the mechano-sensing processes of TCR microclusters during T cell activation.

7.2. Determination of cellular adhesion forces

The determination of rupture forces between T cell-APC conjugates has already revealed that the development of adhesion forces correlates with dynamics of IS formation [102, 275]. Therefore, future studies could address the presence and development of adhesion forces between T cell and substrate in order to better understand the role of pMHC – TCR complexes in adhesion and spreading, since both are required for a successful activation of T cells.

Numerous assays have been developed to quantify cell adhesion forces. Historically, physical properties of the cell, such as membrane elasticity have been studied using very basic washing assays [276] or micropipettes [277], which are still applied to determine the strength of adhesion to a substrate [278–280]. More recently invented approaches include specially designed centrifuges [281, 282] or laminar flow chambers [283], which are of particular interest to investigate the so-called catch bonds, bonds that strengthen their adhesion as soon as a force is acting on them [284, 285]. A more sophisticated method is the usage of an optical tweezers [286], which exerts forces by a strongly focused beam of light to trap and move objects ranging in size from tens of nanometers to tens of micrometers [287]. Optical tweezers have proven to permit characterization of forces between cell pairs [288], cell and adhesive substrates [289] or cells and proteins [290]. Finally a powerful approach to determine cellular adhesion forces is the use of an AFM, whose working principle has been previously described in subsection 3.1.4 (See next subsection 7.2.1 for details of the approach.).

7.2.1. The AFM - a tool to measure adhesion forces of single cells

The use of an AFM for single cell force spectroscopy (SCFS) has recently been established and a wide a variety of studies have already been published [291–293]. It is sufficiently sensitive to characterize the interaction of even single molecules [294–296] and has been applied to determine single adhesion receptor ligand interactions such as ICAM-1 and LFA-1 interactions [297–299] or to study integrin-mediated adhesion of live cells at the single molecular level under near-physiological conditions [300]. It has been used to identify total adhesion forces of live cells to substrates [191, 301, 302] and also between live cell pairs [102, 275]. Among all SCFS techniques the AFM allows for

the widest practical force range from 10 pN to 10^6 pN.

In 2009, the first long time AFM measurements between live cell pairs were performed in our laboratory [102, 303]. We separated T cell/APC conjugates at different contact time points and could for the first time demonstrate that AFM is capable of measuring long-time adhesion forces (up to 60 min). We were able to demonstrate that a single measurement yields total adhesion forces as well as molecular features of the interaction. Our results verified that T cells adhere strongly to APCs if foreign antigen is present. The adhesion forces correlated with the dynamics of IS formation since we detected forces to be maximal after 30 min and to significantly decrease after 60 min. By measuring cells, which did not express the main adhesion contributor, the integrin LFA-1, we could show that only the peptide interaction is below 2 nN and thus, cannot be responsible for the high adhesion forces. These findings indicate that apparently on live APCs the density of pMHC molecules is not sufficient for the generation of stable intercellular contacts. In the natural case it seems that integrin-ligand interactions are crucial for the formation of synapse-like structures.

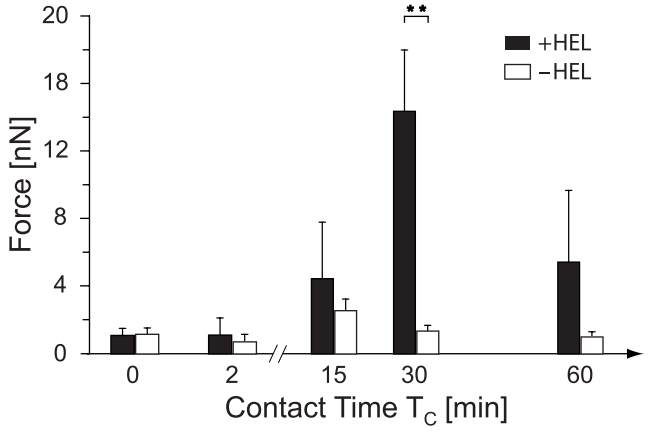

Figure 7.2: Adhesion force dynamics of T cell/APC conjugates APCs pulsed with antigen (black bars) or without (white bars) were allowed to contact T cells for the indicated time period, T_C. T cells were separated from the APCs by means of an AFM and force curves were analyzed in order to determine interaction forces. In the presence of antigen, interaction forces increase after $T_C = 15$ min, reach a maximum after 30 min, and decrease after 60 min, whereas values remain low in the absence of antigen (All bars, between 4 and 21 measurements. ** $p = 0.003$.; adapted from [102]).

In future studies it would be of high interest how adhesion dynamics of T cells develop on artificial APC surfaces. Especially, the absolute values of total adhesion forces of T cells which are presented only with pMHCs could help to understand to what extent pMHC – TCR bonds are able to overtake the function of integrin-ligand interactions and contribute to the adhesion process. There are indications that the TCR is force sensitive and hence, the adhesive role of pMHC – TCR bonds presumably plays a crucial role during IS formation. Consequently, a deeper understanding of adhesion force dynamics would help to understand what exact role adhesion forces

play during the activation process and to what extent TCR microclusters contribute to the development of contact forces.

7.3. Perspectives of APC analogs in immunological research and therapies

The beneficial impact of modifying and targeting immune response is becoming increasingly accepted in the treatment of different diseases. However, cell-based immunotherapy remains difficult, since the guidance and exquisite regulation of immune processes *ex vivo* has turned out to be very challenging. T cell behavior is not solely regulated by the presence of certain molecules on the surface of APCs but also by their density, their spatial micro- and nanometerscale distribution and also the rigidity of the support. Therefore, APC analogs that are able to simulate signals originating from naturally occurring APCs have impressively demonstrated to be a very important vehicle on the long and winding road towards an extensive understanding of the immune response. Recent significant progress in this field, including this study, suggest that advanced artificial APCs could be an effective strategy to culture, to govern and to direct immune cells *ex vivo*. For instance, APC surrogates might provide very efficient methods to generate T cells of desired activation or differentiation states for therapeutic applications. A continuos progress in understanding the needs of T cells is required for an eventual extensive comprehension of the immune system. Innovations in material design resulting in elaborate APC analogs, in combination with novel microscopy or analytic techniques provide a strong and solid basis guaranteeing for an accelerating and amazing future progress finally leading to novel immuno-based therapies.

Bibliography

[1] M Kalos, B L Levine, D L Porter, S Katz, S A Grupp, A Bagg, and C H June. T Cells with Chimeric Antigen Receptors Have Potent Antitumor Effects and Can Establish Memory in Patients with Advanced Leukemia. *Science Translational Medicine*, 3(95):95ra73–95ra73, August 2011. 1

[2] S A Grupp, M Kalos, D Barrett, R Aplenc, D L Porter, S R Rheingold, D T Teachey, A Chew, B Hauck, J F Wright, M C Milone, B L Levine, and C H June. Chimeric Antigen Receptor-Modified T Cells for Acute Lymphoid Leukemia. *New England Journal of Medicine*, pages 1–10, March 2013. 1

[3] K Murphy, P Travers, and M Walport. *Janeway's Immunobiology*. Garland Science, 2008. 1.1, 1.1.1, 1.1.2, 1.1.3, 1.2, 4

[4] R N Germain and D H Margulies. The biochemistry and cell biology of antigen processing and presentation. *Annual Review of Immunology*, 11:403–450, 1993. 1.1.2

[5] K Natarajan, H Li, R A Mariuzza, and D H Margulies. MHC class I molecules, structure and function. *Rev Immunogenet*, 1:32–46, 1999. 1.1.2, 1.1.2

[6] E R Unanue and J C Cerottini. Antigen presentation. *The FASEB journal: official publication of the Federation of American Societies for Experimental Biology*, 3:2496–2502, 1989. 1.1.2

[7] C Duke. Apoptosis in cytotoxic T lymphocytes and their targets. *Seminars in Immunology*, 4:407–412, 1992. 1.1.3

[8] D H Raulet. Missing self recognition and self tolerance of natural killer (NK) cells. *Seminars in Immunology*, 18:145–150, 2006. 1.1.3

[9] K Kärre. Natural killer cell recognition of missing self. *Nature immunology*, 9(5):477–480, 2008. 1.1.3

[10] P E Jensen. Antigen unfolding and disulfide reduction in antigen presenting cells. *Seminars in Immunology*, 7:347–353, 1995. 1.1.3

[11] A J Stagg and S C Knight. Antigen-presenting Cells, 2001. 1.1.3

[12] M F Lipscomb and B J Masten. Dendritic cells: immune regulators in health and disease. *Physiological Reviews*, 82:97–130, 2002. 1.1.3

[13] R N Barker, L-P Erwig, K S K Hill, A Devine, W P Pearce, and A J Rees. Antigen presentation by macrophages is enhanced by the uptake of necrotic, but not apoptotic, cells. *Clinical and experimental immunology*, 127(2):220–5, March 2002. 1.1.3

[14] T W Lebien and T F Tedder. B lymphocytes : how they develop and function (ASH 50th anniversary review). *History*, 112:1570–1580, 2009. 1.1.3

[15] E Market and F N Papavasiliou. V(d)J recombination and the Evolution of the Adaptive Immune System. *PLoS biology*, 1(1):24–27, 2003. 1.2

[16] A Saalmüller, T Werner, and V Fachinger. T-helper cells from naive to committed. *Veterinary Immunology and Immunopathology*, 87:137–145, 2002. 1.2, 1.3

[17] D F Tough and J Sprent. Turnover of naive- and memory-phenotype T cells. *The Journal of experimental medicine*, 179:1127–1135, 1994. 1.2

[18] D F Tough and J Sprent. Life span of naive and memory T cells. *Stem cells*, 13:242–249, 1995. 1.2

[19] M Vongsakul. Characterization of immunological memory cells. A minireview. *Asian Pacific journal of allergy and immunology launched by the Allergy and Immunology Society of Thailand*, 13:75–79, 1995. 1.2

[20] F Sallusto, J Geginat, and A Lanzavecchia. Central memory and effector memory T cell subsets: function, generation, and maintenance. *Annual Review of Immunology*, 22:745–63, 2004. 1.2

[21] D L Farber. T cell memory: heterogeneity and mechanisms. *Clinical immunology Orlando Fla*, 95:173–181, 2000. 1.2

[22] K Wing and S Sakaguchi. Review: Regulatory T cells exert checks and balances on self tolerance and autoimmunity. *Nature Immunology*, 11:7–13, 2009. 1.2

[23] N Campell and J Reece. *Campell Biology*. Pearson Education, 2008. 1.3

[24] D R Fooksman, S Vardhana, G Vasiliver-Shamis, J Liese, D A Blair, J Waite, C Sacristán, Gabriel D Victora, A Zanin-Zhorov, and M L Dustin. Functional anatomy of T cell activation and synapse formation. *Annual review of immunology*, 28:79–105, January 2010. 1.3

[25] M L Dustin, S K Bromley, Z Kan, D A Peterson, and E R Unanue. Antigen receptor engagement delivers a stop signal to migrating T lymphocytes. *Proceedings of the National Academy of Sciences of the United States of America*, 94:3909–3913, 1997. 1.3, 4.1.2, 4.1.2

[26] E Donnadieu, G Bismuth, and A Trautmann. Antigen recognition by helper T cells elicits a sequence of distinct changes of their shape and intracellular calcium. *Current Biology*, 4:584–595, 1994. 1.3, 4.1

[27] C Wülfing, M D Sjaastad, and M M Davis. Visualizing the dynamics of T cell activation: intracellular adhesion molecule 1 migrates rapidly to the T cell/B cell interface and acts to sustain calcium levels. *Proceedings of the National Academy of Sciences of the United States of America*, 95:6302–6307, 1998. 1.3

[28] M Huse. Microtubule-organizing center polarity and the immunological synapse: protein kinase C and beyond. *Frontiers in immunology*, 3:235, 2012. 1.3, 4.1.3

[29] C R F Monks, B A Freiberg, H Kupfer, N Sciaky, and A Kupfer. Three-dimensional segregation of supramolecular activation clusters in T cells. *Nature*, 395(1986):82–86, 1998. 1.3, 1.4, 1.4.1

[30] A Grakoui, S K Bromley, C Sumen, M M Davis, A S Shaw, P M Allen, and M L Dustin. The Immunological Synapse : A Molecular Machine Controlling T Cell Activation. *Science*, 221(1999), 1999. 1.3, 1.4, 1.5, 1.4, 1.4.1, 2.1, 2.1.1, 4.1.2

[31] J B Huppa and M M Davis. T-cell-antigen recognition and the immunological synapse. *Nature reviews. Immunology*, 3(12):973–83, December 2003. 1.3, 1.4.1, 1.6, 2.1.1, 4.1, 4.1.2

[32] M L Dustin. A dynamic view of the immunological synapse. *Seminars in Immunology*, 17:400–410, 2005. 1.3

[33] T Saito and T Yokosuka. Immunological synapse and microclusters: the site for recognition and activation of T cells. *Current opinion in immunology*, 18(3):305–13, June 2006. 1.3, 1.4.2, 5.2.2

[34] Kenneth M Yamada and Edna Cukierman. Modeling tissue morphogenesis and cancer in 3D. *Cell*, 130(4):601–10, August 2007. 1.4

[35] M A Norcross. A synaptic basis for T-lymphocyte activation. *Annales dimmunologie*, 135D:113–134, 1984. 1.4

[36] W E Paul and R A Seder. Lymphocyte Responses and Cytokines Review. *Cell*, 76:241–251, 1994. 1.4

[37] K-H Lee, A D Holdorf, M L Dustin, A C Chan, P M Allen, and A S Shaw. T cell receptor signaling precedes immunological synapse formation. *Science*, 295:1539–1542, 2002. 1.4

[38] K-H Lee, A R Dinner, C Tu, G Campi, S Raychaudhuri, R Varma, T N Sims, W R Burack, H Wu, J Wang, O Kanagawa, M Markiewicz, P M Allen, M L Dustin, A K Chakraborty, and A S Shaw. The immunological synapse balances T cell receptor signaling and degradation. *Science*, 302:1218–1222, 2003. 1.4

[39] J C Stinchcombe, G Bossi, S Booth, and G M Griffiths. The immunological synapse of CTL contains a secretory domain and membrane bridges. *Immunity*, 15:751–761, 2001. 1.4

[40] S J Davis and P A van der Merwe. The immunological synapse: required for T cell receptor signalling or directing T cell effector function? *Current Biology*, 11(8):R289 – R290, 2001. 1.4

[41] R A Maldonado, D J Irvine, R Schreiber, and L H Glimcher. A role for the immunological synapse in lineage commitment of CD4 lymphocytes. *Nature*, 431:527–532, 2004. 1.4

[42] S Cemerski and A Shaw. Immune synapses in T-cell activation. *Current Opinion in Immunology*, 18:298–304, 2006. 1.4

[43] P Friedl, A T Den Boer, and M Gunzer. Tuning immune responses: diversity and adaptation of the immunological synapse. *Nature Reviews Immunology*, 5:532–545, 2005. 1.4

[44] S K Bromley, W R Burack, K G Johnson, K Somersalo, T N Sims, C Sumen, M M Davis, A S Shaw, P M Allen, and M L Dustin. The immunological synapse. *Annual Review of Immunology*, 19:375–396, 2001. 1.4.1

[45] M L Dustin. The cellular context of T cell signaling. *Immunity*, 30:482–92, 2009. 1.4.1

[46] D J Lenschow, T L Walunas, and J A Bluestone. CD28/B7 system of T cell costimulation. *Annual Review of Immunology*, 14:233–258, 1996. 1.4.1, 5.2.1

[47] N Isakov and A Altman. Protein kinase C(theta) in T cell activation. *Annu Rev Immunol*, 20:761–794, 2002. 1.4.1

[48] R Alon and M L Dustin. Force as a facilitator of integrin conformational changes during leukocyte arrest on blood vessels and antigen-presenting cells. *Immunity*, 26(1):17–27, January 2007. 1.4.1, 1.4.2

[49] B A Freiberg, H Kupfer, W Maslanik, J Delli, J Kappler, D M Zaller, and A Kupfer. Staging and resetting T cell activation in SMACs. *Nat Immunol*, 3:911–917, 2002. 1.4.1

[50] E J Allenspach, P Cullinan, J Tong, Q Tang, A G Tesciuba, J L Cannon, S M Takahashi, R Morgan, J K Burkhardt, and A I Sperling. ERM-dependent movement of CD43 defines a novel protein complex distal to the immunological synapse. *Immunity*, 15:739–750, 2001. 1.4.1

[51] J Delon, K Kaibuchi, and R N Germain. Exclusion of CD43 from the immunological synapse is mediated by phosphorylation-regulated relocation of the cytoskeletal adaptor moesin. *Immunity*, 15:691–701, 2001.

[52] S Stoll, J Delon, T M Brotz, and R N Germain. Dynamic imaging of T cell-dendritic cell interactions in lymph nodes. *Science*, 296:1873–6, 2002. 1.4.1

[53] B Alarcón, D Mestre, and N Martínez-Martín. The immunological synapse: a cause or consequence of T-cell receptor triggering? *Immunology*, 133(4):420–5, August 2011. 1.4.1, 1.4.1, 5.2.2

[54] D J Irvine and J Doh. Synthetic surfaces as artificial antigen presenting cells in the study of T cell receptor triggering and immunological synapse formation. *Seminars in immunology*, 19(4):245–54, August 2007. 1.4.1, 2.1, 2.1.1, 2.1.1, 2.2

[55] M A Purbhoo, D J Irvine, J B Huppa, and M M Davis. T cell killing does not require the formation of a stable mature immunological synapse. *Nature immunology*, 5(5):524–30, May 2004. 1.4.1, 1.4.2

[56] L I Richie, P J R Ebert, L C Wu, M F Krummel, J J T Owen, and M M Davis. Imaging Synapse Formation during Thymocyte Selection : Inability of CD3 to Form a Stable Central Accumulation during Negative Selection. *Immunity*, 16:595–606, 2002. 1.4.1, 1.4.2

[57] E Hailman, W R Burack, A S Shaw, M L Dustin, and P M Allen. Immature CD4 CD8 Thymocytes Form a Multifocal Immunological Synapse with Sustained Tyrosine Phosphorylation. *Immunity*, 16:839–848, 2002. 1.4.1, 1.4.2

[58] C Brossard, V Feuillet, A Schmitt, C Randriamampita, M Romao, G Raposo, and A Trautmann. Multifocal structure of the T cell - dendritic cell synapse. *European journal of immunology*, 35(6):1741–53, June 2005. 1.4.1, 1.4.2

[59] T Rothoeft, S Balkow, M Krummen, S Beissert, G Varga, K Loser, P Oberbanscheidt, F Van Den Boom, and S Grabbe. Structure and duration of contact between dendritic cells and T cells are controlled by T cell activation state. *European Journal of Immunology*, 36:3105–3117, 2006. 1.4.1

[60] M L Dustin. T-cell activation through immunological synapses and kinapses. *Immunological reviews*, 221:77–89, February 2008. 1.4.1

[61] J E Smith-Garvin, G A Koretzky, and M S Jordan. T cell activation. *Annual review of immunology*, 27:591–619, January 2009. 1.4.2

[62] S M Alam, P J Travers, J L Wung, W Nasholds, S Redpath, S C Jameson, and N R Gascoigne. T-cell-receptor affinity and thymocyte positive selection. *Nature*, 381:616–620, 1996. 1.4.2

[63] S Alberti. A high affinity T cell receptor? *Immunol.Cell Biol.*, 74:292–297, 1996. 1.4.2

[64] K Matsui, J J Boniface, P Steffner, P A Reay, and M M Davis. Kinetics of T-cell receptor binding to peptide/I-Ek complexes: correlation of the dissociation rate with T-cell responsiveness. *Proceedings of the National Academy of Sciences of the United States of America*, 91(26):12862–6, December 1994. 1.4.2

[65] J Huang, V I Zarnitsyna, B Liu, L J Edwards, N Jiang, B D Evavold, and C Zhu. The kinetics of two-dimensional TCR and pMHC interactions determine T-cell responsiveness. *Nature*, 464:932–936, 2010. 1.4.2

[66] J D Stone, A S Chervin, and D M Kranz. T-cell receptor binding affinities and kinetics: impact on T-cell activity and specificity. *Immunology*, 126:165–176, 2009. 1.4.2

[67] P Robert, M Aleksic, O Dushek, V Cerundolo, P Bongrand, and P Anton van der Merwe. Kinetics and Mechanics of Two-Dimensional Interactions between T Cell Receptors and Different Activating Ligands. *Biophysj*, 102(2):248–257, 2012. 1.4.2

[68] S Tian, R Maile, E J Collins, and J A Frelinger. CD8+ T cell activation is governed by TCR-peptide/MHC affinity, not dissociation rate. *Journal of immunology*, 179(5):2952–60, September 2007. 1.4.2

[69] J D Rabinowitz, C Beeson, D S Lyons, M M. Davis, and H M McConnell. Kinetic discrimination in T-cell activation. *Proceedings of the National Academy of Sciences of the United States of America*, 93(4):1401–5, February 1996. 1.4.2

[70] G J Schütz, M Axmann, M M Davis, and J B Huppa. Determination of Interaction Kinetics between the T Cell Receptor and Peptide-Loaded MHC Class II via Single-Molecule Diffusion Measurements. *Biophysical Journal*, 103:L17–L19, 2012. 1.4.2

[71] J B Huppa, M Axmann, M A Mörtelmaier, B F Lillemeier, E W Newell, M Brameshuber, L O Klein, G J Schütz, and M M Davis. TCR-peptide-MHC interactions in situ show accelerated kinetics and increased affinity. *Nature*, 463:963–967, 2010. 1.4.2, 2.1.1

[72] A Brodovitch, P Bongrand, and A Pierres. T lymphocytes sense antigens within seconds and make a decision within one minute. *Journal of immunology (Baltimore, Md. : 1950)*, 191(5):2064–71, September 2013. 1.4.2

[73] E R Christinck, M A Luscher, B H Barber, and D B Williams. Peptide binding to class I MHC on living cells and quantitation of complexes required for CTL lysis. *Nature*, 352:67–70, 1991. 1.4.2

[74] R C Brower, R England, T Takeshita, S Kozlowski, D H Margulies, J A Berzofsky, and C Delisi. Minimal requirements for peptide mediated activation of CD8+ CTL. *Molecular immunology*, 31:1285–1293, 1994. 1.4.2

[75] Y Sykulev, M Joo, I Vturina, T J Tsomides, and H N Eisen. Evidence that a Single Peptide MHC Complex on a Target Cell Can Elicit a Cytolytic T Cell Response. *Immunity*, 4:565–571, 1996. 1.4.2

[76] C V Harding and E R Unanue. Quantitation of antigen-presenting cell MHC class II/peptide complexes necessary for T-cell stimulation. *Nature*, 346:574–576, 1990. 1.4.2

[77] S Demotz, H M Grey, and A Sette. The minimal number of class II MHC-antigen complexes needed for T cell activation. *Science*, 249:1028–1030, 1990.

[78] K Kimachi, M Croft, and H M Grey. The minimal number of antigen-major histocompatibility complex class II complexes required for activation of naive and primed T cells. *European journal of immunology*, 27:3310–3317, 1997. 1.4.2

[79] D J Irvine, M A Purbhoo, M Krogsgaard, and M M Davis. Direct observation of ligand recognition by T cells. *Nature*, 419(6909):845–9, October 2002. 1.4.2, 4.1.1, 4.1.6, 5.2.1

[80] B N Manz, B L Jackson, R S Petit, M L Dustin, and J Groves. T-cell triggering thresholds are modulated by the number of antigen within individual T-cell receptor clusters. *Proceedings of the National Academy of Sciences of the United States of America*, 108(22):9089–94, May 2011. 1.4.2, 2.1.1, 2.2, 4.1.6, 5.2.1, 5.2.2

[81] G Campi, R Varma, and M L Dustin. Actin and agonist MHC-peptide complex-dependent T cell receptor microclusters as scaffolds for signaling. *The Journal of experimental medicine*, 202(8):1031–6, October 2005. 1.4.2, 4.1

[82] T Yokosuka, K Sakata-Sogawa, W Kobayashi, M Hiroshima, A Hashimoto-Tane, M Tokunaga, M L Dustin, and T Saito. Newly generated T cell receptor microclusters initiate and sustain T cell activation by recruitment of Zap70 and SLP-76. *Nature Immunology*, 6:1253–1262, 2005. 1.4.2

[83] M L Dustin and J T Groves. Receptor signaling clusters in the immune synapse. *Annual review of biophysics*, 41:543–56, January 2012. 1.4.2, 2.1.1

[84] T Yokosuka and T Saito. Dynamic regulation of T-cell costimulation through TCR-CD28 microclusters. *Immunological reviews*, 229(1):27–40, May 2009. 1.4.2, 1.7, 4.1.2

[85] T Saito, T Yokosuka, and A Hashimoto-Tane. Dynamic regulation of T cell activation and co-stimulation through TCR-microclusters. *FEBS letters*, 584(24):4865–71, December 2010. 1.4.2, 1.7, 4.1, 5.2.2

[86] K D Mccoy, I F Hermans, J H Fraser, G Le Gros, and F Ronchese. Cytotoxic T lymphocyte-associated antigen 4 (CTLA-4) can regulate dendritic cell-induced activation and cytotoxicity CD8(+) T cells independently of CD4(+) T cell help266, 1999. 1.4.2

[87] C Wulfing, C Sumen, M D Sjaastad, L C Wu, M L Dustin, and M M Davis. Costimulation and endogenous MHC ligands contribute to T cell recognition. *Nature Immunology*, 3:42–47, 2002. 1.4.2

[88] E Hailman and P M Allen. Self help for T cells. *Nature immunology*, 5(8):780–1, August 2004. 1.4.2

[89] R Varma, G Campi, T Yokosuka, T Saito, and M L Dustin. T cell receptor-proximal signals are sustained in peripheral microclusters and terminated in the central supramolecular activation cluster. *Immunity*, 25(1):117–27, July 2006. 1.4.2, 5.2.2

[90] B F Lillemeier, M A Mörtelmaier, M B Forstner, J B Huppa, J T Groves, and M M Davis. Erratum: TCR and Lat are expressed on separate protein islands on T cell membranes and concatenate during activation. *Nature Immunology*, 11:543, 2010. 1.4.2, 4

[91] S J Davis and P A Van Der Merwe. The kinetic-segregation model: TCR triggering and beyond. *Nature Immunology*, 7:803–809, 2006. 1.4.2

[92] V Horejsí. Lipid rafts and their roles in T-cell activation. *Microbes and infection Institut Pasteur*, 7:310–316, 2005. 1.4.2

[93] M K Wild, A Cambiaggi, M H Brown, E A Davies, H Ohno, T Saito, and P A van der Merwe. Dependence of T cell antigen recognition on the dimensions of an accessory receptor-ligand complex. *The Journal of experimental medicine*, 190:31–41, 1999. 1.4.2

[94] K Choudhuri, M Parker, A Milicic, D K Cole, M K Shaw, A K Sewell, G Stewart-Jones, T Dong, K G Gould, and P A van der Merwe. Peptide-major histocompatibility complex dimensions control proximal kinase-phosphatase balance during T cell activation. *The Journal of biological chemistry*, 284(38):26096–105, September 2009. 1.4.2

[95] S Y Qi, J T Groves, and A K Chakraborty. Synaptic pattern formation during cellular recognition. *Proceedings of the National Academy of Sciences of the United States of America*, 98:6548–6553, 2001. 1.4.2

[96] W C Moss, D J Irvine, M M Davis, and M F Krummel. Quantifying signaling-induced reorientation of T cell receptors during immunological synapse formation. *Proceedings of the National Academy of Sciences of the United States of America*, 99:15024–15029, 2002. 1.4.2

[97] M L Dustin and J A Cooper. The immunological synapse and the actin cytoskeleton: molecular hardware for T cell signaling. *Nature immunology*, 1:23–29, 2000. 1.4.2

[98] A S Sechi and J Wehland. Interplay between TCR signalling and actin cytoskeleton dynamics. *Trends in immunology*, 25(5):257–65, May 2004. 1.4.2

[99] E Judokusumo, E Tabdanov, S Kumari, M L Dustin, and L C Kam. Mechanosensing in T lymphocyte activation. *Biophysical journal*, 102(2):L5–7, January 2012. 1.4.2, 2.1.1, 7.1.2

[100] R S O'Connor, X Hao, K Shen, K Bashour, T Akimova, W W Hancock, L C Kam, and M C Milone. Substrate rigidity regulates human T cell activation and proliferation. *Journal of immunology (Baltimore, Md. : 1950)*, 189(3):1330–9, August 2012. 1.4.2, 2.1, 2.1.1, 7.1.2

[101] B Geiger, J P Spatz, and A D Bershadsky. Environmental sensing through focal adhesions. *Nature reviews. Molecular cell biology*, 10(1):21–33, January 2009. 1.4.2, 2, 2.1, 3.2

[102] B H Hosseini, I Louban, D Djandji, G H Wabnitz, J Deeg, N Bulbuc, Y Samstag, M Gunzer, J P Spatz, and G J Hämmerling. Immune synapse formation determines interaction forces between T cells and antigen-presenting cells measured by atomic force microscopy. *Proceedings of the National Academy of Sciences of the United States of America*, 106(42):17852–7, October 2009. 1.4.2, 7.2, 7.2.1, 7.2

[103] Z Ma, K A Sharp, P A Janmey, and T H Finkel. Surface-anchored monomeric agonist pMHCs alone trigger TCR with high sensitivity. *PLoS biology*, 6(2):0328–0342, 2008. 1.4.2, 2.1.1

[104] J L Bednarczyk, T K Teague, J N Wygant, L S Davis, P E Lipsky, and B W McIntyre. Activation of human T lymphocytes by crosslinking of anti-CD3 monoclonal antibodies. *Journal of Leukocyte Biology*, 46:214–220, 1989. 15

[105] Y-C Li, B-M Chen, P-C Wu, T-L Cheng, L-S Kao, M-H Tao, A Lieber, and S R Roffler. Cutting Edge: mechanical forces acting on T cells immobilized via the TCR complex can trigger TCR signaling. *Journal of immunology (Baltimore, Md. : 1950)*, 184(11):5959–63, June 2010. 1.4.2

[106] A Buxboim, I L Ivanovska, and D E Discher. Matrix elasticity, cytoskeletal forces and physics of the nucleus: how deeply do cells ‚Äòfeel‚Äô outside and in? *Journal of Cell Science*, 123:297–308, 2010. 2

[107] D E Discher, P Janmey, and Y-L Wang. Tissue cells feel and respond to the stiffness of their substrate. *Science*, 310:1139–1143, 2005. 2

[108] A J Engler, S Sen, H L Sweeney, and D E Discher. Matrix elasticity directs stem cell lineage specification. *Cell*, 126:677–689, 2006.

[109] I Platzman, J-W Janiesch, and J P Spatz. Synthesis of Nanostructured and Biofunctionalized Water-in-Oil Droplets as Tools for Homing T Cells. *Journal of the American Chemical Society*, 135:3339–42, 2013. 2, 2.1.1

[110] V Vogel and M Sheetz. Local force and geometry sensing regulate cell functions. *Nature Reviews Molecular Cell Biology*, 7:265–275, 2006. 2

[111] J P Spatz and B Geiger. Molecular engineering of cellular environments: cell adhesion to nano-digital surfaces. *Methods In Cell Biology*, 83:89–111, 2007. 2

[112] M Théry, V Racine, M Piel, A Pépin, A Dimitrov, Y Chen, J-B Sibarita, and M Bornens. Anisotropy of cell adhesive microenvironment governs cell internal organization and orientation of polarity. *Proceedings of the National Academy of Sciences of the United States of America*, 103:19771–19776, 2006. 2

[113] N F Huang and S Li. Regulation of the matrix microenvironment for stem cell engineering and regenerative medicine. *Annals of Biomedical Engineering*, 39:1201–1214, 2011. 2, 2.1

[114] G M Walker, H C Zeringue, and D J Beebe. Microenvironment design considerations for cellular scale studies. *Lab on a Chip*, 4:91–97, 2004. 2.1

[115] T Lohmüller, D Aydin, M Schwieder, C Morhard, I Louban, C Pacholski, and J P Spatz. Nanopatterning by block copolymer micelle nanolithography and bioinspired applications. *Biointerphases*, 6(1):MR1, March 2011. 2.1, 2.1.1, 5.1.1, 7.1.2, 7.1

[116] P S Lienemann, M Karlsson, A Sala, H M Wischhusen, F E Weber, R Zimmermann, W Weber, Matthias P Lutolf, and Martin Ehrbar. A Versatile Approach to Engineering Biomolecule-Presenting Cellular Microenvironments. *Advanced healthcare materials*, pages 1–5, 2012. 2.1

[117] J Y Park, D H Lee, E J Lee, and S-H Lee. Study of cellular behaviors on concave and convex microstructures fabricated from elastic PDMS membranes. *Lab on a Chip*, 9:2043–2049, 2009. 2.1

[118] P Guyot-Sionnest. Quantum dots: A new quantum state? *Nature Materials*, 2005. 2.1

[119] S Noda, T Asano, and M Imada. Novel nanostructures for light: photonic crystals. *2003 Third IEEE Conference on Nanotechnology 2003 IEEENANO 2003*, 1, 2003. 2.1

[120] M Baxendale. Biomolecular applications of carbon nanotubes. *IEE proceedings Nanobiotechnology*, 150:3–8, 2003. 2.1

[121] J Lee, Z-b Li, and D-x Yao. Quantum computation with two-dimensional graphene. *arXiv*, page 1202.5227, 2012. 2.1

[122] N Chancellor and S Haas. Scalable universal holonomic quantum computation realized with an adiabatic quantum data bus and potential implementation using superconducting flux qubits. *Physical Review A*, 87:042321, 2013. 2.1

[123] R Jayakumar, M Prabaharan, K T Shalumon, K P Chennazhi, and S V Nair. Biomedical Applications of Polymer/Silver Composite Nanofibers. *Biomedical Applications of Polymeric Nanofibers*, 246:263–282, 2012. 2.1

[124] D Aydin, I Louban, N Perschmann, J Blümmel, T Lohmüller, E A Cavalcanti-Adam, T L Haas, H Walczak, H Kessler, R Fiammengo, and J P Spatz. Polymeric substrates with tunable elasticity and nanoscopically controlled biomolecule presentation. *Langmuir : the ACS journal of surfaces and colloids*, 26(19):15472–80, October 2010. 2.1, 7.1.2

[125] E T Castellana and P S Cremer. Solid supported lipid bilayers: From biophysical studies to sensor design. *Surface Science Reports*, 61:429–444, 2006. 2.1

[126] J T Groves. Supported Lipid Bilayers as Mimics for Cell Surfaces and as Tools in Biotechnology. In *BioMEMS Biomed Nanotechnol*, volume 3, pages 305–323. Springer Verlag, 2007. 2.1

[127] J J Ramsden. Concepts in Self-Assembly. In *Advanced Nanomaterials*, pages 767–790. Wiley-VCH Verlag, 2010. 2.1, 3.1

[128] S V Graeter, J Huang, N Perschmann, M López-García, H Kessler, J Ding, and J P Spatz. Mimicking cellular environments by nanostructured soft interfaces. *Nano letters*, 7(5):1413–8, May 2007. 2.1, 7.1.2

[129] F Pi, P Dillard, L Limozin, A Charrier, and K Sengupta. Nanometric Protein-Patch Arrays on Glass and Polydimethylsiloxane for Cell Adhesion Studies. *Nano letters*, 13:3372–3378, June 2013. 2.1

[130] B Cortese, G Gigli, and M O Riehle. Mechanical gradient cues for guided cell motility and control of cell behavior on uniform substrates. *Advanced Functional Materials*, 19:2961–2968, 2009. 2.1

[131] A N Akbar and M Salmon. Cellular environments and apoptosis: Tissue microenvironments control activated T-cell death. *Immunology today*, 18:72–76, 1997. 2.1

[132] B Prakken, M Wauben, D Genini, R Samodal, J Barnett, a Mendivil, L Leoni, and S Albani. Artificial antigen-presenting cells as a tool to exploit the immune 'synapse'. *Nature medicine*, 6(12):1406–10, December 2000. 2.1

[133] H Han, J-R Peng, P-C Chen, L Gong, S-S Qiao, W-Z Wang, Z-Q Cui, X Yu, Y-H Wei, and X-S Leng. A novel system of artificial antigen-presenting cells efficiently stimulates Flu peptide-specific cytotoxic T cells in vitro. *Biochemical and biophysical research communications*, 411(3):530–5, August 2011. 2.1

[134] C Sarraf, A B Harris, A D McCulloch, and M Eastwood. Cell proliferation rates in an artificial tissue-engineered environment. *Cell Proliferation*, 38:215–221, 2005. 2.1

[135] S Even-Ram, V Artym, and K M Yamada. Matrix control of stem cell fate. *Cell*, 126:645–647, 2006. 2.1

[136] K Wingate, W Bonani, Y Tan, S J Bryant, and W C Tan. Compressive elasticity of three-dimensional nanofiber matrix directs mesenchymal stem cell differentiation to vascular cells with endothelial or smooth muscle cell markers. *Acta Biomaterialia*, 8:1–9, 2012.

[137] G C Reilly and A J Engler. Intrinsic extracellular matrix properties regulate stem cell differentiation. *Journal of Biomechanics*, 43:55–62, 2010.

[138] A J Engler, F Rehfeldt, S Sen, and D E Discher. Microtissue elasticity: measurements by atomic force microscopy and its influence on cell differentiation. *Methods In Cell Biology*, 83:521–45, 2007. 2.1

[139] F Liu and J Wu. Artificial skin cultured in vitro. *Sheng wu yi xue gong cheng xue za zhi Journal of biomedical engineering Shengwu yixue gongchengxue zazhi*, 17:223–225, 230, 2000. 2.1

[140] W W Minuth, M Sittinger, and S Kloth. Tissue engineering: generation of differentiated artificial tissues for biomedical applications. *Cell and Tissue Research*, 291:1–11, 1998.

[141] W W Minuth, R Strehl, and K Schumacher. Tissue factory: conceptual design of a modular system for the in vitro generation of functional tissues. *Tissue Engineering*, 10:285–294, 2004. 2.1

[142] O Z Fisher, A Khademhosseini, R Langer, and N A Peppas. Bioinspired materials for controlling stem cell fate. *Accounts of Chemical Research*, 43:419–428, 2010. 2.1

[143] D A Brafman, C Phung, N Kumar, and K Willert. Regulation of endodermal differentiation of human embryonic stem cells through integrin-ECM interactions. *Cell death and differentiation*, 20:369–81, 2013. 2.1

[144] Y K Tam, J A Martinson, K Doligosa, and H-G Klingemann. Ex vivo expansion of the highly cytotoxic human natural killer-92 cell-line under current good manufacturing practice conditions for clinical adoptive cellular immunotherapy. *Cytotherapy*, 5:259–272, 2003. 2.1

[145] T L Whiteside and C Odoux. Dendritic cell biology and cancer therapy. *Cancer immunology immunotherapy CII*, 53:240–248, 2004.

[146] C Yee. Adoptive T cell therapy: Addressing challenges in cancer immunotherapy. *Journal of Translational Medicine*, 3:17, 2005. 2.1

[147] G Chen, T Ushida, and T Tateishi. Scaffold Design for Tissue Engineering. *Macromolecular Bioscience*, 2:67–77, 2002. 2.1

[148] Q L Feng. Materials selection and scaffold construction for liver tissue engineering. *Materials Science Forum*, 475-479:2391–2394, 2005.

[149] R El-Ayoubi, C DeGrandpré, R DiRaddo, A-M Yousefi, and P Lavigne. Design and dynamic culture of 3D-scaffolds for cartilage tissue engineering. *Journal of Biomaterials Applications*, 25:429–444, 2011.

[150] J W Haycock. 3D cell culture: a review of current approaches and techniques. *Methods In Molecular Biology Clifton Nj*, 695:1–15, 2011.

[151] Y Hwang, A Phadke, and S Varghese. Engineered microenvironments for self-renewal and musculoskeletal differentiation of stem cells. *Regenerative Medicine*, 6:505–524, 2011. 2.1

[152] A E Foster, K Forrester, D J Gottlieb, G W Barton, J A Romagnoli, and K F Bradstock. Large-scale expansion of cytomegalovirus-specific cytotoxic T cells in suspension culture. *Biotechnology and Bioengineering*, 85:138–146, 2004. 2.1

[153] H-G Klingemann. Natural killer cell-based immunotherapeutic strategies. *Cytotherapy*, 7:16–22, 2005.

[154] S J Albon, C Mancao, K Gilmour, G White, I Ricciardelli, J Brewin, G Lugthart, R Wallace, and P J Amrolia. Optimization of methodology for production of CD25/CD71 allodepleted donor t cells for clinical use, 2013. 2.1

[155] A Douglass and R Vale. Single-molecule microscopy reveals plasma membrane microdomains created by protein. *Cell*, 2005. 2.1.1

[156] C-J Hsu and T Baumgart. Spatial Association of Signaling Proteins and F-Actin Effects on Cluster Assembly Analyzed via Photoactivation Localization Microscopy in T Cells. *PLoS ONE*, 6:13, 2011. 2.1.1

[157] M L Dustin. Insights into function of the immunological synapse from studies with supported planar bilayers. *Current Topics in Microbiology and Immunology*, 340:1–24, 2010. 2.1.1, 2.1.1

[158] K D Mossman, G Campi, J T Groves, and M L Dustin. Altered TCR signaling from geometrically repatterned immunological synapses. *Science*, 310:1191–1193, 2005. 2.1.1

[159] J Doh and D J Irvine. Immunological synapse arrays: patterned protein surfaces that modulate immunological synapse structure formation in T cells. *Proceedings of the National Academy of Sciences of the United States of America*, 103(15):5700–5, April 2006. 2.1.1, 2.1.1, 2.3, 3.2, 5.2.1

[160] J Deeg, M Axmann, J Matic, A Liapis, D Depoil, S Curado, M L Dustin, and J P Spatz. T cell activation is determined by the number of presented antigens. *Nano letters*, October 2013. 2.1.1, 4.2

[161] D Delcassian, D Depoil, D Rudnicka, M Liu, D M Davis, M L Dustin, and I E Dunlop. Nanoscale Ligand Spacing Influences Receptor Triggering in T Cells and NK Cells. *Nano letters*, October 2013. 5.3

[162] J Matic, J Deeg, A Scheffold, I Goldstein, and J P Spatz. Fine tuning and efficient T cell activation with stimulatory aCD3 nano-arrays. *Nano letters*, October 2013. 2.1.1, 5.3

[163] H T Tien and A L Ottova. The lipid bilayer concept and its experimental realization: from soap bubbles, kitchen sink, to bilayer lipid membranes. *Journal of Membrane Science*, 189:83–117, 2001. 2.1.1

[164] B N Manz and J T Groves. Spatial organization and signal transduction at intercellular junctions. *Nature Reviews Molecular Cell Biology*, 11:342–352, 2010. 2.1.1

[165] I Platzman, J-W Janiesch, J Matic, and JP Spatz. Artificial Antigen-Presenting Interfaces in the Service of Immunology. *Israel Journal of Chemistry*, 53:1–15, 2013. 2.1.1, 5.3

[166] G M Whitesides, J P Mathias, and C T Seto. Molecular self-assembly and nanochemistry: a chemical strategy for the synthesis of nanostructures. *Science*, 254:1312–1319, 1991. 3.1

[167] I Lee. Molecular Self-Assembly: Smart Design of Surface and Interface via Secondary Molecular Interactions. *Langmuir the ACS journal of surfaces and colloids*, 29:2476–89, 2013. 3.1

[168] K Ariga, J P Hill, M V Lee, A Vinu, R Charvet, and S Acharya. Challenges and breakthroughs in recent research on self-assembly. *Science and Technology of Advanced Materials*, 9:014109, 2008. 3.1

[169] J S Lindsey. Self-Assembly in Synthetic Routes to Molecular Devices - Biological Principles and Chemical Perspectives - a Review. *New Journal of Chemistry*, 15:153–180, 1991. 3.1

[170] C-S Chang, R-H Wang, K-C Chen, and E Wu. Self-assembly of microchips on substrates. *56th Electronic Components and Technology Conference 2006*, pages 1533–1538, 2006. 3.1

[171] R Glass, M Müller, and J P Spatz. Block copolymer micelle nanolithography. *Nanotechnology*, 14(10):1153–1160, October 2003. 3.1, 3.1.2, 3.1.3, 5.1.1

[172] E L Schwartz and C K Ober. Phase-Selective Chemistry in Block Copolymer Systems. In *Advanced Nanomaterials*, pages 1–66. Wiley, 2010. 3.1.1

[173] V Abetz and P Simon. Phase Behaviour and Morphologies of Block Copolymers. In *Block Copolymers I*, volume 189, pages 125–212. Springer-Verlag Heidelberg, 2005. 3.1.1

[174] N Hadjichristidis, S Pispas, and G Floudas. *Block Copolymers: Synthetic Strategies, Physical Properties, and Applications*, volume null. Wiley, 2002. 3.1.1

[175] D Izzo and C M Marques. Formation of micelles of diblock and triblock copolymers in a selective solvent. *Macromolecules*, 26:7189–7194, 1993. 3.1.1, 3.1.2

[176] J P Spatz, S Sheiko, and M Möller. Ion-Stabilized Block Copolymer Micelles : Film Formation and Intermicellar Interaction. *Macromolecules*, 29:3220–3226, 1996. 3.1.1, 3.1.2, 3.1.2, 3.1.3

[177] J P Spatz, S Mössmer, C Hartmann, M Möller, T Herzog, M Krieger, H-G Boyen, P Ziemann, and B Kabius. Ordered Deposition of Inorganic Clusters from Micellar Block Copolymer Films. *Langmuir*, 16(2):407–415, January 2000. 3.1.2, 3.1.3

[178] J Deeg. *Cell adhesion on nano- and micronanostructured surfaces*. Diplomarbeit, University of Heidelberg, 2010. 3.1, 3.7, 3.15, 3.4.1, 7.1

[179] J P Spatz, A Roescher, S Sheiko, G Krausch, and M Moeller. Noble metal loaded block ionomers. Micelle organization, adsorption of free chains, and formation of thin films. *Advanced Materials*, 7:731–735, 1995. 3.1.2, 3.1.3

[180] N Denkov, O Velev, P Kralchevski, I Ivanov, H Yoshimura, and K Nagayama. Mechanism of formation of two-dimensional crystals from latex particles on substrates. *Langmuir*, 8(12):3183–3190, 1992. 3.1.3

[181] N D Denkov, O D Velev, P A Kralchevsky, I B Ivanov, H Yoshimura, and K Nagayama. Two-dimensional crystallization. *Nature*, 361:26, 1993.

[182] M Arnold. *Molecularly defined nanostructured interfaces as tools for the regulation and measurement of functional length scales in cell adhesion mediating protein clusters*. Phd thesis, University of Heidelberg, 2005. 3.1.3, 3.1.4

[183] J Bansmann, S Kielbassa, H Hoster, F Weigl, H G Boyen, U Wiedwald, P Ziemann, and R J Behm. Controlling the interparticle spacing of Au-salt loaded micelles and Au nanoparticles on flat surfaces. *Langmuir The Acs Journal Of Surfaces And Colloids*, 23:10150–10155, 2007. 3.1.3, 3.1.4

[184] M Arnold, E A Cavalcanti-Adam, R Glass, J Blümmel, W Eck, M Kantlehner, H Kessler, and J P Spatz. Activation of integrin function by nanopatterned adhesive interfaces. *Chemphyschem : a European journal of chemical physics and physical chemistry*, 5(3):383–8, March 2004. 3.1.3, 3.3.1

[185] S Krishnamoorthy, C Hinderling, and H Heinzelmann. Nanoscale patterning with block copolymers. *Materials Today*, 9:40–47, 2006. 3.1.3

[186] A A Darhuber, S M Troian, S M Miller, and S Wagner. Morphology of liquid microstructures on chemically patterned surfaces. *Journal of Applied Physics*, 87:7768, 2000. 3.1.3, 3.1.4

[187] V C Hirschfeld-Warneken, M Arnold, E A Cavalcanti-Adam, M López-García, H Kessler, and J P Spatz. Cell adhesion and polarisation on molecularly defined spacing gradient surfaces of cyclic RGDfK peptide patches. *European Journal of Cell Biology*, 87:743–750, 2008. 3.1.3

[188] R Glass, M Arnold, J Blümmel, A Küller, M Möller, and J P Spatz. Micro-Nanostructured Interfaces Fabricated by the Use of Inorganic Block Copolymer Micellar Monolayers as Negative Resist for Electron-Beam Lithography. *Advanced Functional Materials*, 13:569–575, 2003. 3.1.4

[189] A E Larsen and D G Grier. Melting of metastable crystallites in charge-stabilized colloidal suspensions. *Physical Review Letters*, 76:3862–3865, 1996. 3.1.4

[190] K C Grabar, K R Brown, C D Keating, S J Stranick, S L Tang, and M J Natan. Nanoscale characterization of gold colloid monolayers:,Äâ a comparison of four techniques. *Analytical Chemistry*, 69(3):471–477, 1997. 3.1.4

[191] J Deeg, I Louban, D Aydin, C Selhuber-Unkel, H Kessler, and J P Spatz. Impact of Local versus Global Ligand Density on Cellular Adhesion. *Nano letters*, 11(4):1469–1476, April 2011. 3.2, 3.2.1, 3.4.2, 7.2.1

[192] J R Cochran, T O Cameron, J D Stone, J B Lubetsky, and L J Stern. Receptor proximity, not intermolecular orientation, is critical for triggering T-cell activation. *The Journal of Biological Chemistry*, 276:28068–28074, 2001. 3.2, 5.2.2

[193] D Aydin, M Schwieder, I Louban, S Knoppe, J Ulmer, T L Haas, H Walczak, and J P Spatz. Micro-Nanostructured Protein Arrays : A Tool for Geometrically Controlled Ligand Presentation **. *Small*, 5(9):1014–1018, 2009. 3.2, 3.2.1, 3.2.1, 3.3.2, 5.1.2

[194] R P Seisyan. Nanolithography in microelectronics: A review. *Technical Physics*, 56:1061–1073, 2011. 3.2.1

[195] E Wagenaars, A Mader, K Bergmann, J Jonkers, and W Neff. Extreme Ultraviolet Plasma Source For Future Lithography. *IEEE Transactions on Plasma Science*, 36, 2008. 3.2.1

[196] C Wagner and N Harned. EUV lithography: Lithography gets extreme. *Nature Photonics*, 4:24–26, 2010. 3.2.1

[197] B Wu and A Kumar. Extreme ultraviolet lithography: A review. *Journal of Vacuum Science and Technology B: Microelectronics and Nanometer Structures*, 25:1743, 2007. 3.2.1

[198] H Ogi, Y Fukunishi, H Nagai, K Okamoto, M Hirao, and M Nishiyama. Nonspecific-adsorption behavior of polyethylenglycol and bovine serum albumin studied by 55-MHz wireless-electrodeless quartz crystal microbalance. *Biosensors and Bioelectronics*, 24:3148–3152, 2009. 3.3.1

[199] M Vert and D Domurado. Poly(ethylene glycol): protein-repulsive or albumin-compatible? *Journal of biomaterials science Polymer edition*, 11:1307–1317, 2000. 3.3.1

[200] L Nieba, S E Nieba-Axmann, A Persson, M Hamalainen, F Edebratt, A Hansson, J Lidholm, K Magnusson, A F Karlsson, and A Pluckthun. BIACORE analysis of histidine-tagged proteins using a chelating NTA sensor chip. *Analytical Biochemistry*, 252:217–228, 1997. 3.3.2

[201] S Knecht, D Ricklin, A N Eberle, and B Ernst. Oligohis-tags: mechanisms of binding to Ni2+-NTA surfaces. *Journal of Molecular Recognition*, 22(4):270–279, 2009. 3.3.2

[202] E Hochuli, H Döbeli, and A Schacher. New metal chelate adsorbent selective for proteins and peptides containing neighbouring histidine residues. *Journal Of Chromatography*, 411:177–184, 1987. 3.3.2

[203] J W Lichtman and J-A A Conchello. Fluorescence microscopy. *Nat Methods*, 2:910–919, 2005. 3.3.2

[204] F Festy, S M Ameer-Beg, T Ng, and K Suhling. Imaging proteins in vivo using fluorescence lifetime microscopy. *Molecular Biosystems*, 3:381–391, 2007. 3.3.2

[205] B Huang, M Bates, and X Zhuang. Super-resolution fluorescence microscopy. *Annual Review of Biochemistry*, 78:993–1016, 2009.

[206] B O Leung and K C Chou. Review of super-resolution fluorescence microscopy for biology. *Applied Spectroscopy*, 65:967–80, 2011. 3.3.2, 3.3.3

[207] B Neupane, F Chen, W Sun, D T Chiu, and G Wang. Tuning donut profile for spatial resolution in stimulated emission depletion microscopy. *The Review of scientific instruments*, 84:043701, 2013. 3.3.3

[208] S Galiani, B Harke, G Vicidomini, G Lignani, F Benfenati, A Diaspro, and P Bianchini. Strategies to maximize the performance of a STED microscope. *Optics Express*, 20:7362–74, 2012. 3.3.3

[209] E Betzig, G H Patterson, R Sougrat, O W Lindwasser, S Olenych, J S Bonifacino, M W Davidson, J Lippincott-Schwartz, and H F Hes. Imaging Proteins Intracellular at Nanometer Fluorescent Resolution. *Science*, 313:1642–1645, 2006. 3.3.3

[210] R Henriques, C Griffiths, E Hesper R, and M M Mhlanga. PALM and STORM: unlocking live-cell super-resolution. *Biopolymers*, 95:322–331, 2011.

[211] M Rust, M Bates, and X Zhuang. Stochastic optical reconstruction microscopy (STORM) provides sub-diffraction-limit image resolution, 2006.

[212] M Bates, S A Jones, and X Zhuang. Stochastic Optical Reconstruction Microscopy (STORM): A Method for Superresolution Fluorescence Imaging. *Cold Spring Harbor protocols*, 2013, 2013. 3.3.3

[213] C Schilling and N Jung. Cycloaddition Reactions with Azides : An Overview. *Reactions*, pages 269–284, 1963. 3.3.4

[214] V D Bock, H Hiemstra, and J H Van Maarseveen. CuI-Catalyzed Alkyne-Azide "Click" Cycloadditions from a Mechanistic and Synthetic Perspective. *European Journal of Organic Chemistry*, 2006:51–68, 2006. 3.3.4

[215] R A Evans. The rise of azide-alkyne 1,3-Dipolar 'click' cycloaddition and its application to polymer science and surface modification. *Australian Journal of Chemistry*, 60:384–395, 2007.

[216] S Dedola, S A Nepogodiev, and R A Field. Recent applications of the Cu(I)-catalysed Huisgen azide-alkyne 1,3-dipolar cycloaddition reaction in carbohydrate chemistry. *Organic and Biomolecular Chemistry*, 5:1006–1017, 2007.

[217] B T Worrell, J A Malik, and V V Fokin. Direct Evidence of a Dinuclear Copper Intermediate in Cu(I)-Catalyzed Azide-Alkyne Cycloadditions. *Science*, 2013. 3.3.4

[218] Y C Lim, M W Wakelin, L Henault, D J Goetz, T Yednock, C Cabañas, F Sánchez-Madrid, a H Lichtman, and F W Luscinskas. Alpha4beta1-integrin activation is necessary for high-efficiency T-cell subset interactions with VCAM-1 under flow. *Microcirculation (New York, N.Y. : 1994)*, 7(3):201–14, June 2000. 3.3.4

[219] C R Blanchard. Atomic Force Microscopy,ÄìAFM. *The Chemical Educator*, 1:1–8, 2000. 3.4.2

[220] R García. Dynamic atomic force microscopy methods. *Surface Science Reports*, 47:197–301, 2002. 3.4.2

[221] N B Martín-Cófreces, J Robles-Valero, J R Cabrero, M Mittelbrunn, M Gordón-Alonso, C-H Sung, B Alarcón, J Vázquez, and F Sánchez-Madrid. MTOC translocation modulates IS formation and controls sustained T cell signaling. *The Journal of Cell Biology*, 182:951–962, 2008. 4, 4.1, 4.1.3

[222] R Testi, J H Phillips, and L L Lanier. T cell activation via Leu-23 (CD69). *The Journal of Immunology*, 143:1123–1128, 1989. 4

[223] M Li, J Yang, G X Shen, Q Zhang, S P Liu, Z B Liu, and W X Ye. Study on lymphocyte activation and proliferation induced by anti-CD3 McAb. *Journal of Tongji Medical University Tong ji yi ke da xue xue bao*, 14:209–212, 1994. 4

[224] T Nakayama and M Yamashita. The TCR-mediated signaling pathways that control the direction of helper T cell differentiation. *Seminars in Immunology*, 22:303–309, 2010. 4

[225] D Masopust and J M Schenkel. The integration of T cell migration, differentiation and function. *Nature reviews Immunology*, 13:309–320, 2013. 4

[226] J Kaye, N J Vasquez, and S M Hedrick. Involvement of the same region of the T cell antigen receptor in thymic selection and foreign peptide recognition. *The Journal of Immunology*, 148:3342–3353, 1992. 4.1

[227] T Yokosuka and T Saito. The immunological synapse, TCR microclusters, and T cell activation. *Current Topics in Microbiology and Immunology*, 340:81–107, 2010. 4.1, 5.2.2

[228] R S Lewis. Calcium signaling mechanisms in T lymphocytes. *Annu Rev Immunol*, 19:497–521, 2001. 4.1.1

[229] B D Freedman. Mechanisms of calcium signaling and function in lymphocytes. *Critical reviews in immunology*, 26:97–111, 2006. 4.1.1

[230] M Vig and J P Kinet. Calcium signaling in immune cells. *Nature Immunology*, 10:21–27, 2009. 4.1.1

[231] S Feske. Calcium signalling in lymphocyte activation and disease. *Nature reviews. Immunology*, 7:690–702, 2007. 4.1.1

[232] M Oh-hora and A Rao. Calcium signaling in lymphocytes. *Current opinion in immunology*, 20:250–258, 2008.

[233] B A Niemeyer, U Becherer, J Rettig, M Pasche, A Quintana, C Junker, P Meraner, H Rieger, M Hoth, D Al-Ansary, C Kummerow, L Nuñez, and C Villalobos. Calcium microdomains at the immunological synapse: how ORAI channels, mitochondria and calcium pumps generate local calcium signals for efficient T-cell activation, 2011. 4.1.1

[234] K.R. Gee, K.A. Brown, W-N.U. Chen, J. Bishop-Stewart, D. Gray, and I. Johnson. Chemical and physiological characterization of fluo-4 Ca2+-indicator dyes. *Cell Calcium*, 27(2):97–106, 2000. 4.1.1

[235] A J Morgan and R Jacob. Ionomycin enhances Ca2+ influx by stimulating store-regulated cation entry and not by a direct action at the plasma membrane. *The Biochemical journal*, 300 (Pt 3:665–72, 1994. 4.1.1

[236] T Chatila, L Silverman, R Miller, and R Geha. Mechanisms of T cell activation by the calcium ionophore ionomycin. *The Journal of Immunology*, 143:1283–1289, 1989. 4.1.1

[237] D M Davis. Mechanisms and functions for the duration of intercellular contacts made by lymphocytes. *Nature Reviews Immunology*, 9:543–555, 2009. 4.1.2

[238] H H Gabriel and W Kindermann. Adhesion molecules during immune response to exercise. *Canadian Journal of Physiology and Pharmacology*, 76:512–523, 1998. 4.1.2

[239] C R Mackay and B A Imhof. Cell adhesion in the immune system., 1993.

[240] T A Springer. Adhesion receptors of the immune system. *Nature*, 346:425–434, 1990. 4.1.2

[241] G A Horridge and S L Tamm. Critical Point Drying for Scanning Electron Microscopic Sthdy of Ciliary Motion. *Science*, 163(3869):817–818, 1969. 4.1.2

[242] G D Cagle. Critical-point drying: rapid method for the determination of bacterial extracellular polymer and surface structures. *Applied Microbiology*, 28:312–316, 1974.

[243] L A Barrett and R E Pendergrass. A method for handling free cells through critical point drying. *Journal of Microscopy*, 109:311–313, 1977. 4.1.2

[244] J C Stinchcombe, E Majorovits, G Bossi, S Fuller, and G M Griffiths. Centrosome polarization delivers secretory granules to the immunological synapse. *Nature*, 443:462–465, 2006. 4.1.3

[245] J R Kuhn and M Poenie. Dynamic polarization of the microtubule cytoskeleton during CTL-mediated killing. *Immunity*, 16:111–121, 2002. 4.1.3

[246] W Knapp and H Ludwig. Developments in immunofluorescence (author's transl). *Wiener Klinische Wochenschrift*, 88:1–5, 1976. 4.1.3

[247] A Kumar, J L Moreau, M Gibert, and J Thèze. Internalization of interleukin 2 (IL-2) by high affinity IL-2 receptors is required for the growth of IL-2-dependent T cell lines. *The Journal of Immunology*, 139:3680–3684, 1987. 4.1.4

[248] S L Swain. Lymphokines and the immune response: the central role of interleukin-2. *Current Opinion in Immunology*, 3:304–310, 1991. 4.1.4

[249] T Wolfram, F Belz, T Schoen, and J P Spatz. Site-specific presentation of single recombinant proteins in defined nanoarrays. *Biointerphases*, 2:44–48, 2007. 5.1.2

[250] H Quill and R H Schwartz. Stimulation of normal inducer T cell clones with antigen presented by purified Ia molecules in planar lipid membranes: specific induction of a long-lived state of proliferative nonresponsiveness. *The Journal of Immunology*, 138:3704–3712, 1987. 5.2

[251] B P Babbitt, P M Allen, G Matsueda, E Haber, and E R Unanue. Binding of immunogenic peptides to Ia histocompatibility molecules. *Nature*, 317:359–61, 1985. 5.2.1

[252] K P Kane and M F Mescher. Activation of CD8-dependent cytotoxic T lymphocyte adhesion and degranulation by peptide class I antigen complexes. *The Journal of Immunology*, 150:4788–4797, 1993. 5.2.1

[253] M L Dustin, J M Miller, S Ranganath, D A Vignali, N J Viner, C A Nelson, and E R Unanue. TCR-mediated adhesion of T cell hybridomas to planar bilayers containing purified MHC class II/peptide complexes and receptor shedding during detachment. *The Journal of Immunology*, 157:2014–2021, 1996. 5.2.1

[254] M L Dustin and T A Springer. T-cell receptor cross-linking transiently stimulates adhesiveness through LFA-1. *Nature*, 341:619–624, 1989. 5.2.1

[255] M Sanchez-Lockhart, M Kim, and J Miller. Cutting Edge: A Role for Inside-Out Signaling in TCR Regulation of CD28 Ligand Binding. *The Journal of Immunology*, 187:5515–9, 2011. 5.2.1

[256] T Yokosuka and T Saito. Dynamic regulation of T-cell costimulation through TCR-CD28 microclusters. *Immunological reviews*, 229(1):27–40, May 2009. 5.2.1

[257] M F Bachmann, K McKall-Faienza, R Schmits, D Bouchard, J Beach, D E Speiser, T W Mak, and P S Ohashi. Distinct roles for LFA-1 and CD28 during activation of naive T cells: adhesion versus costimulation. *Immunity*, 7:549–557, 1997. 5.2.1

[258] Stephen C Bunnell. Immunological Synapse. *Cell*, 340:123–154, 2010. 5.2.2

[259] S C Bunnell. T cell receptor ligation induces the formation of dynamically regulated signaling assemblies. *The Journal of Cell Biology*, 158(7):1263–1275, September 2002. 5.2.2

[260] J J Boniface, J D Rabinowitz, C Wülfing, J Hampl, Z Reich, J D Altman, R M Kantor, C Beeson, H M McConnell, and M M Davis. Initiation of Signal Transduction through the T Cell Receptor Requires the Multivalent Engagement of Peptide/MHC Ligands. *Immunity*, 9(4):459–466, October 1998. 5.2.2, 5.2.2

[261] J R Cochran, T O Cameron, and L J Stern. The relationship of MHC-peptide binding and T cell activation probed using chemically defined MHC class II oligomers. *Immunity*, 12:241–250, 2000. 5.2.2

[262] M Krogsgaard, Q-J Li, C Sumen, J B Huppa, M Huse, and M M Davis. Agonist/endogenous peptide-MHC heterodimers drive T cell activation and sensitivity. *Nature*, 434(7030):238–43, March 2005. 5.2.2

[263] R König and W Zhou. Signal transduction in T helper cells: CD4 coreceptors exert complex regulatory effects on T cell activation and function. *Current Issues in Molecular Biology*, 6:1–15, 2004. 5.2.2

[264] S J Davis, S Ikemizu, E J Evans, L Fugger, T R Bakker, and P A van der Merwe. The nature of molecular recognition by T cells. *Nature immunology*, 4(3):217–24, March 2003. 5.2.2

[265] J V Kim, J-B Latouche, I Rivière, and M Sadelain. The ABCs of artificial antigen presentation. *Nature biotechnology*, 22:403–410, 2004. 5.3

[266] C H June. Principles of adoptive T cell cancer therapy. *J Clin Invest*, 117:1204–1212, 2007. 5.3

[267] A Trickett and Y L Kwan. T cell stimulation and expansion using anti-CD3/CD28 beads. *Journal of immunological methods*, 275:251–255, 2003. 5.3

[268] J Polleux, M Rasp, I Louban, N Plath, A Feldhoff, and J P Spatz. Benzyl alcohol and block copolymer micellar lithography: a versatile route to assembling gold and in situ generated titania nanoparticles into uniform binary nanoarrays. *ACS nano*, 5(8):6355–64, August 2011. 7.1.1

[269] C E Kandow, P C Georges, P A Janmey, and K A Beningo. Polyacrylamide hydrogels for cell mechanics: steps toward optimization and alternative uses. *Methods in cell biology*, 83:29–46, 2007. 7.1.2

[270] F Chambon. Linear Viscoelasticity at the Gel Point of a Crosslinking PDMS with Imbalanced Stoichiometry, 1987. 7.1.2

[271] M N Collins and C Birkinshaw. Physical properties of crosslinked hyaluronic acid hydrogels. *Journal of materials science. Materials in medicine*, 19:3335–3343, 2008. 7.1.2

[272] I Platzman, C A Muth, C Lee-Thedieck, D Pallarola, R Atanasova, I Louban, E Altrock, and J P Spatz. Surface properties of nanostructured bio-active interfaces: impacts of surface stiffness and topography on cell-surface interactions. *RSC Adv.*, 3(32):13293–13303, 2013. 7.1.2, 7.1.2

[273] C-J Wu, J J Wilker, and G Schmidt. Robust and adhesive hydrogels from crosslinked poly(ethylene glycol) and silicate for biomedical use. *Macromolecular bioscience*, 13:59–66, 2013. 7.1.2

[274] F Brandl, M Henke, S Rothschenk, R Gschwind, M Breunig, T Blunk, J Tessmar, and A Göpferich. Poly(Ethylene Glycol) Based Hydrogels for Intraocular Applications. *Advanced Engineering Materials*, 9:1141–1149, 2007. 7.1.2

[275] S Hoffmann, B H Hosseini, M Hecker, I Louban, N Bulbuc, N Garbi, G H Wabnitz, Y Samstag, J P Spatz, and G J Hämmerling. Single cell force spectroscopy of T cells recognizing a myelin-derived peptide on antigen presenting cells. *Immunology letters*, 136:13–20, November 2010. 7.2, 7.2.1

[276] R J Klebe. Cell attachment to collagen: the requirement for energy. *Journal of cellular physiology*, 86:231–236, 1975. 7.2

[277] J M Mitchison and M M Swann. The mechanical properties of the cell surface I. The cell elastimeter. *Journal of Experimental Biology*, 31:443–460, 1954. 7.2

[278] E Evans, K Ritchie, and R Merkel. Sensitive force technique to probe molecular adhesion and structural linkages at biological interfaces. *Biophysical journal*, 68:2580–2587, 1995. 7.2

[279] J-Y Shao, G Xu, and P Guo. Quantifying cell-adhesion strength with micropipette manipulation: principle and application. *Frontiers in bioscience: a journal and virtual library*, 9:2183–2191, 2004.

[280] Z Gao, S Wang, H Zhu, and J Xu. Modification and application of the micropipette aspiration method for measuring the cell adhesion force on material surface. *Journal of biomedical engineering*, 26:508–511, 2009. 7.2

[281] L Chu, L A Tempelman, C Miller, and D A Hammer. Centrifugation Assay of IgE-Mediated Cell Adhesion to Antigen-Coated Gels. *AIChE Journal*, 40:692–70, 1994. 7.2

[282] O Thoumine, A Ott, and D Louvard. Critical centrifugal forces induce adhesion rupture or structural reorganization in cultured cells. *Cell motility and the cytoskeleton*, 33:276–287, 1996. 7.2

[283] G Kaplanski, C Farnarier, O Tissot, A Pierres, A M Benoliel, M C Alessi, S Kaplanski, and P Bongrand. Granulocyte-endothelium initial adhesion. Analysis of transient binding events mediated by E-selectin in a laminar shear flow. *Biophysical journal*, 64:1922–1933, 1993. 7.2

[284] W Thomas. Catch bonds in adhesion. *Annual review of biomedical engineering*, 10:39–57, 2008. 7.2

[285] W E Thomas, V Vogel, and E Sokurenko. Biophysics of catch bonds. *Annual review of biophysics*, 37:399–416, 2008. 7.2

[286] M C Williams. Optical Tweezers : Measuring Piconewton Forces. *Physics*, pages 1–14, 2002. 7.2

[287] D G Grier. A revolution in optical manipulation. *Nature*, 424:810–816, 2003. 7.2

[288] O Thoumine, P Kocian, A Kottelat, and J J Meister. Short-term binding of fibroblasts to fibronectin: optical tweezers experiments and probabilistic analysis. *European biophysics journal : EBJ*, 29:398–408, 2000. 7.2

[289] G Weder, O Guillaume-Gentil, N Matthey, F Montagne, H Heinzelmann, J Vörös, and M Liley. The quantification of single cell adhesion on functionalized surfaces for cell sheet engineering. *Biomaterials*, 31(25):6436–43, September 2010. 7.2

[290] C O Mejean, A W Schaefer, E A Millman, P Forscher, and E R Dufresne. Multiplexed force measurements on live cells with holographic optical tweezers. *Optics express*, 17:6209–6217, 2009. 7.2

[291] P-H Puech, A Taubenberger, F Ulrich, M Krieg, D J Muller, and C-P Heisenberg. Measuring cell adhesion forces of primary gastrulating cells from zebrafish using atomic force microscopy. *Journal of cell science*, 118(Pt 18):4199–206, September 2005. 7.2.1

[292] Jonne Helenius, Carl-philipp Heisenberg, Hermann E Gaub, and Daniel J Muller. Single-cell force spectroscopy. *Journal of Cell Science*, 2008.

[293] C M Franz and P-H Puech. Atomic Force Microscopy: A Versatile Tool for Studying Cell Morphology, Adhesion and Mechanics. *Cellular and Molecular Bioengineering*, 1:289–300, 2008. 7.2.1

[294] J Zlatanova, S M Lindsay, and S H Leuba. Single molecule force spectroscopy in biology using the atomic force microscope. *Prog.Biophys.Mol.Biol.*, 74:37–61, 2000. 7.2.1

[295] R H Eibl and V T Moy. Atomic force microscopy measurements of protein-ligand interactions on living cells. *Methods Mol Biol*, 305:439–450, 2005.

[296] M Kawakami and Y Taniguchi. Recent Advances in Single-Molecule Biophysics with the Use of Atomic Force Microscopy. *Single-Molecule Biophysics: Experiment and Theory, Vol 146*, 146:89–132, 2012. 7.2.1

[297] X Zhang, E P Wojcikiewicz, and V T Moy. Force spectroscopy of the leukocyte function-associated antigen-1/intercellular adhesion molecule-1 interaction. *Biophysical Journal*, 83:2270–2279, 2002. 7.2.1

[298] E P Wojcikiewicz, X Zhang, and V T Moy. Force and Compliance Measurements on Living Cells Using Atomic Force Microscopy (AFM). *Biological procedures online*, 6:1–9, 2004.

[299] E P Wojcikiewicz, M H Abdulreda, X Zhang, and V T Moy. Force spectroscopy of LFA-1 and its ligands, ICAM-1 and ICAM-2. *Biomacromolecules*, 7:3188–3195, 2006. 7.2.1

[300] C M Franz, A Taubenberger, P-H Puech, and D J Muller. Studying integrin-mediated cell adhesion at the single-molecule level using AFM force spectroscopy. *Science's STKE : signal transduction knowledge environment*, 406:pl5, October 2007. 7.2.1

[301] C Selhuber-Unkel, T Erdmann, M López-García, H Kessler, U S Schwarz, and J P Spatz. Cell adhesion strength is controlled by intermolecular spacing of adhesion receptors. *Biophysical journal*, 98(4):543–51, February 2010. 7.2.1

[302] J Friedrichs, J Helenius, and D J Muller. Quantifying cellular adhesion to extracellular matrix components by single-cell force spectroscopy. *Nature protocols*, 5:1353–1361, 2010. 7.2.1

[303] B Hosseini. *Cellular Separation Forces Studied by Force Spectroscopy and Microplate Manipulation*. PhD thesis, University of Heidelberg, 2008. 7.2.1

Appendix

Appendix

A

Publications

In preparation:

"Quantification of substrate and cellular strain in 3D cell culture - an experimental and computational framework"

Paula Gonzales Avalos[*a,b], Marlies Mürnseer[*c], **Janosch Deeg[d,e]**, Anastasia Bachmann[f], Joachim P. Spatz[d,e], Steven Dooley[c], Roland Eils[a,b], Evgeny Gladilin[b]

* These authors contributed equally to the work and the manuscript presented.

a Bioquant, University of Heidelberg, Heidelberg, Germany

b German Cancer Research Center, Heidelberg, Germany

c Medical Faculty Mannheim, University of Heidelberg, Mannheim, Germany

d Max-Planck-Institute for Intelligent Systems, Stuttgart, Germany

e Biophysical Chemistry, University of Heidelberg, Heidelberg, Germany

f BG Trauma Centre, University of Tübingen, Tübingen, Germany

Nanoletters 2013

"T Cell Activation is Determined by the Number of Presented Antigens"

Janosch Deeg[a,b], Markus Axmann[a], Jovana Matic[a], Anastasia Liapis[c], David Depoil[c], Jehan Afrose[c], Silvia Curado[c], Michael L. Dustin[c,d], and Joachim P. Spatz[a,b]

a Department of New Materials and Biosystems, Max Planck Institute for Intelligent Systems, Heisenbergstraße 3, D-70569 Stuttgart, Germany
b Department of Biophysical Chemistry, University of Heidelberg, INF 253, D-69120 Heidelberg, Germany c Skirball Institute of Biomolecular Medicine and Department of Pathology, New York University School of Medicine, New York, New York 10016, United States
d Kennedy Institute of Rheumatology, Nuffield Department of Orthopedics, Rheumatology and Musculoskeletal Sciences, University of Oxford, Oxford, OX37FY, United Kingdom

Abstract: Antigen recognition is a key event during T cell activation. Here, we introduce nanopatterned antigen arrays that mimic the antigen presenting cell surface during T cell activation. The assessment of activation related events revealed the requirement of a minimal density of 90 – 140 stimulating major histocompatibility complex class II proteins (pMHC) molecules per μm^2. We demonstrate that these substrates induce T cell responses in a pMHC dose-dependent manner and that the number of presented pMHCs dominates over local pMHC density.

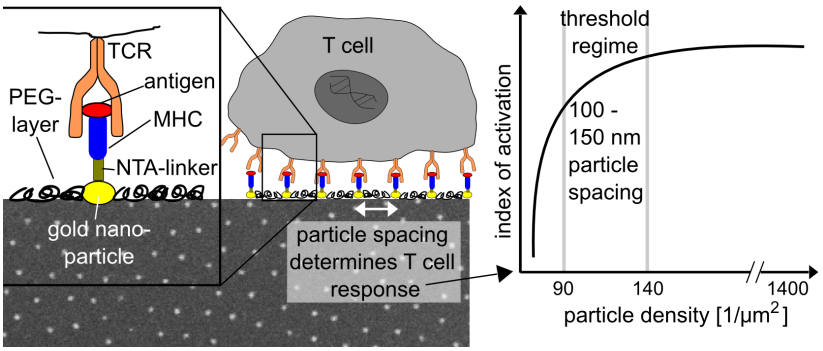

Nanoletters 2013

"Fine Tuning and Efficient T Cell Activation with Stimulatory aCD3 Nanoarrays"

Jovana Matic[a], **Janosch Deeg**[a,b], Alexander Scheffold[c,d], Itamar Goldstein[e,f], and Joachim P. Spatz[a,b]

a Department of New Materials and Biosystems, Max Planck Institute for Intelligent Systems, Heisenbergstrasse 3, 70569 Stuttgart, Germany
b Department of Biophysical Chemistry, University of Heidelberg, INF 253, Germany
c Department of Cellular Immunology, Clinics for Rheumatology and Clinical Immunology, Charité University Medicine Berlin, Berlin, Germany
d German Rheumatism Research Centre (DRFZ) Berlin, Leibniz Association, Berlin, Germany
e Immunology Core Laboratory, Sheba Cancer Research Center, Chaim Sheba Medical Center, Tel Hashomer 52621, Israel
f Sackler Faculty of Medicine, Tel Aviv University, Israel

Abstract: Anti-CD3 (aCD3) nanoarrays fabricated by self-assembled nanopatterning combined with site-directed protein immobilization techniques represent a novel T cell stimulatory platform that allows tight control over ligand orientation and surface density. Here, we show that activation of primary human CD4+ T cells, defined by CD69 upregulation, IL-2 production and cell proliferation, correlates with aCD3 density on nanoarrays. Immobilization of aCD3 through nanopatterning had two effects: cell activation was significantly higher on these surfaces than on aCD3-coated plastics and allowed unprecedented fine-tuning of T cell response.

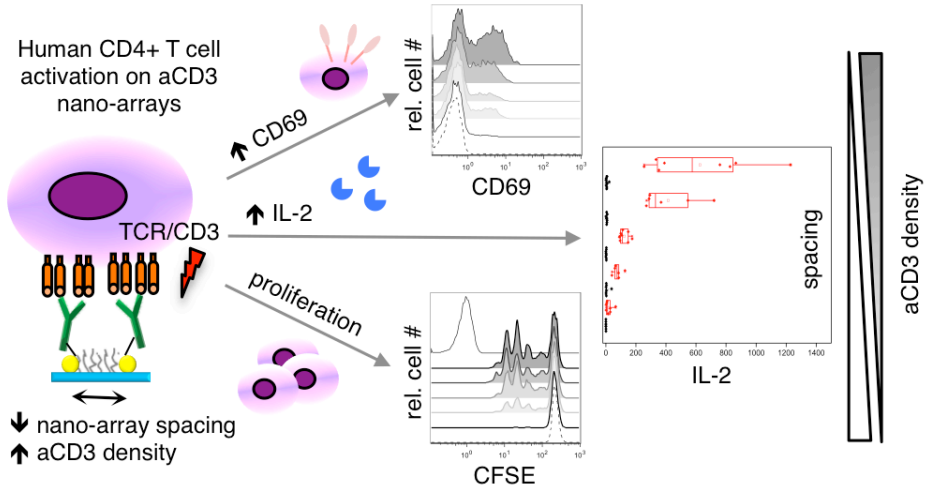

Nanoletters 2011

"Impact of Local versus Global Ligand Density on Cellular Adhesion"

Janosch Deeg[a,b], Ilia Louban[a,b], Daniel Aydin[a,b], Christine Selhuber-Unkel[c], Horst Kessler[c], and Joachim P. Spatz[a,b]

a Department of New Materials and Biosystems, Max Planck Institute for Metals Research, Heisenbergstrasse 3, 70569 Stuttgart, Germany
b Department of Biophysical Chemistry, University of Heidelberg, Germany
c Zoological Institute, University of Kiel, Germany
d Institute for Organic Chemistry und Biochemistry, Lehrstuhl II, Technical University of Munich, Lichtenbergstrasse 4, 985747 Garching, Germany

Abstract: $\alpha_v\beta_3$ integrin-mediated cell adhesion is crucially influenced by how far ligands are spaced apart. To evaluate the impact of local ligand density versus global ligand density of a given surface, we used synthetic micronanostructured cell environments with user-defined ligand spacing and patterns to investigate cellular adhesion. The development of stable focal adhesions, their number, and size as well as the cellular adhesion strength proved to be influenced by local more than global ligand density.

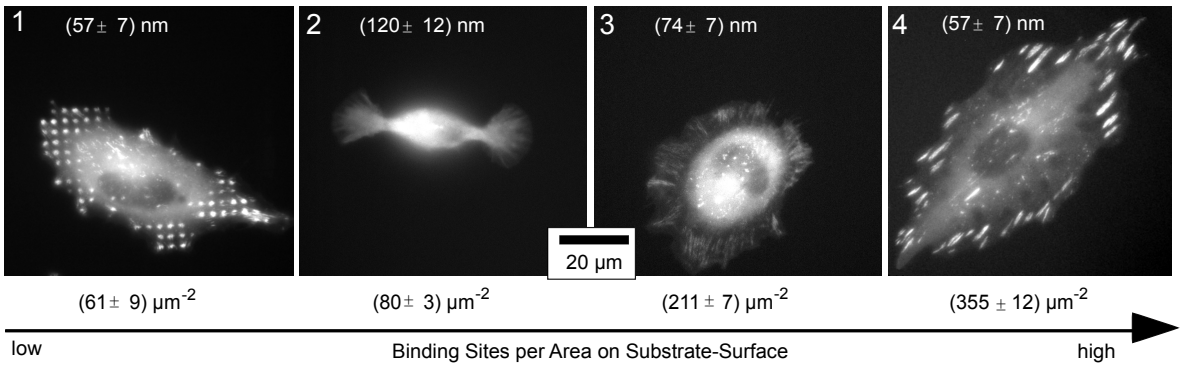

PNAS 2010

"Immune synapse formation determines interaction forces between T cells and antigen-presenting cells measured by atomic force microscopy"

Babak H. Hosseini[a], Ilia Louban[a], Dominik Djandji[b], Guido H. Wabnitz[c], **Janosch Deeg[a]**, Nadja Bulbuc[b], Yvonne Samstag[c], Matthias Gunzer[d], Joachim P. Spatz[a], and Günter J. Hämmerling[b,1]

a Department of New Materials and Biosystems, Max-Planck-Institute for Metals Research, Stuttgart, Germany, and Department of Biophysical Chemistry, University of Heidelberg, Heisenbergstrasse 3, D-70569 Stuttgart, Germany

b Department of Molecular Immunology, German Cancer Research Center, D-69120 Heidelberg, Germany

c Institute for Immunology, University of Heidelberg, Im Neuenheimer Feld 305, D-69120 Heidelberg, Germany

d Institute of Molecular and Clinical Immunology, Otto-von-Guericke-University-Magdeburg, Leipziger-Strasse 44, D-39120 Magdeburg, Germany

Abstract: During adaptive immune responses, T lymphocytes recognize antigenic peptides presented by MHC molecules on antigen-presenting cells (APCs). This recognition results in the formation of a so-called immune synapse (IS) at the T-cell/APC interface, which is crucial for T-cell activation. The molecular composition of the IS has been extensively studied, but little is known about the biophysics and interaction forces between T cells and APCs. Here, we report the measurement of interaction forces between T cells and APCs employing atomic force microscopy (AFM). For these investigations, specific T cells were selected that recognize an antigenic peptide presented by MHC-class II molecules on APCs. Dynamic analysis of T-cell/APC interaction by AFM revealed that in the presence of antigen interaction forces increased from 1 to 2 nN at early time-points to a maximum of 14 nN after 30 min and decreased again after 60 min. These data correlate with the kinetics of synapse formation that also reached a maximum after 30 min, as determined by high-throughput multispectral imaging flow cytometry. Because the integrin lymphocyte function antigen-1 (LFA-1) and its counterpart intercellular adhesion molecule-1 (ICAM-1) are prominent members of a mature IS, the effect of a small molecular inhibitor for LFA-1, BIRT377, was investigated. BIRT377 almost completely abolish the interaction forces, emphasizing the importance of LFA-1/ICAM-1-interactions for firm T-cell/ APC adhesion.

In conclusion, using biophysical measurements, this study provides precise values for the interaction forces between T cells and APCs and demonstrates that these forces develop over time and are highest when synapse formation is maximal.

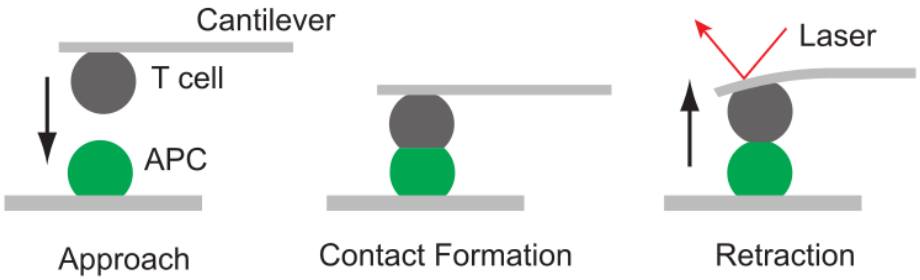

Danksagung

"Es gibt so viele Dinge, die man nicht mit Geld bezahlt, wohl aber mit einem Lächeln, einer Aufmerksamkeit, einem "Danke"." **Léon-Joseph Suenens**

Danke, an all diejenigen unzähligen, guten Seelen, die mich bei dieser Arbeit unterstützt haben, mir beigestanden sind, mich begleitet haben und mir gezeigt haben, dass kleine Dinge - ein Lächeln, eine Aufmerksamkeit - oft die wertvollsten Güter auf dieser Erde sind.

Mein Doktorvater Prof. Dr. Spatz hat mir stets sein volles Vertrauen entgegengebracht, mich und meine Ideen immer unterstützt und mir gleichzeitig alle Freiheiten gelassen, mich in einem interdisziplinären und spannenden Forschungsfeld auszuprobieren. Er hat es mir ermöglicht unter perfekten Bedingungen in einem internationalen Projekt tätig zu sein und hierbei mein Wissen in viele Richtungen zu erweitern, als auch wertvolle Kontakte zu knüpfen. Das alles schätze ich sehr. Vielen herzlichen Dank, Joachim, dass ich bei Dir meine Promotion durchführen durfte!

Bei Prof. Dr. Fink möchte ich mich sehr herzlich für die bereitwillige Zusage bedanken an meiner Disputation teilzunehmen, als auch sich in die Materie einzuarbeiten, um ein Zweitgutachten dieser Arbeit anzufertigen. Ebenfalls danke ich Prof. Dr. Schwarz und Prof. Dr. Dubbers, dass sie sich spontan bereit erklärt haben, mich zu prüfen und bezüglich des Prüfungstermins sehr flexibel waren!

Ein großer Dank geht an meine Arbeitskollegen in New York! Hauptsächlich möchte ich mich bei Anastasia Liapis bedanken, die mir zu Beginn alle Tricks und Kniffe bei der Arbeit mit Zellen verraten hat und sowohl das Konzept der Arbeit mit ausgearbeitet hat. Ausserdem danke ich Prof. Dr. Michael Dustin, David Depoil und David Blair für die vielen überaus kompetenten Anregungen und die Geduld die sie meinen Fragen entgegenbrachten, sowie Silvia Curado für die Organisation des internationalen Projekts und die zahlreichen Videokonferenzen und Projektmeetings!

Um eine Doktorarbeit anzufertigen, braucht es Ausdauer und Durchhaltevermögen! Ohne meine netten und stets hilfsbereiten Kollegen hätte ich es wohl nicht auf diese Art gemeistert. Vielen, vielen Dank an alle aus der Spatz-Crew, die mich über die Jahre begleitet haben und immer für ein angenehmes Arbeitsklima gesorgt haben. Bei Markus Axmann möchte ich mich dafür bedanken, dass er stets geduldig mit mir an seinem Hightech-Mikroskop gemessen hat! Gleiches gilt für Timo Maier, der immer sofort bereit war mir beim "Zellen mikroskopieren" mit dem RICM zu helfen, wenn es mal wieder nicht so klappte wie es sollte. Auch für seine vielen leckeren Kuchen, vielen Dank! Ausserdem möchte ich mich bei meinen netten, sympathischen und lustigen

Zimmerkollegen Catharina, Jan, Sabri und Gerri, sowie die beiden “Ehemaligen”, Seba und Tobi, bedanken. Ich hatte immer Spaß im Büro und falls ich Hilfe brauchte war immer jemand da! Catharina gilt besonderer Dank, da sie sehr sorgfältig meine Doktorabeit gelesen und korrigiert hat und auch sonst oft mit Rat und Tat zur Seite stand. Gleiches gilt für Dimitris, den T-Zell-Experten der Großartiges geleistet hat, um meine Dissertation zu verbessern. Vielen Dank für deine vielen kompetenten Anmerkungen und Ideen! Danke auch an Björn, meinen Masterstudenten, Jan und Timo die ebenfalls Teile meiner Arbeit gewissenhaft korrigiert haben. An Björn schätze ich außerdem sehr, dass er selbständig forscht und es mir nicht übel nimmt, dass ich in der letzten Phase meiner Arbeit kaum Zeit für ihn hatte. Rebecca habe ich als sehr kompetente Zellexpertin kennengelernt. Sie hatte für Fragen und Probleme immer ein offenes Ohr. Danke!

Den ehemaligen Kollegen, Ilia, Daniel, Babak gilt ebenfalls ein großer Dank, da sie mich geduldig mit allerlei Techniken vertraut gemacht haben, meine ersten Schritte im Arbeitskreis begleitet haben und mit Rat und Tat zur Seite standen.

Für die anregenden fachlichen Gespräche, Vorschläge und neue Ideen und Hilfen möchte ich mich vor allem bei Tamas, Seraphine, Franzi, Jovana, Chrissy, Ada, Ilia P., Katharina, Martin, Heike und Vera bedanken. Sicherlich gibt es noch einige, die jetzt nicht namentlich genannt wurden, aber mir ebenfalls immer wieder neue Anregungen geliefert und mit ihren fleißigen Händen unterstützt haben. Deshalb noch mal vielen Dank an alle aus der Spatz Gruppe für die große Hilfsbereitschaft und Kollegialität!

Ich bedanke mich ganz herzlich bei den Sekretärinnen Frau Ulshöfer, Frau Hess und Frau Pfeilmeier für ihre stete Hilfe und den reibungslosen Ablauf aller organisatorischen Dinge. Nina Grunze möchte ich Danke sagen für die sehr wertvollen Korrekturen meiner Publikationen. Sigrid Riese für die wichtige und wertvolle Arbeit die sie in unserem Arbeitskreis leistet.

Wieder mal ein großer Dank an meine Fetzer-Crew da draussen. Was würde ich bloß ohne euch machen? Und nicht zu vergessen meine Homies, Jelli, Judith und Imer. Vielen Dank für viele lustige Stunden, gutes Essen und sonstige Ablenkungen.

Meine Eltern haben mich immer bedingungslos unterstützt und keine meiner Entscheidungen in Frage gestellt. Für dieses wertvolle Vertrauen möchte ich mich ganz, ganz herzlich bedanken und ich weiß es sehr zu schätzen! Mein Schwester ist immer für mich da wenn ich sie brauche und sie wird es immer sein. Vielen, vielen Dank an meine Familie!

Julie, ich danke dir von ganzem Herzen für deine fortwährende Unterstützung, dein Vertrauen und deine Zuneigung! Danke, dass es dich gibt!

Ich erkläre hiermit, dass ich die vorgelegte Dissertation selbst verfasst und mich keiner anderen als der von mir ausdrücklich bezeichneten Quellen und Hilfen bedient habe.

Heidelberg, den 04. November 2013 .....

Janosch Deeg

"We are all visitors to this time, this place. We are just passing through. Our purpose here is to observe, to learn, to grow, to love... and then we return home"

Aboriginal Proverb